Print ISSN 0033-9008
Online ISSN 1880-1765

QUARTERLY REPORT of RTRI

Feb. 2025 Vol. 66 No. 1

CONTENTS

H Human factors
I Infrastructure
N Natural hazards
O Operations
R Rolling stock
T Technical system integration and interaction

RAILWAY TECHNICAL RESEARCH INSTITUTE

QUARTERLY REPORT of RTRI

Print ISSN 0033-9008
Online ISSN 1880-1765

February 2025 Vol. 66 No. 1

CONTENTS

H Human factors
I Infrastructure
N Natural hazards
O Operations
R Rolling stock
T Technical system integration and interaction

Survey of Railway Customer Perception of Men's Restroom Cleanliness in Railway Stations

Takashi KYOTANI
Comfort Science and Engineering Laboratory, Human Science Division

Yoshiki IKEDA
East Japan Railway Company

Hiroshi OISHI
Tohoku Institute of Technology

Tamami KAWASAKI
Comfort Science and Engineering Laboratory, Human Science Division

In order to extract factors that affect customer evaluations of men's restrooms in railway stations, we conducted surveys to understand railway customer perception of men's restroom cleanliness in railway stations. Statistical analysis of the survey results revealed that two indicators, "odor satisfaction" and "urine stains on skirting boards," affect user perception of cleanliness and their decision to use the same restroom again. It also became clear that user perception of the cleanliness of men's railway restrooms cleaned using dry methods in terms of odor was statistically significantly higher than those cleaned with wet methods.

Key words: *station, restroom, cleaning, customer perception, hygiene*

1. Introduction

To attract more customers to use railways, which are a form of public transport, it is very important to create an inviting environment (inside stations and trains, etc.). Station restrooms in particular, in terms of appearance and odor, are one of the passenger facilities that most shape opinions about the quality of a station environment. Past surveys [1, 2], have found that about 20% of all respondents consider odor to be an important factor determining the attractiveness of station facilities. In addition, Ozaki et al. [3] found that there was a high correlation between overall evaluation items such as "Would you choose to use this restroom again?" and "Has your perception of the facility improved?" and evaluation items such as "odor," "cleanliness," and "comfort" in shaping user perception of restrooms in commercial facilities. In addition, Takahashi et al. [4, 5] reported that it was confirmed that the trap and flush methods of urinals, the presence or absence of urinal backsplash stones and gutters, and the size of floor tiles in men's restrooms at stations affected odor acceptability. One reason for this is that in men's restrooms, the urinals are located on the walking surface of the floor, and urine stains scattered on the floor may be spread by user movement around the restroom. In general, restrooms in stations are cleaned by cleaning companies contracted by railway operators, and the quality of the cleaning work is evaluated by inspections carried out by the cleaning companies themselves using evaluation criteria set for each cleaning area. On the other hand, there are few reports on user evaluation of the cleanliness of station restrooms, and it is not clear how users evaluate the quality of current cleaning work, and what kind of cleaning quality would improve user perception of cleanliness.

In recent years, an increasing number of stations have introduced a method (dry cleaning) that does not use water to clean the floor of restrooms in stations to suppress the growth of bacteria [6], which is considered to be one of the causes of odors in restrooms. It has been reported that dry cleaning reduces restroom odors compared to restrooms cleaned using conventional water-based methods (wet cleaning) [7, 8]. However, cleaning evaluations are carried out using almost the same criteria regardless of cleaning method.

Therefore, we conducted a survey to investigate customer perceptions of station restroom cleanliness (hereafter referred to as "monitor survey") with the aim of understanding how railway customers evaluate station restroom cleanliness, in order to contribute to the improvement of cleaning quality for users. When analyzing data collected from these surveys, we considered the indicators that affect the answer to the question "Would you choose to use this restroom again?" based on the contents of the previous study [3] mentioned above. Based on the contents of previous studies [4, 5], the restrooms included in the survey were limited to men's restrooms. We also examined whether differences in cleaning methods (dry or wet) would produce differences in survey results. In this paper, we report on the contents and results.

2. Survey outline

2.1 Surveyed restrooms

The restrooms surveyed were men's restrooms at two stations (hereafter referred to as "Station A" and "Station B") where dry cleaning was carried out on the floor, and men's restrooms at two stations (hereafter referred to as "Station C" and "Station D") where wet cleaning was carried out. These four stations were selected from stations that met the following conditions.

Condition (1) The number of passengers must be approximately the same.
Condition (2) The renovation of the restroom, including the change of the floor of the restroom, was carried out at about the same time.

However, for Station D, since there were no other stations that met Condition (2) in the restroom for wet cleaning, a station that met Condition (1) was selected from a station in the vicinity of Station B where the survey was to be conducted on the same day. Table 1 shows the number of passengers at each station, how the restrooms are cleaned, and photos of the flooring. In addition, the schematic diagram of each restroom and the approximate dimensions and area are shown in Fig. 1.

Here, we briefly describe the differences in cleaning methods used in the surveyed restrooms. In restrooms where dry cleaning is used, the floor is wiped using a flat mop equipped with a cleaning sheet during the day, and about once a month outside of business hours (late at night), dust is sucked up with a vacuum cleaner, and urine stains are wiped with a sponge soaked in water and wrung out tightly. On the other hand, in restrooms where wet cleaning is being carried out, the floor is wiped with a tightly wrung mop during the day, and about once a month outside of business hours, water containing detergent is sprinkled on the entire floor, scrubbed with a brush or rotating brush, and finally drained via the gutter into the sewer pipe.

2.2 Monitor attributes and survey itinerary

This survey was conducted a total of three times from 2018 to 2019. The first survey conducted in 2018 was designated as the "preliminary survey," and the second and third surveys conducted in 2019 as the "main survey" after additional questions were added on the basis of the results of the preliminary survey. Table 2 shows the dates and the stations to be surveyed of each survey. The surveys were about men's restrooms, therefore all participants were men. Table 3 (a) shows the number of people and the breakdown by age group, Table 3 (b) shows the results of the question about the frequency of regular use of the stations, and Table 3 (c) shows the results of the question about the frequency of use of the restrooms in the stations.

The number of participants was determined in consultation with the railway operator responsible for the stations to be surveyed, as it was necessary to conduct the survey within the constraints of not interfering with the operation of the station, the passage of general customers, and the use of restrooms.

The age groups were those in their 20s to 50s, who frequently used stations and could participate during the daytime on the day of the survey (weekdays). We thought that high school students were included in the 10-year-olds and could not participate due to commuting to school, etc., and that those in their 60s and older would not use stations frequently, and that the risk of developing heat stroke would increase in the survey conducted in the summer (main survey). As a result of the above considerations, we decided to exclude these age groups from the participants. On the days of the

Table 1 Surveyed restrooms [7][9][10]

Station	A	B	C	D
Floor cleaning method	Dry		Wet	
Number of renewals	2	2	1	2
Year of last renewal	2015	2015	2014	2006
Cleaning tools (normal)	• Flat mop with cleaning sheet		• Tightly squeezed mop	
Cleaning tools (midnight) (About once a month)	• Vacuum cleaner • Tightly squeezed sponge		• Brush • Rotating brush	
Examples of cleaning tools [7]	 (Flat mop)		 (Tightly squeezed mop)	
Floor structure	Rubber tiles		Porcelain tiles + joints	
Photo of the inside of restrooms (example)				
Photo of flooring	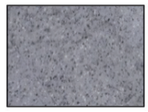			
Average number of passengers getting on and off per day (Approximate values) *)	70,000	35,000	70,000	30,000

*) The average number of passengers getting on and off per day was calculated based on the "Number of passengers at each station FY2017" published by JR East (https://www.jreast.co.jp/passenger/2017.html). However, the published figures are only for the number of passengers getting on, and do not include the number of them getting off. Therefore, we estimated that the "Number of passengers" is twice as many as the number of passengers getting on and calculated the figures (approximate values) in Table 1.

Table 2 Date of survey and stations with surveyed restrooms

Date of survey		Stations with surveyed restrooms
1st (Preliminary survey)	2018.12.2	A, C
2nd (Main survey)	2019.7.23	A, C
3rd (Main survey)	2019.7.30	B, D

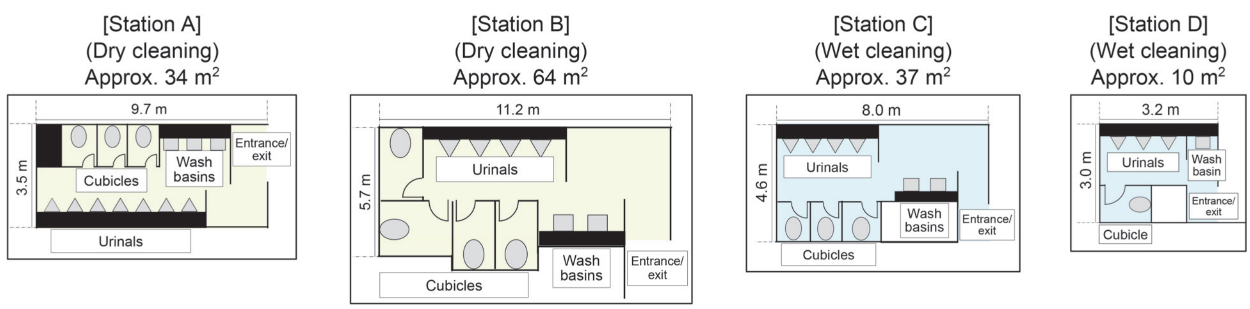

Fig. 1 Schematic diagram of the surveyed restrooms

survey, each participant was taken once to the restrooms in the two stations (Table 2) and asked to answer the evaluation items described below.

2.3 Survey content

In a total of three monitoring surveys, we instructed the participants to first enter the surveyed men's restroom and check the facilities inside, and then to answer their impressions of the cleanliness of each facility (hereafter referred to as "cleaning status evaluation"). Specifically, we instructed the participants to evaluate the cleanliness of each surveyed facility based on the evaluation items set for each facility using a four-case method. Table 4 shows the facilities to be surveyed and the evaluation items for each facility, and Table 5 shows the options for answering. Among the evaluation items in Table 4, those indicated by "●" were set in both the preliminary survey and the main survey, and those indicated by "◇" were additional items set in the main survey based on the results of the preliminary survey. In addition, the items indicated by "●" were set with reference to previous studies [11, 12] and the quality evaluation items of the cleaning work carried out by the company in charge of cleaning the surveyed restrooms (hereafter referred to as "previous cleaning quality evaluation item [13]"). We also divided the surveyed facilities into "floor (around urinals)" and "floor (other than around urinals)," as we thought that the evaluation results of the floor might differ between the area around the urinal and the rest of the facility. In addition, the "grating (around the drain)," "lining (shelf behind the urinal)," and "entrance/exit," which were not included in the previous study and the previous cleaning quality evaluation items, were newly added as facilities to be surveyed, considering that they are easily visible to users and may affect the impression of the restroom used.

For the preliminary survey (first survey) only, in order to search for items that could be used as criteria for evaluating the cleanliness

Table 3 Participant attributes

(a) age

Age	Number of respondents			Total
	1st (Preliminary survey)	2nd (Main survey)	3rd (Main survey)	
20s	7	2	2	11
30s	7	5	7	19
40s	8	3	2	13
50s	3	2	2	7
Total	25	12	13	50

(b) Usual frequency of use of stations

Frequency of use of stations	Number of respondents			
	1st survey	2nd survey	3rd survey	Total
Almost every day	16	5	6	27
Several times a week	9	7	7	23

(c) Usual frequency of use of restrooms in stations

Frequency of use of restrooms in stations	Number of respondents			
	1st survey	2nd survey	3rd survey	Total
Use	20	7	8	35
Sometimes use	4	5	5	14
Never use	1	0	0	1

Table 4 Facilities to be surveyed for cleaning status evaluation and evaluation items (●: Common to the preliminary survey and the main survey) (◇: Added in the main survey)

Surveyed facilities	Evaluation items
Urinal	● Is there any dirt around the equipment? ● Is there dust or dirt accumulated inside the equipment (inner surface) or on the perforated plates? ◇Are there "water drops or wetness?" ◇Are there "urine stains?"
Floor (around urinal)	● Is there dirt under the urinal? ● Is there any uneven wiping or unwiped residue? ● Is there sticking gum? Is there dust or dirt in the corners? ◇Are there "water drops or wetness?" ◇Are there "urine stains?"
Floor (except around urinal)	● Are footprints not noticeable? ● Are dirt and sediment not noticeable? ● Is there sticking gum? Is there dust or dirt in the corners? ◇Are there "water drops or wetness?" ◇Are there "urine stains?"
Grating	● Is there any trash? ● Is there a puddle? ◇Are there "water drops or wetness?" ◇Are there "urine stains?"
Lining	● Is there any trash left in the lining? ●Are there any dust or dirt in the corners? ◇Are there "water drops or wetness?"
Wall	● Is there any dirt around the urinal? ● Is there any graffiti? ◇Are there "water drops or wetness?" ◇Are there "urine stains?"
Skirting board	● Is dust not noticeable? ● Are any scratches not noticeable? ● Is there any sewage or wax adhesion? ◇Are there "water drops or wetness?" ◇Are there "urine stains?"
Cubicle door (outside surface)	● Is there dust around the door? ● Is the bottom of the door dirty? ● Is there any graffiti? ◇Are there "water drops or wetness?" ◇Are there "urine stains?"
Air vent	● Is dust not noticeable? ● Are any scratches not noticeable? ◇Are there "water drops or wetness?"
Mirror	● Is there an uneven wipe at the top? ● Is there any water stain on the bottom? ● Is there dust attached? ◇Are there "water drops or wetness?"
Wash basin	● Is the wash basin clean with no water stains? ● Is there any garbage on the dressing table (luggage table)? ● Is the faucet clean and shiny? ◇Are there "water drops or wetness?"
Entrance/exit	● Is the pictogram (restroom mark, etc.) dirty? ● Is there any trash falling near the entrance? ● Is the brightness of the entrance enough? ◇Are there "water drops or wetness?"
The whole restroom	● Overall impression about cleaning

Table 5 Answer options to cleaning status evaluation (Table 4)

Options	Contents
1	Overall bad
2	Acceptable if cleaned
3	Acceptable
4	Overall good

of restrooms, other than the items listed in "●," and to confirm whether there were any contents that should be added to the evaluation items in Table 4 for the main survey, we asked the participants to freely describe any "points of concern such as dirt" for each surveyed facility and the air in the surveyed restroom space. The format of the answers was a fixed free-form format as shown in Table 6. The answers were organized according to the following procedure.

(1) Exclude answers with the same content as the evaluation items in "●" in Table 4.
(2) Extract the facilities for which the answer remains for each station as results of the procedure (1).
(3) Categorize each answer according to the cause of "worrisome stains" (including water, toilet paper, and odors).
(4) As a result of the classification, exclude the answer with the content with only one mention and with the content that cannot be removed by cleaning.

Table 7 summarizes the contents of the answers, and the number of mentions made by two or more participants (referred to as "a"), the total number of mentions made for the same surveyed facility (referred to as "b"), and the ratio of "a" to "b."

The reason why the number of answers was described as "number of mentions" instead of "number of participants who answered" was that there were participants who submitted two answers for the same facility in the same restroom, and we identified several cases where the value of "b" did not match the number of participants who answered.

In both Station A and Station C restrooms, the air in the restroom space smelled of human waste, accounting for 50% of the total number of answers in Station A and 73% in Station C. In addition, the remaining responses to the spatial air in the restroom in Station C were all related to odors. In addition, 25% and 50% of the mentions pointed out "water wetness" and "splashing water on the walls and floor" on the floor (other than around the urinal) and sinks in Station A, and 80% of the mentions pointed out "dirt on the floor and walls" at the entrance of Station C.

Table 6 Answer column for "Points of concern such as dirt" (Preliminary survey only)

"Specific part of equipment"	"Concerns"	"Condition"
[Answer example]		
"Urinal"	"Darkening"	"Remained"

Checking the evaluation items of "●" in Table 4, "floor" and "wall" include evaluation items related to dirt, but "water wetness" is not included in the evaluation items of facilities other than the "floor (around urinals)," "grating," and "mirror," and evaluation items related to "human waste" are not included in any facility. In addition, the toilet paper scraps on the floor (other than around urinals) and the tape marks on the walls that were pointed out in the restroom in Station A are not usually seen in station restrooms (toilet paper scraps may occasionally fall in cubicles, but they are rarely found on other floors), and they are easy to remove as soon as they are found, as are the plastic bottles and empty cans that are sometimes seen. Based on these findings, we considered that it is necessary to understand users' awareness of "water droplets and water wetness" and "urine stains" for the surveyed facilities shown in Table 4, and as described above, these two evaluation items were additionally set in the main survey.

For the evaluation of odors in the restroom, we instructed people to answer regarding five evaluation items (common to all three surveys): "odor intensity," "odor concern," "odor pleasantness/unpleasantness," "odor satisfaction," and "odor tolerance." The answer options for each evaluation item are shown in Table 8.

In addition, we asked about two points: whether this station restroom was generally clean (hereafter referred to as "cleanliness") and whether they would like to use this station restroom again (hereafter referred to as "reuse") (common to all three times). Tables 9 and 10 show the answer options for each question.

3. Survey results and discussion

3.1 Confirmation of significant differences in the results of each evaluation due to different cleaning methods

The differences in the results of monitor surveys due to the different cleaning methods (dry or wet) were examined using a non-parametric test. Specifically, we compiled the results of a total of three surveys for each station restroom with dry cleaning (Station A and Station B) and wet cleaning (Station C and Station D) and performed a Mann-Whitney U-test to see if there were significant differences in the results of the survey. The results are shown in Table 11. Table 11 (a) shows the results for the surveyed facilities and evaluation items in Table 4, and Table 11 (b) shows the results

Table 7 "Points of concern" other than the evaluation items of "●" in Table 4

Station	Facilities	Answer contents	Number of answers **(a)**	Total number of answers to the equipment **(b)**	a/b
A	Floor (except around urinal)	• Wet	3	12	25%
		• Toilet paper waste	4		33%
	Wall	• Trace of tape	3	8	38%
	Wash basin	• Water splash (to wall or floor)	3	6	50%
	Space air	• Odor of human waste	2	4	50%
C	Entrance/exit	• Dirty floor and wall	4	5	80%
	Space air	• Odor of human waste	11	15	73%
		• Strong odor	2		13%
		• Anxious odor	2		13%

(Points with only one answer were excluded)

Table 8 Answer options for evaluation items related to odor (Common to all 3 surveys)

(a) Odor Intensity

Odor intensity	Contents
0	Undetectable (odorless)
1	Odor that can be detected barely
2	Weak odor that can still be identified as to what odor it is
3	Odor easily perceived
4	Strong odor
5	Intense odor

(b) Odor concern

Answer options	Contents
1	Be concerned
2	Not be concerned

(c) Odor pleasantness/unpleasantness

Pleasantness/unpleasantness	Contents
−4	Extremely unpleasant
−3	Very unpleasant
−2	Unpleasant
−1	Somewhat unpleasant
0	Neither
1	Somewhat pleasant
2	Pleasant
3	Very pleasant
4	Extremely pleasant

(d) Odor satisfaction

Answer options	Contents
1	Dissatisfied
2	Somewhat dissatisfied
3	Neither
4	Somewhat satisfied
5	Satisfied

(e) Odor acceptance

Answer options	Contents
1	Acceptable
2	Unacceptable

Table 9 Answer options to "cleanliness" (Common to all 3 surveys)

Answer options	Contents
1	It was clean
2	If anything, it was clean
3	Neither
4	If anything, it was dirty
5	It was dirty

Table 10 Answer options to "reuse" (Common to all 3 surveys)

Answer options	Contents
1	I would choose to use
2	If anything, I would choose to use
3	Neither
4	If anything, I would choose not to use
5	I would choose not to use

for the five odor-related evaluation items (Table 8), "cleanliness" (Table 9), and "reuse" (Table 10).

The significance probability was less than 0.05 only for the five odor-related evaluation items (intensity, concern, pleasantness/unpleasantness, satisfaction, and tolerance) as shown in Table 11 (b). When compared with the graph (Fig. 2) showing the results of these five evaluations, it was found that all the results were significantly better in the restrooms in Station A and Station B, where dry cleaning was used, than those in Station C and Station D, where wet cleaning was used.

3.2 Indicators influencing "reuse"

In a previous study [3], one of the overall evaluation items of the restroom was "Would you choose to use this restroom again?" For this reason, in this study, when analyzing the users' evaluation results, we considered the indicators that affect the answer to "reuse." Therefore, we conducted a correlation analysis between the answers to "reuse" and the results of the cleanliness evaluation of the surveyed facilities (Tables 4 and 5), odor-related (Table 8), and "cleanliness" (Table 9). The correlation coefficient was Kendall's rank correlation coefficient because all options shown in Tables 5

Table 11 Significance probability obtained as a result of the Mann-Whitney U-test (Differences in cleaning methods)

(a) Cleaning status evaluation of the surveyed facilities shown in Table 4

Facilities	Significance probability		
	Evaluation items: "●" in Table 4	Evaluation items: "◇" in Table 4	
		Are there "water drops or wetness?"	Are there "urine stains?"
Urinal	0.866	0.708	0.456
Floor (around urinal)	0.440	0.162	0.470
Floor (except around urinal)	0.924	0.454	0.900
Grating	0.247	0.099	0.307
Lining	0.504	0.792	-
Wall	0.536	0.475	0.488
Skirting board	0.408	0.054	0.688
Cubicle door (outside surface)	0.533	0.601	0.885
Air vent	0.799	0.895	-
Mirror	0.722	0.570	-
Wash basin	0.145	0.103	-
Entrance/exit	0.887	0.455	-
The whole restroom	0.441	-	-

(b) Odor, "cleanliness" and "reuse"

Evaluation items	Significance probability
Odor intensity	0.037
Odor concern	0.008
Odor pleasantness/unpleasantness	0.048
Odor satisfaction	0.011
Odor acceptance	0.028
"Cleanliness"	0.473
"Reuse"	0.437

and 8-10 were ordinal data [14]. Table 12 shows the results of this analysis for the common evaluation items for all three surveys (Tables 4, 5, 8, and 9, except for the evaluation items indicated by "◇" in Table 4) and the evaluation items added in the main survey (the evaluation items indicated by "◇" in Table 4). In Table 12, the absolute value of the correlation coefficient that exceeded 0.4 was shaded to indicate that the absolute value was larger than that of the others (strong correlation with "reuse").

From Table 12 (a), it was found that the absolute value of the correlation coefficient with the answer to "reuse" exceeded 0.4 for the following evaluation items. The preliminary survey and main survey are listed separately.

Preliminary survey: Four odor-related evaluation items ("odor intensity," "odor concern," "odor pleasantness/unpleasantness," and "odor satisfaction") and "cleanliness" in the restroom as a whole.

Main survey: Evaluation of the same evaluation items as the preliminary survey, and the cleaning status of "urinal," "lining," and "entire restroom."

The absolute values of the correlation coefficient for the "urinal" and "lining" in the preliminary survey exceeded 0.3, which were larger than that of other facilities surveyed. In addition, these facilities are easily visible when using the urinals. From these results, it was considered that it would be possible to encourage users to "use the restroom again" by improving the above four odor-related evaluation items and the cleanliness of the urinal and lining to improve customer perceptions.

On the other hand, from Table 12 (b), the facilities that were found to have an absolute correlation coefficient value of more than 0.4 with the response to "reuse" are listed below by evaluation item.

"Are there water drops or wetness?": linings, walls, skirting boards, cubicle doors, ventilation openings

"Are there urine stains?": urinals, gratings, skirting boards, cubicle doors

As with the odor evaluation items and "cleanliness" shown in Table 12(a), these items were not included in the previous study [11, 12] or in the previous cleaning quality evaluation items, so we con-

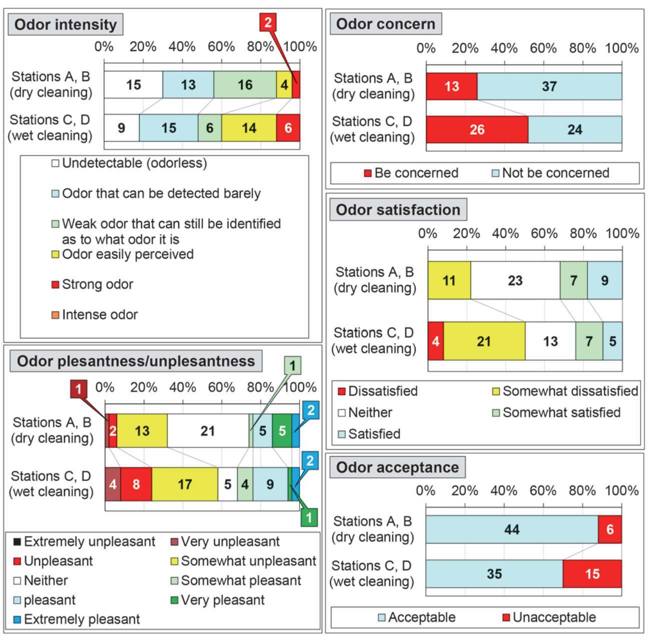

Fig. 2 Comparison of odor-related evaluation results by cleaning method

Table 12 Correlation with "reuse"

(a) Common evaluation items for all 3 surveys

Reference table	Evaluation target (facilities, odor, etc.)	(Preliminary survey) Kendall's rank correlation coefficient	(Preliminary survey) Frequency	(Main survey) Kendall's rank correlation coefficient	(Main survey) Frequency
Table 4	Urinal	−0.308*	49	−0.457**	50
	Floor (around urinal)	−0.110	49	−0.360**	50
	Floor (except around urinal)	−0.141	48	−0.263*	50
	Grating	−0.104	49	−0.340**	50
	Lining	−0.336**	49	−0.418**	50
	Wall	−0.109	49	−0.248	50
	Skirting board	−0.169	49	−0.275*	50
	Cubicle door (outside surface)	−0.146	49	−0.385**	50
	Air vent	−0.063	49	−0.242*	50
	Mirror	−0.104	49	−0.265*	50
	Wash basin	−0.041	49	−0.280*	50
	Entrance/exit	−0.182	49	−0.200	50
	The whole restroom	−0.278*	49	−0.533**	50
Table 8	Odor intensity	0.543**	49	0.455**	50
	Odor concern	−0.508**	49	−0.448**	50
	Odor pleasantness/ unpleasantness	−0.546**	49	−0.479**	50
	Odor satisfaction	−0.614**	49	−0.552**	50
	Odor acceptance	0.388**	49	0.258	50
Table 9	"Cleanliness"	0.505**	49	0.538**	50

**: The correlation coefficient is significant at the 1% level (two-sided).
*: The correlation coefficient is significant at the 5% level (two-sided).

(b) Evaluation items added in the main survey

Evaluation target (facilities, odor, etc.)	Evaluation items	Kendall's rank correlation coefficient	Frequency
Urinal	Are there "water drops or wetness?"	−0.314*	50
	Are there "urine stains?"	−0.435**	50
Floor (around urinal)	Are there "water drops or wetness?"	−0.279*	50
	Are there "urine stains?"	−0.251*	50
Floor (except around urinal)	Are there "water drops or wetness?"	−0.219	50
	Are there "urine stains?"	−0.316*	50
Grating	Are there "water drops or wetness?"	−0.375**	46
	Are there "urine stains?"	−0.412**	46
Lining	Are there "water drops or wetness?"	−0.460**	50
Wall	Are there "water drops or wetness?"	−0.417**	50
	Are there "urine stains?"	−0.252	50
Skirting board	Are there "water drops or wetness?"	−0.445**	50
	Are there "urine stains?"	−0.573**	49
Cubicle door (outside surface)	Are there "water drops or wetness?"	−0.431**	50
	Are there "urine stains?"	−0.446**	50
Air vent	Are there "water drops or wetness?"	−0.470**	50
Mirror	Are there "water drops or wetness?"	−0.194	50
Wash basin	Are there "water drops or wetness?"	−0.193	50
Entrance/exit	Are there "water drops or wetness?"	−0.186	50

**. The correlation coefficient is significant at the 1% level (two-sided).
*. The correlation coefficient is significant at the 5% level (two-sided).

sider that these items are necessary to improve the perception of cleanliness and encourage "reuse" by customers.

In addition, a stepwise multiple regression analysis was performed on the results of the main survey to confirm the degree of influence on "reuse." The objective variable was "reuse," and the explanatory variables were all the evaluation items except the following items: "reuse," the evaluation items found that the correlation coefficient is not significant at the 5% level (Table 12), "overall restroom" (Table 4) and "cleanliness" (Table 9) in the cleaning status evaluation. "Overall restrooms" and "cleanliness" were excluded from the explanatory variables because they were evaluations of the station restroom as a whole and were not indicators of specific facilities. Note that these variables are ordinal data, but they were treated as quantitative data here. As a result, two explanatory variables with a high degree of influence on the objective variable "reuse" were identified: "odor satisfaction" and "urine stains on skirting boards." Table 13 shows the standardized partial regression coefficients (hereinafter referred to as "β"), significance probability, VIF (variance inflation factors) for each explanatory variable, coefficient of determination, adjusted coefficient of determination.

Comparing β, it was estimated that the impact of "odor satisfaction" ($\beta = -0.443$) on "reuse" was greater than that of "urine stains on skirting boards" ($\beta = -0.415$). In addition, since the VIF values were sufficiently small for all explanatory variables, multicollinearity between explanatory variables was not observed [15]. Furthermore, since the coefficient of determination was 0.540 and the adjusted coefficient of determination was 0.519, and the multiple regression equation was relatively good, we considered that these two explanatory variables are appropriate variables for evaluating "reuse" [16].

From the results of the correlation analysis described above (Table 12), the Kendall rank correlation coefficients for "odor satisfaction" and "urine stains on skirting boards" in the main survey were −0.552 and −0.573, respectively. Among the explanatory variables included in the multiple regression analysis by the stepwise method, the absolute value of the correlation coefficient is the highest, indicating that these two evaluation items have the strongest correlation with "reuse." These results suggest that although simple comparisons cannot be made due to the difference in the handling of data between ordinal data and quantitative data, "odor satisfaction" and "urine stains on skirting boards" extracted by the stepwise method are the most effective indicators that encourage users to "reuse."

Section 3.1 showed that the five odor-related evaluation results were significantly better for the station restrooms using dry cleaning than the station restrooms for those using wet cleaning, and this section showed that the four evaluation items related to odor were included among the evaluation items that had a strong correlation with "reuse." Considering these results together, it is believed that the introduction of dry cleaning is one of countermeasures which could improve "odor satisfaction" and increase the percentage of customers who want to use the station restroom again.

Table 13 Results of multiple linear regression analysis (main survey) (Objective Variable: "reuse")

Explanatory variables	Standardized partial regression coefficients (β)	Significance probability	VIF
Odor satisfaction	−0.443	< 0.001	1.278
Urine stains on skirting boards	−0.415	0.001	1.278

Coefficient of determination: 0.540
Adjusted coefficient of determination: 0.519

4. Conclusions

In order to assess the cleaning quality of restrooms in railway stations from the perspective of railway customers, we conducted a monitor survey of men's restrooms in railway stations with different cleaning methods (dry or wet) with the aim of extracting factors that affect users' satisfaction and intention to reuse. The results are shown below.

(1) The significant difference in the results of each evaluation conducted in the main survey due to the different cleaning methods (dry or wet) was examined using the Mann-Whitney U-test. It was found that the evaluation results of the dry-cleaned restroom were significantly better than those of the wet-cleaned restroom for the five odor-related evaluation items (intensity, concern, pleasantness/unpleasantness, satisfaction, and tolerance).

(2) A total of three monitor surveys were conducted in two station restrooms with dry cleaning and two station restrooms with wet cleaning. Of these, the first survey was conducted as a "preliminary survey" and the second and third surveys were conducted as the "main survey." Correlation analysis was performed on the results of the survey, and evaluation items that were strongly correlated with "repeat use" were identified. As for the results of the survey, evaluation items strongly correlated with "reuse" were extracted by correlation analysis. The results of the main survey were examined using the stepwise method to confirm the relationship between "reuse" and other evaluation items. The result confirmed that the two evaluation items of "odor satisfaction" and "urine stains on skirting boards" had the strongest correlation with "reuse." Therefore, it was found that it was possible to increase the percentage of customers who think they would like to use the station restroom again by adding content that reflects these evaluation items to the cleaning quality evaluation items and by performing cleaning that is highly rated by users.

(3) "Odor satisfaction" was extracted as one of the appropriate explanatory variables for evaluating "reuse," and the results of the users' odor evaluation were significantly better for dry-cleaned restrooms than for wet-cleaned restrooms. These results suggest that the introduction of dry cleaning is one of the countermeasures that could improve "odor satisfaction" and thereby increase the percentage of customers who think they would "like to use the restroom again" in the station.

Although new knowledge has been obtained from the user evaluations of the cleaning quality of the station restrooms targeted in this study, it is necessary to conduct a similar survey of more station restrooms and to accumulate data in order to obtain more general conclusions in the future. On top of that, by scrutinizing and optimizing the items of cleaning quality evaluation, we aim to develop a maintenance and management method that can provide comfortable station restrooms that customers think they would like to use again.

This article is a reprint of the Journal of Environmental Engineering, Architectural Institute of Japan (Vol. 88, No. 807, pp. 421-428, May 2023 [17]) with some additions and corrections.

References

[1] Kawasaki, T., Kyotani, T., Ushiogi. T., Fujinami. K. and Hayakawa, T., "Assessment of the Effects of Airborne Microorganisms on Indoor Air Quality of Railway Stations," *RTRI Report*, Vol. 22, No. 5, pp. 35-40, 2008 (in Japanese).

[2] Suzuki. H., Fujinami. K., Saito. A., Kawasaki, T., Izumi, Y. and Iino. N., "Passengers' Hygienic Assessment of the Railway Station Environment," *RTRI Report*, Vol. 19, No. 1, pp. 15-20, 2005 (in Japanese).

[3] Kozaki, M., Koga, T. and Hirate, K., "Research on Impressive Evaluation and Environment of Toilet," *Summary of Technical Papers of Annual Meeting, Environmental Engineering I, Architectural Institute of Japan*, pp.13-14, 2015 (in Japanese).

[4] Takahashi, A., Yasui, M., Ikeda, Y., Aoyama, H. and Yamaguchi, Y., "Study on Offensive Odor Control of Restroom at Railway Stations Part1: Result of Field Survey 1," *Summary of Technical Papers of Annual Meeting, Environmental Engineering I, Architectural Institute of Japan*, pp. 671-672, 2018 (in Japanese).

[5] Aoyama, H., Yasui, M., Takahashi, A., Yamaguchi, Y. and Ikeda, Y., "Study on Offensive Odor Control of Restroom at Railway Stations Part1: Result of Field Survey 2," *Summary of Technical Papers of Annual Meeting, Environmental Engineering I, Architectural Institute of Japan*, pp. 673-674, 2018 (in Japanese).

[6] Kawasaki, T., Kyotani, T., Ushiogi. T., Hayakawa. T., Kameda, A. and Sakamoto, K., "Research on Countermeasures to Reduce Unpleasant Odors in Toilets of Railway Stations (Part 2): Relationship between Concentrations of Bacteria and Ammonia on the Floor Tiles of Railway Station," *Annual Meeting of the Society of Indoor Environment*, pp. 60-61, 2012 (in Japanese).

[7] Ikeda, Y., et al., "Study on cleaning method of dry process at railway station Part 1: Outline and result of laboratory survey," *Summary of Technical Papers of Annual Meeting, Environmental Engineering I*, *Architectural Institute of Japan,* pp. 591-592, 2015 (in Japanese).

[8] Ikebe, T., et al., "Study on cleaning method of dry process at railway station Part 2: Result of field survey," *Summary of Technical Papers of Annual Meeting, Environmental Engineering I*, *Architectural Institute of Japan,* pp. 593-594, 2015 (in Japanese).

[9] Kawasaki, T., Kyotani, T., Ushiogi, T. and Yoshie, S., "Quantitative and Qualitative Research of Surface Bacteria on the Floor of Station Restrooms with Two Types of Cleaning Methods," *RTRI Report*, Vol. 35, No. 2, pp. 35-40, 2021 (in Japanese).

[10] Kawasaki, T., Yoshie, S., Kyotani, T. and Ushiogi, T., "Comparison of Microbiomes on Floors of Men's Restrooms, before and after Cleaning with Different Cleaning Methods at Two Railway Stations," *Japan Architectural Review*, Vol. 5, No. 4, pp. 633-643, 2022.
(DOI: https://doi.org/10.1002/2475-8876.12285)

[11] Masada, K. and Kakitsuba, N., "A Study of Standardizing the Inspection Sheets for Evaluation of Quality of Building Maintenance," *AIJ Journal of Technology and Design*, Vol. 23, No. 54, pp. 607-611, 2017 (in Japanese).
(DOI: https://doi.org/10.3130/aijt.23.607)

[12] Sugita, H., Sato, T., Murakawa, S., Hiraga, M. and Oishi, H., "A Study on the Evaluation for the Quality of Cleaning in the Government Office Building," *Journal of Architectural Planning (Transaction of AIJ)*, Vol. 71, No. 600, pp. 153-159, 2006 (in Japanese).
(DOI: https://doi.org/10.3130/aija.71.153_1)

[13] Tokyo Building Maintenance Association, Building Sanitation Management Committee, "Building Cleaning Quality Evaluation and Specifications – Introduction to Inspection (3rd Edition)," 2017 (in Japanese).

[14] Ishimura, Y., Kato, C. and Ryu, C., "*Questionnaire Processing to Learn Easily with SPSS (5th Edition)*," Tokyo Tosho, 2020 (in Japanese).

[15] Ishimura, S. and Ishimura, K., "*First Multivariate Analysis*," Tokyo Tosho, 2007 (in Japanese).

[16] Ishimura, S. and Ishimura, K., *"Procedure for Multivariate Data Analysis by SPSS (5th Edition)*," Tokyo Tosho, 2016 (in Japanese).

[17] Kyotani, T., Ikeda, Y., Oishi, H. and Kawasaki, T., "Survey on Consciousness of Railway Customers about Cleaning Status at Men's Restrooms in Railway Stations Aimed at Improving Customers' Evaluation," *Journal of Environmental Engineering (Transaction of AIJ)*, Vol. 88, No. 807, pp. 421-428, 2023 (in Japanese).
(DOI: https://doi.org/10.3130/aije.88.421)

Authors

Takashi KYOTANI
Senior Researcher, Comfort Science and Engineering Laboratory, Human Science Division
Research Areas: Analytical Chemistry, Biological Chemistry

Yoshiki IKEDA, Dr.Eng.
Assistant Center Chief, East Japan Railway Company
Omiya Architecture Technology Center
Research Areas: Architectural Environment Psychology

Hiroshi OISHI, Ph.D.
Associate Professor, Department of Architecture, Tohoku Institute of Technology
Research Areas: Architectural Environmental Engineering

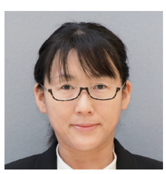

Tamami KAWASAKI, Ph.D.
Senior Researcher, Comfort Science and Engineering Laboratory, Human Science Division
Research Areas: Environmental Biochemistry

Increased Perception of Strain and Related Cognitive Functions in Drivers with Aging

Ryo NAKAMURA **Ayanori SATO** **Takayuki MASUDA**
Safety Psychology Laboratory, Human Science Division

Yasuhiro KITAMURA **Munendo FUJIMICHI**
Safety Psychology Laboratory, Human Science Division

Ayano SAITO
Ergonomics Laboratory, Human Science Division.

With age, physical and cognitive functions generally tend to decline. However, with appropriate measures, it is possible for older train drivers to continue their duties safely and confidently. The first step in this study was to obtain fundamental data to investigate measures needed to enable older drivers to continue driving. Based on a survey result, we identified tasks for which perceived strain increases with age. Furthermore, it was revealed that the increase in perceived strain of these tasks is associated with age-related declines in attention, vison, decision making and reaction time.

Key words*: *aging, crew shortage, older driver, attention, vision

1. Introduction

In Japan, labor shortages due to a declining birth rate and aging population are accelerating. Securing enough train drivers is therefore one of the most important issues for railway operators. One possible solution to this problem is an extension of the retirement age for drivers. To achieve this, it is necessary to identify the tasks for which the strain increases (physical and mental) with age, and to support older drivers. However, there has been no comprehensive study on the effects of aging on driver tasks. Therefore, we first conducted a survey to identify the tasks that drivers find more difficult with age. Next, we conducted a survey to investigate the functional changes with age that affect the increase in perceived strain. Older drivers and young drivers in this study were defined as follows.

Older driver: over 55 years old.
Young driver: more than 3 years of driving experience and under 39 years old.

2. Identification of tasks for which strain is perceived to increase with age

Two surveys were carried out to identify which tasks drivers perceived as more strenuous with age. First, we conducted a survey of perceived driver strain for each task and identified tasks which were perceived as more strenuous by older drivers compared to young drivers. This was followed by interviews to gain deeper understanding of what older drivers considered more strenuous than younger drivers, in the tasks identified during the first survey.

2.1 Questionnaire on perceived strenuousness of driver tasks

Drivers from two railway operators participated in the survey. The number and average age of the participants is shown in Table 1. Participants responded to questions on a 5 - point scale (1: Not difficult at all to 5: Very difficult) on how difficult they perceived each task to be. The tasks to be evaluated were selected with reference to a previous study that organized the train driver's task. The questionnaire surveyed ordinary tasks performed by drivers and excluded tasks which would be carried out in abnormal situations. The questionnaire included 84 tasks for rail operator A and 83 for rail operator B.

Table 1 The number and mean age of the participants in the questionnaire survey

Railway operator	Older driver	Young driver
A	37 $Mean_{age}$ = 61.5 SD = 1.32	56 $Mean_{age}$ = 31.4 SD = 2.93
B	35 $Mean_{age}$ = 61.7 SD = 1.50	35 $Mean_{age}$ = 32.5 SD = 2.82

We conducted a *t*-test to compare the difference between the means of older and younger driver scores. The results showed that the perceived level of strenuousness for 27 out of 84 tasks was statistically higher for older drivers than younger drivers at railway operator A. At railway operator B, the perceived level of strenuousness was statistically higher among older drivers for 34 out of 83 tasks (5% level of significance).

2.2 Follow-up interviews to understand strenuousness of tasks

From the questionnaire, it was found that many tasks were perceived by older drivers to be more strenuous. However, not all the strain can be attributed to aging. Therefore, to identify the tasks where perceived strain may have increased with aging, we conducted semi-structured interviews to understand what exactly was perceived as strenuous in the tasks rated as more strenuous by older drivers, compared to younger drivers. We asked participants about how hard the tasks are, in terms of physical, mental, and other aspects, and added questions depending on participants' answers. The number and mean age of the participants is shown in Table 2

Table 2 The number and mean age of the participants in the interview survey

Railway operator	Older driver	Young driver
A	5 $Mean_{age}$ = 60.2 SD = 0.45	5 $Mean_{age}$ = 29.8 SD = 2.22
B	4 $Mean_{age}$ = 61.5 SD = 1.29	6 $Mean_{age}$ = 30.7 SD = 1.63

2.3 Results of perceived strenuousness of driver tasks

The average rating of perceived strenuousness of each task is shown in Fig. 1. Tasks in red font are those for which the perceived strain increases with age.

Several older drivers answered that the perceived strain of some tasks had increased due to changes in the working environment, rules, and procedures. The increase in the perceived strain of these tasks was not considered to be due to aging. Furthermore, among the tasks where older drivers rated the perceived strain higher than younger drivers, some had an average rating which was low for both age groups. Therefore, tasks which had a mean score of less than 3.0 and which were described by all the drivers in interviews as “not hard” were categorized as tasks with no increase in the perception of strain. On the other hand, even if a task obtained a score of 3 or less, if many older drivers mentioned in interviews that the strain increased with age, it was categorized as a task for which perceived strain increases with aging.

3. Evaluation of age-related functional changes associated with increased perceived strain

This chapter describes an evaluation conducted by experts to estimate the impact of age-related functional changes on increased perceived strain.

3.1 Evaluation items

During the interviews to elucidate specific strain, it became clear that some of the evaluation items (train driver’s tasks) in the questionnaire survey were not appropriate for expert evaluation. For such items, we revised them. The final set of evaluation items is shown in Table 3.

3.2 Expert evaluation

The functions to be evaluated (Table 4) were selected on the basis of previous studies on age-related changes in various functions [1-5], the opinions of managers who supervise drivers, the responses of older drivers from the interviews, and the tests conducted for older drivers when they renew their car driving licenses in Japan.

A total of 22 experts with sufficient knowledge of train driver tasks participated in expert evaluations from railway operators A and B (A: 10, $Mean_{age}$ = 37.5, SD = 5.42; B: 12, $Mean_{age}$ = 42.8, SD = 4.75). They evaluated the degree to which each function (Table 4) was related to each task (Table 3) on a 5 - point scale (1: not related at all ~ 5: highly related).

3.3 Results of expert evaluation

The results are shown in Table 5. Yellow cells in the table indicate an average rating of 3.5 or higher, and red cells indicate 4.0 or higher. These results indicate that the functions corresponding to vision, judgment, attention, and reaction time are particularly related to the tasks for which the perceived strain increases with age.

Vision was particularly relevant to tasks that falls into the categories of “Signal check,” “Check timetable and instrument panel.” It was also relevant for “Check signal and platform when entering a non-stop station,” “Check one-man mirror at departure” and “High-speed driving.” These tasks are confirmation procedures using eyes and are susceptible to the decline in vison with aging [3].

The judgment was particularly relevant to “Check signal while high-speed driving,” “Check signal during dark hours,” “Check signal and platform when entering a non-stop station,” “Check departure signal when departing,” “Check the mirrors on the platform when departing,” “High-speed driving” and “Operation under delay.” In the interview survey, many participants answered that they are particularly careful and feel a high strain in these tasks, since a misjudgment in these tasks can lead to a serious accident. Many older drivers who are aware of the decline in their judgment ability considered to feel more strain.

The attention was particularly relevant to the tasks that falls into the categories of “Signal check.” It was also relevant to “Check signal and platform when entering a non-stop station,” “Check platform and open/close the door,” “Check departure signal when departing,” “Check one-man mirror at departure,” “High-speed driving,” “Operation under delay” and “Pointing check throughout entire job.” The attention is one of the functions that is strongly affected by aging [4, 5]. These tasks, which involve checking multiple objects simultaneously or frequently performing a series of checking actions, are severely affected by aging.

Reaction time was particularly relevant to tasks in the “Signal check” category. It was also relevant to “Check signal and platform when entering a non-stop station,” “Check one-man mirror at departure” and “High-speed driving.” Reaction time increases with age. It is particularly important to react quickly when an anomaly is detected when checking a signal or checking a platform or when driving at high-speed. Older drivers, who are aware of a delay in their reaction time, are likely to find these tasks more stressful.

4. Conclusions

From the train driver surveys, we identified tasks for which perceived strain increases with age. We also confirmed that age-related changes in vision, decision-making, attention, and reaction time were responsible for the increased perception of strain. Even if some functions decline with age, taking measures such as being aware of these declines and checking more carefully than when you are younger could allow older drivers to continue to drive safely.

In the medical field, it has been confirmed that cognitive training for older people has been shown to improve attention and other functions [6, 7]. If cognitive training for train drivers can be developed, it may be possible to reduce the strain on older drivers. In the future, we aim to develop specific support measures based on the age-related driver stress or burden and related functions identified in this study.

Fig. 1　The driver's tasks for which the perceived strain increases with age

Table 3 Evaluation Items

No.	Work category	Evaluation items to be checked
1	Inspection before departure from depot	Walk to the train with their luggage
2		Check train number from the ground
3	Signal check	Check signal (general)
4		Check signal while high-speed driving
5		Check signal during dark hours
6		Pointing and calling out to the signals in mainline operation
7		Pointing and calling out to the objects other than signal in mainline operation
8	Check timetable and instrument panel	Check timetable
9		Check watch
10		Check instrument panel
11		Check speed limits for entering and exiting switches listed in timetable
12	Confirmation of course of operation	Check signal and platform when entering a non-stop station
13	Handling of arrival and departure (one-man)	Braking after stopping (prevention of rolling)
14		Check platform and opening/closing doors
15		Check departure signal before departure
16		Check departure time
17		Handle ATS chime (ringing noise and the procedure for turning off)
18		Check departure signal when departing
19		Check speed limit at departure
20		Check the mirrors on the platform when departing
21		Pressing public announcement button after departure and before arrival
22	Others	High-speed driving
23		Operation when there are delays
24		Tablet implementation (e.g., new devices)
25		Pointing check while working
26		Calling check while working

Table 4 Functions targeted by functional assessment in relation to increased strain

Function		Explanation of each function.
Vision	Dynamic visual acuity	Vision to see moving objects
	Night vision	Vision to see things in the dark
	Accommodation	Ability to focus on an object
	Color discrimination	Distinguishing between colors
	Field of view	Range of vision that can be seen without the movement of eyes or head
	Glare vision	Ability to see clearly in bright or glaring light
	Dark adaptation	Time it takes to become visible when suddenly moving from a bright place to a dark place
Hearing	Recruitment Hearing	A phenomenon in which soft sounds are hard to hear and loud sounds are loud.
	Discrimination of sound	Distinguish necessary sounds in the presence of multiple sounds and noises
Decision-making		Make appropriate decisions based on the situation.
Memory	Working memory	Temporarily store and process information required for a task or operation.
	Knowledge	Knowledge obtained through training, experience, etc.
	Learning ability	Ability to learn new things
Attention	Divided attention	Divide attention to multiple targets simultaneously
	Switch attention	Shift attention from one to another in succession
	Inhibition	Suppress attention to irrelevant things when there is something to focus on
Reaction time		Time between noticing things and reacting to them
Speediness		Perform a series of movements quickly

Table 5　Expert evaluation results

No.		1		2		3		4		5		6		7	
Work category		Inspection before departure from depot				Signal check									
Evaluation items / Function		Walk to the train with their luggage		Check train number from the ground		Check signal (general)		Check signal while high-speed driving		Check signal during dark hours		Pointing and calling out to the signals in mainline operation		Pointing and calling out to the objects other than signal in mainline operation	
		Results of evaluation													
		Ave.	SD	Ave	SD	Ave	SD	Ave	SD	Ave	SD	Ave	SD	Ave	SD
Vision	Dynamic visual acuity	1.68	0.95	1.55	0.86	4.14	1.25	4.82	0.50	4.55	0.86	3.82	1.44	3.36	1.47
	Night vision	1.91	1.19	2.36	1.36	3.23	1.63	3.50	1.71	4.68	0.72	3.00	1.63	2.77	1.48
	Accommodation	1.55	0.86	2.64	1.22	4.27	1.16	4.55	0.74	4.32	1.17	3.73	1.24	3.59	1.33
	Color discrimination	1.50	0.80	2.05	1.05	4.09	1.19	4.41	0.85	3.91	1.34	3.73	1.32	2.86	1.39
	Field of view	2.55	1.18	2.36	1.29	3.91	0.97	4.50	0.67	4.14	1.17	3.73	1.24	3.45	1.10
	Glare vision	1.68	1.04	2.23	1.31	3.82	1.40	4.18	1.18	2.95	1.46	3.59	1.33	3.27	1.20
	Dark adaptation	1.55	0.86	1.82	1.14	3.86	1.21	3.91	1.19	3.50	1.44	3.32	1.29	3.14	1.28
Hearing	Recruitment Hearing	1.73	0.88	1.59	1.05	2.05	1.13	2.00	1.15	1.77	1.02	2.05	1.09	2.27	1.12
	Discrimination of sound	1.91	1.15	1.45	0.96	1.95	1.40	1.86	1.36	1.73	1.20	2.05	1.25	2.32	1.25
Decision-making		1.82	0.80	1.86	1.17	3.73	1.28	4.36	0.85	4.32	1.21	3.95	1.36	3.59	1.26
Memory	Working memory	2.00	1.27	2.32	1.17	3.32	1.17	3.45	1.22	3.23	1.34	3.41	1.37	3.36	1.14
	Knowledge	1.55	0.74	1.95	1.29	3.36	1.26	3.32	1.36	3.18	1.40	3.18	1.40	3.36	1.29
	Learning ability	1.41	0.80	1.95	1.21	2.82	1.50	2.82	1.33	2.64	1.40	2.64	1.40	2.82	1.26
Attention	Divided attention	2.41	1.10	2.05	1.13	3.82	1.14	4.32	1.04	4.09	1.23	3.91	1.02	3.82	1.10
	Switch attention	2.05	1.09	1.64	1.05	4.18	0.91	4.50	0.60	4.32	0.95	4.09	0.92	3.77	1.15
	Inhibition	2.09	0.92	1.95	1.13	4.18	1.05	3.91	1.27	3.91	1.34	3.95	1.00	3.77	1.11
Reaction time		2.27	1.24	1.55	0.80	4.27	0.94	4.64	0.49	4.36	1.09	4.32	0.78	4.05	1.00
Speediness		2.36	1.26	1.73	1.24	3.50	1.14	4.14	1.13	3.77	1.45	3.91	1.06	3.68	1.17

No.		8		9		10		11		12	
Work category		Check timetable and instrument panel								Confirmation of course of operation	
Evaluation items / Function		Check timetable		Check watch		Check instrument panel		Check speed limits for entering and exiting switches listed in timetable		Check signal and platform when entering a non-stop station	
		Results of evaluation									
		Ave	SD	Ave	SD	Ave	SD	Ave	SD	Ave	SD
Vsion	Dynamic visual acuity	2.55	1.37	2.86	1.42	2.91	1.11	2.77	1.34	4.59	0.80
	Night vision	3.55	1.22	3.59	1.30	3.41	1.22	3.55	1.34	3.64	1.36
	Accommodation	4.27	0.98	4.23	0.97	3.77	1.11	4.05	1.29	4.14	1.04
	Color discrimination	3.05	1.09	2.05	1.13	3.23	1.19	2.36	1.09	3.64	1.36
	Field of view	3.55	1.10	3.00	1.07	3.45	1.01	3.05	1.05	4.36	0.95
	Glare vision	3.18	1.18	3.09	1.27	2.95	1.05	3.09	1.27	3.91	1.38
	Dark adaptation	3.32	1.29	3.32	1.39	3.05	1.13	3.05	1.21	3.82	1.18
Hearing	Recruitment Hearing	1.41	0.73	1.32	0.72	1.95	1.17	1.36	0.66	2.18	1.10
	Discrimination of sound	1.32	0.65	1.23	0.53	1.95	1.24	1.36	0.66	2.32	1.25
Decision-making		3.32	1.25	2.91	1.34	3.90	0.89	3.36	1.05	4.27	0.98
Memory	Working memory	3.45	1.18	2.91	1.23	2.86	1.28	3.10	1.48	3.27	1.35
	Knowledge	2.82	1.30	2.14	1.04	3.32	1.25	2.82	1.37	3.18	1.26
	Learning ability	2.36	1.09	1.91	0.97	2.95	1.09	2.36	1.14	2.50	1.06
Attention	Divided attention	3.45	1.37	3.36	1.29	3.36	0.85	3.68	0.99	3.95	1.09
	Switch attention	3.36	1.26	3.09	1.23	3.36	0.95	3.73	0.98	4.27	0.77
	Inhibition	3.41	1.33	3.18	1.22	3.27	1.20	3.68	0.89	4.00	0.93
Reaction time		3.09	1.27	3.32	1.32	3.23	1.02	3.23	1.15	4.27	0.83
Speediness		2.77	1.34	2.95	1.46	2.95	1.21	2.82	1.37	3.77	1.31

No.		13		14		15		16		17		18		19		20		21	
Work category		Handling of arrivals and departures (one man)																	
Evaluation items / Function		Braking after stopping (prevention of rolling)		Check platform and open/close the door		Check departure signal before departure		Check departure time		Handle ATS chime (ringing noise and the procedure to turning off)		Check departure signal when departing		Check speed limit at departure		Check one-man mirror at the departure		Press public announcing button after departure and before arrival	
		Results of evaluation																	
		Ave	SD	Ave	SD	Ave	SD	Ave	SD	Ave	SD	Ave	SD	Ave	SD	Ave	SD	Ave	SD
Vision	Dynamic visual acuity	1.64	0.79	3.09	1.60	2.00	1.38	1.95	1.46	1.91	1.11	2.95	1.59	2.55	1.47	4.05	1.17	1.82	1.10
	Night vision	1.77	0.97	2.68	1.39	2.41	1.33	2.73	1.39	1.77	1.07	2.95	1.46	2.95	1.40	3.59	1.33	1.77	1.07
	Accommodation	1.91	0.87	3.36	1.62	3.68	1.36	3.59	1.50	2.18	1.26	3.77	1.27	3.68	1.32	4.09	1.06	1.86	1.04
	Color discrimination	1.73	0.98	2.41	1.50	3.59	1.33	2.27	1.49	2.32	1.52	3.68	1.29	1.91	1.06	2.91	1.51	1.77	1.07
	Field of view	2.32	1.21	3.82	1.22	3.27	1.16	2.73	1.45	2.50	1.26	3.59	1.10	2.91	1.11	4.09	1.02	2.18	1.18
	Glare vision	1.73	0.77	3.23	1.38	3.14	1.58	2.82	1.50	2.14	1.21	3.36	1.47	2.95	1.46	3.73	1.42	1.55	0.96
	Dark adaptation	1.77	0.87	2.50	1.41	2.55	1.47	2.32	1.36	1.86	1.13	3.05	1.59	2.86	1.46	3.18	1.50	1.64	1.00
Hearing	Recruitment Hearing	1.73	0.98	1.95	1.21	1.45	0.91	1.36	0.58	4.14	1.17	1.45	0.67	1.18	0.39	1.64	0.95	1.77	0.92
	Discrimination of sound	2.00	1.38	2.09	1.27	1.32	0.57	1.23	0.43	3.73	1.32	1.45	0.80	1.18	0.39	1.73	1.03	2.18	1.33
Decision-making		3.27	1.20	4.00	1.11	3.55	1.10	2.95	1.25	3.68	1.25	4.09	1.02	3.59	1.01	4.18	0.96	2.55	1.18
Memory	Working memory	2.64	1.40	3.05	1.33	3.32	1.39	2.91	1.48	3.18	1.47	3.14	1.42	3.18	1.26	3.45	1.50	3.14	1.39
	Knowledge	2.73	1.24	3.18	1.37	3.32	1.36	2.41	1.26	3.68	1.32	3.27	1.39	3.27	1.16	3.10	1.30	2.50	1.47
	Learning ability	1.95	0.95	2.09	1.02	2.41	1.33	1.64	0.85	2.55	1.34	2.50	1.26	2.18	1.01	2.14	1.17	1.73	1.08
Attention	Divided attention	3.14	1.42	4.00	0.76	3.64	1.36	3.18	1.26	3.64	1.36	4.00	1.27	3.86	1.08	4.45	0.74	3.05	1.29
	Switch attention	3.05	1.36	4.09	0.75	3.55	1.37	3.32	1.29	3.77	1.31	3.95	1.29	3.95	1.00	4.36	1.00	3.09	1.19
	Inhibition	3.41	1.26	4.27	0.88	3.95	1.25	3.32	1.39	3.86	1.21	4.23	0.92	3.95	1.09	4.45	0.86	2.91	1.27
Reaction time		2.77	1.45	3.91	0.97	2.73	1.16	2.32	1.13	3.50	1.34	3.68	1.25	3.14	1.28	4.18	0.91	2.45	1.57
Speediness		2.91	1.31	3.50	1.34	2.50	1.22	2.27	1.20	3.50	1.34	3.14	1.31	2.82	1.26	3.41	1.33	2.45	1.47

No.		22		23		24		25		26	
Work category		Others									
Evaluation items / Function		High-speed driving		Operation under delay		Tablet implementation (e.g., new devices)		Pointing check throughout entire job		Calling check throughout entire job	
		Results of evaluation									
		Ave	SD	Ave	SD	Ave	SD	Ave	SD	Ave	SD
Vision	Dynamic visual acuity	4.77	0.43	3.55	1.44	2.36	1.40	3.64	1.18	3.32	1.52
	Night vision	3.73	1.42	3.00	1.54	2.73	1.55	3.73	1.24	3.05	1.40
	Accommodation	4.45	0.91	3.41	1.59	3.45	1.50	3.73	0.98	3.23	1.41
	Color discrimination	4.05	1.36	3.41	1.50	3.18	1.65	3.45	1.14	3.00	1.31
	Field of view	4.55	0.74	3.55	1.50	3.09	1.15	3.50	1.01	2.90	1.30
	Glare vision	3.95	1.33	3.18	1.62	2.82	1.47	3.68	0.95	2.82	1.40
	Dark adaptation	3.82	1.37	3.05	1.59	2.95	1.46	3.45	1.01	2.82	1.44
Hearing	Recruitment Hearing	2.59	1.40	2.59	1.53	2.50	1.47	2.64	1.09	2.91	1.15
	Discrimination of sound	2.82	1.47	2.76	1.67	2.90	1.48	2.68	1.13	3.09	1.11
Decision-making		4.41	0.80	4.05	1.25	3.36	1.43	3.73	1.24	3.23	1.38
Memory	Working memory	3.59	1.26	3.82	1.37	3.68	1.29	3.32	1.13	3.00	1.27
	Knowledge	3.32	1.36	3.50	1.44	4.14	1.13	3.18	1.22	3.18	1.05
	Learning ability	2.59	1.44	2.82	1.40	4.68	0.57	3.18	1.30	3.05	1.25
Attention	Divided attention	4.45	0.80	4.18	1.18	3.09	1.48	3.86	0.89	3.55	1.14
	Switch attention	4.41	0.80	4.09	1.19	2.95	1.46	4.09	0.87	3.64	1.18
	Inhibition	4.14	0.89	3.95	1.33	2.95	1.40	3.71	1.19	3.45	1.34
Reaction time		4.73	0.55	3.64	1.33	3.00	1.41	3.73	1.03	3.55	1.22
Speediness		4.32	1.09	3.45	1.50	2.95	1.53	3.55	1.06	3.55	1.30

References

[1] Baddeley, A. D., *Working memory*, New York, Oxford University Press, 1986.
[2] Schaie, K. W., "The course of adult intellectual development," *American Psychologist,* 49, pp. 304-313, 1994.
[3] Park, D. C., Lautenschlager, G., Hedden, T., Davidson, N. S., Smith, A. D., & Smith, P. K., "Models of visuospatial and verbal memory across the adult life span," Psychology and Aging, 17, 2, pp. 299-320, 2002.
[4] Rogers, W., "Attention and aging," *Cognitive aging: A primer*, New York, Psychology Press, pp. 57-73, 2000.
[5] Zacks, R., & Hasher, L., "Cognitive gerontology and attentional inhibition: A reply to Burke and McDowd," *Journal of Gerontology, Series B, Psychological Science and Social Science*, 52 (6), pp. 274-283, 1997.
[6] Karlene, B., Daniel, B. B., Karin, F. H., Jared, B. J., Mary, D. L., Michael, M., John, N. M., George, W. R., David, M. S., Sharon, L. T., Frederick, W. U., & Sherry, L. W., "Effects of cognitive training intervention with older adults: A randomized control trial," *The Journal of American Medical Association*, 288, 18, pp. 2271-2281, 2002.
[7] Nouchi, R., Taki, Y., Takeuchi, H., Nozawa, T., Sekiguchi, A., Kawashima, R., "Reading Aloud and Solving Simple Arithmetic Calculation Intervention (Learning Therapy) Improves Inhibition, Verbal Episodic Memory, Focus Attention and Processing Speed in Healthy Older Frontiers in Human," *Neuroscience*, 2016.

Authors

Ryo NAKAMURA, Ph.D.
Senior Researcher, Safety Psychology Laboratory, Human Science Division
Research Areas: Cognitive Psychology, Brain Science, Aging

Yasuhiro KITAMURA.
Technical Manager, Senior Researcher, Safety Psychology Laboratory, Human Science Division
Research Areas: Psychology, Human Error, Decision Making

Ayanori SATO, Doctor of Psychology
Senior Researcher, Safety Psychology Laboratory, Human Science Division
Research Areas: Cognitive Psychology, Memory, Human Error

Munendo FUJIMICHI, Ph.D.
Researcher, Safety Psychology Laboratory, Human Science Division
Research Areas: Cognitive Psychology, Evacuation Behavior

Takayuki MASUDA, Ph.D.
Senior Researcher, Safety Psychology Laboratory, Human Science Division
Research Areas: Traffic Psychology

Ayano SAITO, Ph.D.
Senior Chief Researcher, Head of Ergonomic Laboratory, Human Science Division
Research Areas: Ergonomics

Proposal for Excitation Acceleration in Vibration Endurance Testing of Signalling Equipment

Yoshikazu OSHIMI **Shunsuke SHIOMI**
Signalling systems Laboratory, Signalling and Operation Technology Division

Tsuyoshi KAMIYA **Ryuto ISSHIKI**
Signalling systems Laboratory, Signalling and Operation Technology Division (Former)

Signalling equipment is installed in positions where it is exposed to vibrations from passing trains transmitted via rails, sleepers, and roadbeds. The design of signalling equipment must therefore take this into account to prevent vibration-related damage. In recent years, the installation environment of signalling equipment has evolved due to faster train running speeds and changes in tracks and structures. However, the details of vibration propagation to signalling equipment have not been investigated so far. In addition to current issues, this paper reports on guidelines for vibration acceleration amplitude in vibration endurance testing.

Key words*: *signalling equipment, vibrations, acceleration, vibration endurance test, acceleration measurement

1. Introduction

Signalling equipment on railways is installed in positions where it is exposed to vibrations from passing trains transmitted via rails, sleepers, and roadbeds. It is therefore necessary to design signalling equipment taking this into account to avoid damage due to vibration. The Japanese Industrial Standard JIS E 3014 (hereinafter referred to as JIS E 3014) for vibration testing of signalling equipment specifies a number of tests to be performed for each installation location of the equipment, as well as the test conditions such as vibration direction, test time, vibration frequency and amplitude. However, since its establishment in 1976, there have been no major revisions to these tests and test conditions of this standard [1, 2, 3].

On the other hand, the installation environment of signalling equipment has changed in recent years due to faster train running speeds and changes in tracks and structures. However, the details of vibration propagation to signalling equipment have not been investigated so far.

In order to indicate vibration endurance test conditions based on the current usage environment of signalling equipment, we investigated the vibration acceleration to which signalling equipment is exposed to better understand the actual situation. This report clarifies the vibration acceleration exerted on signalling equipment in current general usage environment, presents the data required for considering the future revision of JIS E 3014, and shows the vibration acceleration amplitude for a sinusoidal vibration test in a vibration endurance test. To compare the domestic and overseas usage environments, we also compared the frequency characteristics of the domestic signalling equipment usage environment obtained this time with the international standard International Electrotechnical Commission IEC 62498-3 (hereinafter referred to as IEC), which specifies the frequency characteristics of vibration acceleration along European railway lines.

2. Vibration endurance test standards for signalling equipment and present issues

2.1 History of establishment and revision of vibration endurance test standards for signalling equipment

JIS E 3014 was established in December 1976 after deliberation by a drafting committee established in 1972 by the Signal Association of Japan [1]. Subsequently, in 1992, the system was changed to the SI unit system and the format of the standard sheet was revised [2]. In 1999, in response to an issue where signalling equipment made of resin such as ATP Balise would heat up due to friction during vibration endurance tests, the standard was revised to allow for measures such as interrupting the test if a rise in temperature occurred during the test [3]. The standard has been revised twice since its establishment, but the test methods and test conditions remain the same as when it was first established.

2.2 Previous vibration environment surveys and their issues

Table 1 shows the conditions under which vibration acceleration measurements were carried out when JIS E 3014 was established. These measurements were mainly carried out on the earth structure sections of the Shinkansen and Meter-gauged railway lines, and measurements on the viaduct sections were carried out at one location each on the Shinkansen and Meter-gauged railway lines. The measured maximum speed of the Shinkansen was 188 km/h on the earth structure section and 205 km/h on the viaduct section, the maximum speed of the Meter-gauged railway line was 112 km/h on the earth structure section and 47.5 km/h on the viaduct section. Since the standard was established, the environment in which signalling equipment is used is expected to have changed due to factors such as increased train speeds and the introduction of new track and structure construction methods. However, there is an issue in that the current JIS E 3014 test conditions do not reflect changes in the vibrations transmitted to the equipment and their effects. To address this issue, we considered it was necessary to conduct a survey to understand the actual conditions of the current operating environments of signalling equipment, and therefore carried out measurements of vibration acceleration in various operating environments.

Table 1 Measurement conditions in past vibration environment surveys

	Rail	Structure type		Maximum speed (km/h)
		Earth structure	Viaduct	
Shinkansen	50T	○	—	188
	50T	—	○	205
Meter-gauged railway line	50N	○	—	112
	50N	○	—	75
	50N	○	—	70
	50N	○	—	65
	40N	○	—	66
	40N	○	—	43
	40N	○	—	20
	37	○	—	65
	37	○	—	54
	37	○	—	47
	37	○	—	20
	50N	—	○	47.5

3. On-site vibration survey of signalling equipment

3.1 Selection of locations for vibration acceleration survey

On current Shinkansen and Meter-gauged railway lines, in addition to sections of ballasted track laid on earth structures and viaducts where vibration environment surveys have been conducted in the past, there are also sections that use track structures such as slab track and ballastless track. In addition, the maximum operating speed has increased to 320 km/h on the Shinkansen and to 130 to 160 km/h on some Meter-gauged railway lines. The purpose of the survey was to grasp the current state of the vibration environment, and vibration acceleration was measured at locations where signal equipment was installed [4, 5]. The survey locations were selected as areas with severe operating conditions, such as sections of the Shinkansen where trains run at high-speed and sections of Meter-gauged railway lines where freight trains and limited express trains run, and surveys were conducted at locations with different types of structures in these sections.

3.2 Measurement items and methods for on-site vibration survey

At each survey location, measurements were required at the bottom of the rail and on the sleepers, and if an instrument box was installed in the vicinity, measurements were taken at three points, including the instrument box. For the measurements, a piezoelectric acceleration sensor (RION Co., Ltd. PV-93) and a charge amplifier (RION Co., Ltd. UV-15, UV-16) were used, and an axle detector (proximity sensor: Copto Co., Ltd. R004-MKII) was installed as a trigger to start the measurements. The acceleration sensors were attached to the bottom of the rail using a mounting jig that matched the taper of the bottom of the rail and fixed with adhesive, while for the sleepers and instrument boxes, a rectangular mounting jig was used and the sensors were fixed to the target objects with adhesive and an insulating acrylic plate between them. Hereinafter, the measurement directions of the three-axis acceleration are defined as the longitudinal direction of the rail as front-to-back, the vertical direction as up-down, and the sleeper direction as left-to-right. The sampling frequency in this measurement was 10 kHz.

3.3 Measurement data processing

The measured vibration acceleration results are recorded as a waveform of the vibration acceleration over time. This waveform was processed as follows.

① Removal of high frequency components using a low-pass filter

② Calculation of peak-to-peak value

Mechanical damage to signalling equipment caused by vibrations due to running trains is thought to be caused by fatigue failure due to resonance of component parts. It is known that the resonant frequency is 1 kHz or less due to the weight and elastic properties of the components. Therefore, the upper limit of resonant frequency exploration in JIS E 3014 is 1 kHz. In addition, in the data processing that has been carried out after vibration acceleration measurement, the signals above 1 kHz are processed to be attenuated. Similarly, in this survey, high-frequency components were removed from the vibration acceleration obtained in each measurement using a low-pass filter (Chebyshev type II, 10th order, stopband attenuation 80 dB) with a cutoff frequency of 1 kHz constructed on a numerical calculation software. Furthermore, the index used to indicate the magnitude of vibration acceleration is not the maximum or minimum values, but rather the difference between the peaks and valleys of a local wave in the acceleration waveform that changes over time (peak-to-peak value, hereafter referred to as the p-p value, Fig. 1). In these measurements, the maximum p-p value for each train (hereafter referred to as the maximum p-p value) was calculated for the waveforms after low-pass filtering, and the data was then organized.

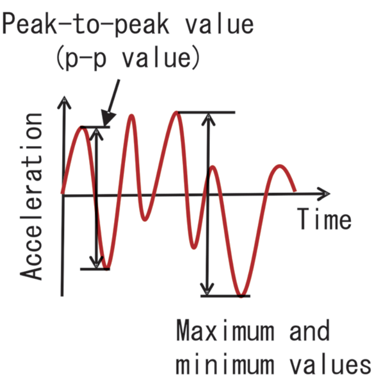

Fig. 1 Peak-to-peak value (p-p value)

4. Overall trends of on-site measurement results

4.1 Measurement location

Vibration acceleration was measured when trains passed at a total of 44 locations on both Shinkansen and Meter-gauged railway lines. The breakdown by structure type, track type, etc. is shown in Table 2.

4.2 Trends in vibration acceleration along railway lines

4.2.1 Acceleration waveform when a train passes

As an example of the results of measuring the acceleration of the rail, sleepers, and instrument boxes when a train passes, Fig. 2 shows the waveform of acceleration in the up-down direction of the rail when a train passes. The acceleration fluctuated greatly when a train passed, and the p-p value generally showed a large value at the moment the wheelsets passed. Following the approach used when formulating the test conditions for the excitation acceleration amplitude for vibration endurance tests in JIS E 3014, it was decided to determine the test conditions for the excitation acceleration amplitude suitable for the current usage environment, based on the p-p values when trains pass at each measurement location.

When some of the wheelsets passed over the installations, significant vibration acceleration was observed in the rails, exceeding the JIS E 3014 test conditions (Type 4C) of 981 m/s^2. Such significant acceleration fluctuations observed on specific wheelsets are believed to be the result of wheel shape irregularities such as wheel flats. In this case, when other wheelsets pass by, the same level of vibration acceleration is measured for each wheelset, but when the rail is hit by the wheel flat, the maximum p-p value becomes significantly higher. In this evaluation, which targets vibration endurance testing, it is necessary to use the vibration acceleration value of the steady vibration when a train passes. If the maximum p-p value is used, it would mean that when a train passes, the rail is considered to be constantly subjected to a vibration acceleration equivalent to the impact caused by a wheel flat. This means that an excessive vibration acceleration is adopted compared to the actual usage of the signal equipment. Therefore, it is desirable to exclude this sporadic impact component from the evaluation.

Table 2 Number of vibration acceleration measurement points

	Structure type	Track type	Track geometry	Measurement points
Shinkansen	Earth structure	Ballasted	Turnout	1
	Viaduct	Ballasted	Turnout	1
		Ballastless	Turnout	1
Meter-gauged railway line	Earth structure	Ballasted	Straight	8
			Curve	6
			Turnout	6
	Viaduct	Ballasted	Straight	3
			Curve	1
			Turnout	4
		Ballastless	Straight	2
			Turnout	4
		Slab	Straight	1
			Turnout	4
	Bridge	Ballastless	Straight	2

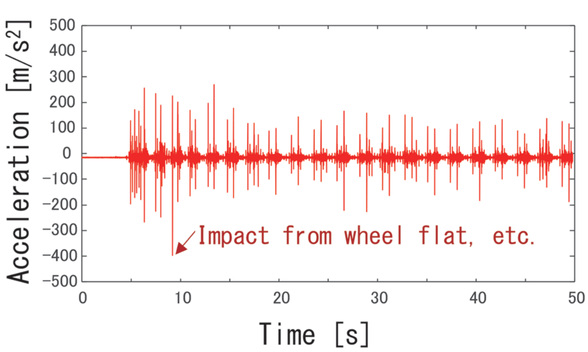

Fig. 2 Vibration acceleration when a train passes (Up-down direction of rail)

4.2.2 Maximum p-p value and wheelset-number average p-p value

To reduce the impact components described above during evaluation, the p-p values were averaged based on the number of wheelsets passing when one trainset passed. The vibration acceleration when a wheelset passes over the installations is measured on the whole as a large p-p value for each passing wheelset. The magnitude of this p-p value varies for each wheelset of a train, as shown in Fig. 3 (a). This is thought to be due to differences in axle loads depending on the vehicle type and number of passengers, the loading conditions of containers and cargo, balance of axle loads, and irreg-

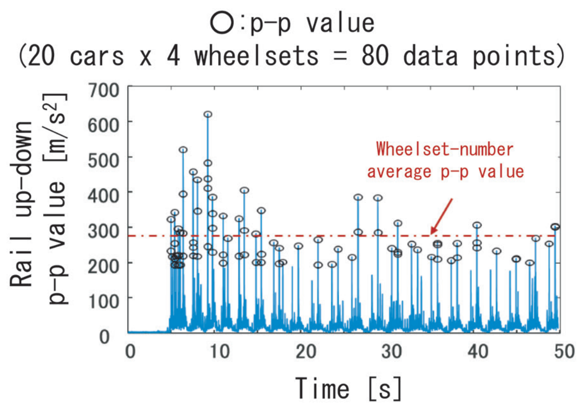

(a) Extracted p-p value and wheelset p-p match

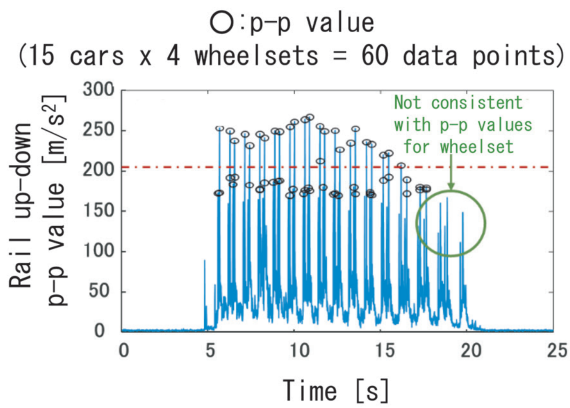

(b) Extracted p-p value and wheelset p-p discrepancy

Fig. 3 Example of the p-p value extracted when calculating the wheelset-number average p-p value ○ : The p-p value used in the calculation

ularities in the shape of wheels such as wheel flats. Assuming that there are no large fluctuations such as impacts caused by wheel flats and that one peak is obtained when one wheelset passes, for a train with N axles, the p-p value for each wheelset can be obtained by extracting the top N p-p values from the measurement data for that single train component. Therefore, the average value obtained by dividing the sum of the top N p-p values by N (hereinafter referred to as the wheelset-number average p-p value) was calculated as an index equivalent to the average p-p value for each wheelset [6].

The maximum p-p value is affected by wheel flats and other factors, and has a large variance. On the other hand, the wheelset-number average p-p value is thought to be able to eliminate to some extent the variation associated with the condition of individual wheelsets (red dot-dash line shown in Fig. 3 (a)). However, Although the variance can be reduced, if there is a large discrepancy between the two values, the wheelset-number averaged p-p value cannot be used to evaluate vibration durability. If there is a large discrepancy between the two values, the wheelset-number average p-p value cannot be used as an evaluation index for vibration durability and the evaluation must be made using the maximum p-p value.

Therefore, the maximum p-p value and the wheelset-number average p-p value were calculated, and the two results were compared. When calculating the wheelset-number average p-p value, the number of data points for the number of wheelsets is extracted from all the p-p values when a train set passes, starting with the largest. Therefore, if several high p-p values are observed on the same wheelset due to a wheel flat or other problem, the extracted p-p value may not necessarily match the p-p value when the wheelset passed (Fig. 3 (b)). However, the calculated wheelset-number average p-p value is greater than the average of the maximum p-p values for all wheelsets (in one train set) when only the sections through which each wheelset has passed are extracted, and therefore is an assessment on the safety side. Moreover, because data processing can be easily automated, in this comparison the wheelset-number average p-p value was calculated using the method described above.

The average value μ and standard deviation σ of the maximum p-p value and the wheelset-number average p-p value of the measurement results were calculated for each speed stage. The calculations showed that the up-down vibration acceleration was the greatest of the three axis directions at each measurement point, so as an example, Fig. 4 shows the maximum p-p value in the up-down direction of the rail and the wheelset-number average p-p value. Each point in the figure is the average value μ for each speed stage, and the tip of the error bar is the value of $\mu + \sigma$. The difference between the average of the wheelset-number average p-p value and the average of the maximum p-p value for each speed stage is generally less than 200 m/s^2 in the up-down direction of the rail. In addition, the standard deviation σ of the wheelset-number average p-p value is smaller than that of the maximum p-p value.

From these results, it was decided that the wheelset-number average p-p value could reduce variance without deviating significantly from the maximum p-p value, and therefore the wheelset-number average p-p value was used in this analysis, which determines the vibration endurance test conditions for steady-state vibration caused by passing trains.

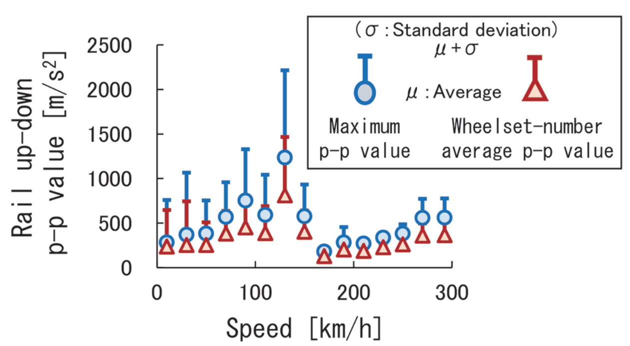

Fig. 4 Average and standard deviation of maximum p-p value and wheelset-number average p-p value by speed stage

4.3 Vibration acceleration distribution for each speed stage of passing trains

This paper describes the distribution of the wheelset-number average p-p values when train speeds are divided into speed steps of 10 km/h, with 5 km/h as the base speed. As an example, Fig. 5 shows the cumulative frequency distribution of wheelset-number average p-p values in the up-down direction of the rail at train speeds of 105 to 115 km/h. Although the distribution of the wheelset-number average p-p value for each speed step differs from a normal distribution, when the mean value μ and standard deviation σ were calculated, the cumulative relative frequency, which indicates the proportion of data falling within the range of $\mu + \sigma$ (wheelset-number average p-p value 0 m/s^2 to 800 m/s^2 in the example in Fig. 5) to the total measurement data, was 0.9. For this reason, we decided to use $\mu + \sigma$ as the value that contains 90% of the measurement data for each speed stage.

5. Analysis of measurement results

The average value μ and standard deviation σ were calculated for each speed stage for the wheelset-number average p-p value of acceleration in each direction at each measurement point obtained from the measurement results. As an example, the results of the rail vibration acceleration are shown in Fig. 6. Each point in the figure indicates the average value μ for each speed stage, and the tip of the error bar indicates the value of $\mu + \sigma$. In addition, since the vibration acceleration in the up-down direction was the largest among the three axial directions at each measurement point, in the following,

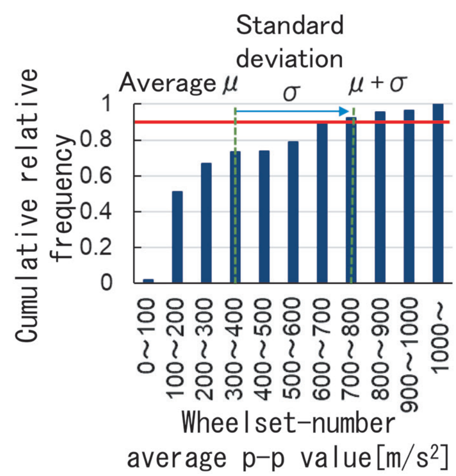

Fig. 5 Frequency of occurrence of up-down vibration acceleration of rail (Speed stage:105～115 km/h)

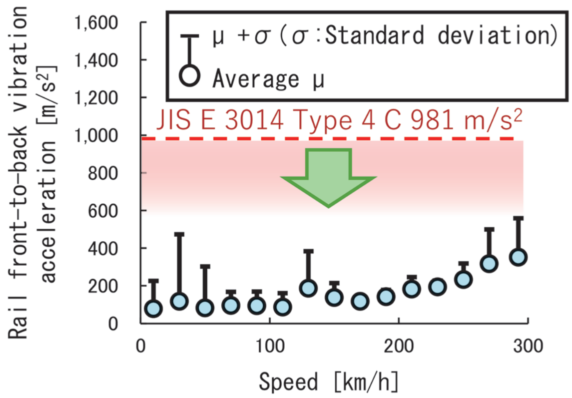

(a) Front-to-back direction of rail

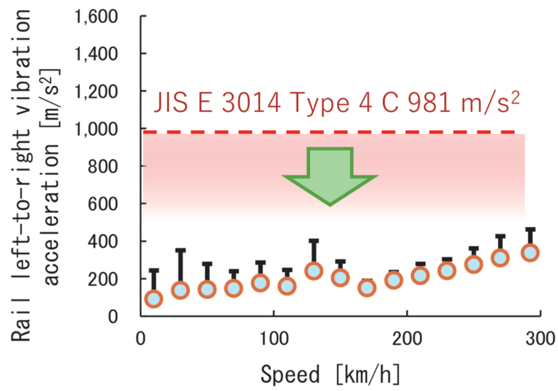

(b) Left-to-right direction of rail

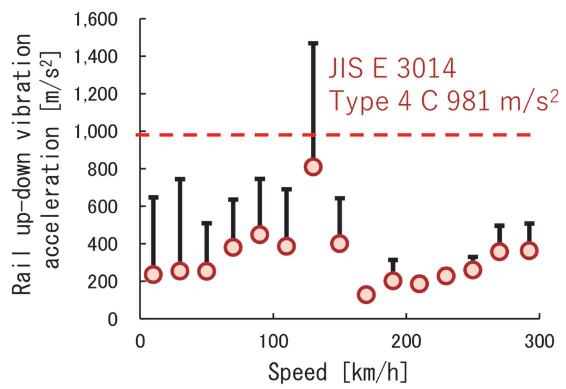

(c) Up-down direction of rail

Fig. 6 Vibration acceleration measurement results

when only one axial direction is shown as an example, the up-down direction will be described.

The magnitude of $\mu+\sigma$ of the wheelset-number average p-p value of the rail was below the current JIS standard of 981 m/s^2 (Type 4 C) in all directions, up-down, left-to-right, and front-to-back, except for some Meter-gauged railway lines (up-down direction at speed stages around 130 km/h). The up-down acceleration of the rail at speeds of around 130 km/h on Meter-gauged railway lines, which exceeded 981 m/s^2, was also significantly increased due to the maintenance conditions at certain measurement points. In the left-to-right and front-to-back directions of the rail, the value of $\mu + \sigma$ is about 500 m/s^2, even at the speed stage of the Shinkansen (around 300 km/h). In addition, the results showed that the wheel-set-number average p-p value generally increased as the train speed increased.

6. Ideal vibration endurance test conditions for signalling equipment

6.1 Ideal vibration acceleration amplitude based on on-site measurement results

In this section, we compare the measurement results with the vibration endurance test conditions of JIS E 3014 and discuss the ideal vibration acceleration amplitude when taking into account the current usage environment. JIS E 3014 specifies that the amplitude of sinusoidal vibration should be the same in all three axial directions for the test specimen, with the vibration being 981 m/s^2 for equipment installed on rails (Type 4C), 147 m/s^2 for equipment installed on sleepers (Type 3C), and 9.81 m/s^2 for equipment installed on instrument boxes (Type 2C). In addition, the excitation frequency must be the resonant frequency of the specimen (100 Hz if there is no resonant point within 1 kHz).

As a guideline for the vibration acceleration to which rails, sleepers, and instrument boxes are exposed under current general operating conditions, the maximum values of $\mu + \sigma$ were compared with the excitation acceleration amplitude specified in JIS E 3014. As a result, as shown in Fig. 6, in the case of rails, the maximum value of $\mu + \sigma$ for the JIS-specified vibration amplitude of 981 m/s^2 was approximately 550 m/s^2 in the front-to-back direction and 450 m/s^2 in the left-to-right direction. Furthermore, considering that the vibration acceleration experienced in an actual installed state contains a variety of frequency components and is not excited only at the resonant frequency, in the case of sinusoidal vibration tests simulating the actual usage environment, results were obtained that support the possibility of mitigating the excitation acceleration amplitude during vibration endurance tests in the front-to-back and left-to-right directions of the rail. Similar studies were also carried out in the up-down direction of rails and in the three axial directions of sleepers and instrument boxes. As a result, it was found that the maximum value of $\mu + \sigma$ obtained from the measurement data was roughly the same as the excitation acceleration amplitude specified by JIS. In addition, it was confirmed that the acceleration was higher at some measurement locations due to the maintenance state of the equipment. Therefore, it is considered that the current excitation amplitude is appropriate for these items [5].

6.2 Comparison of frequency characteristics with international standards

In recent years, in fields such as railway vehicles, random wave excitation has been added as a new test condition in addition to the conventional sine wave excitation vibration durability tests in order to reproduce excitation conditions that are closer to the actual usage environment, making it possible to select the excitation method [7]. In addition, the IEC describes the characteristics of the usage environment along railway lines using power spectral density (PSD), which assumes random waves. Therefore, in order to compare with the international standard, we performed FFT (Fast Fourier Transformation) on the acquired data on time changes in vibration acceleration and calculated the PSD versus frequency.

Among the measurement items, the PSD related to the vibration acceleration of rails and sleepers is specified by the IEC as the frequency characteristics of vibration along railway lines in Europe. The measurement results were compiled using the 1/3 octave band in the same way as the IEC.

Figure 7 shows the result of superimposing the calculated PSD (hereafter referred to as on-site measured PSD). The purple line in the figure is the envelope of the maximum value of the PSD measured at each frequency, and shows the maximum value of the PSD at each frequency in all measurement results (maximum value at the site). This PSD is the PSD that encompasses all measurement results. Also, the green line is the PSD specified by the IEC. Comparing the results of these measurements with the IEC standards, which were established based on the vibration environment along European railways, no prominent PSD peaks were observed in any particular frequency range for rails and sleepers, and up to 1 kHz, the PSD increases as the frequency increases, showing that the distribution between Japan and Europe is similar. In addition, in the range above 1 kHz, the PSD in domestic on-site environments showed high results, but the reason for this is currently unknown.

7. Summary

In order to understand the trends in vibration acceleration to which signalling equipment is exposed when trains pass, this report measured the vibration acceleration at a total of 44 locations, on Shinkansen and Meter-gauged railway lines, for steady-state vibration from passing trains, and clarified the vibration acceleration to which signalling equipment is exposed under current general operating conditions. From the results, we presented the data necessary for the consideration of future revisions of the JIS standard, and also showed the ideal vibration acceleration amplitude for sinusoidal vibration tests in vibration endurance tests. Regarding the effects of impacts due to occasional wheel flats, which were not included in this study, we believe that it will be necessary to discuss this when revising the test methods defined in JIS E 3015 (Railway signalling safety components - Impact test methods) [8], and we plan to continue our study on this issue.

In addition, from the vibration acceleration data acquired, a domestic PSD was derived that can be compared with the IEC on the same scale. Comparison of these results with the PSD indicated by the IEC showed that no prominent PSD peaks were observed in any particular frequency range for rails and sleepers, and that the PSD increased with increasing frequency up to 1 kHz, showing that the distributions in Japan and Europe were similar. In addition, the PSD in the domestic on-site environment showed high results in the 1 kHz range and above. Regarding the difference with the distribution specified by the IEC, we believe that it is necessary to collect more data on the characteristics of PSD in Japan and to clarify the causes.

In the future, based on the PSD characteristics obtained this time, we plan to study the excitation time when conducting vibration endurance tests using vibration acceleration waveforms (random waves) converted to the time domain to reproduce the actual usage environment.

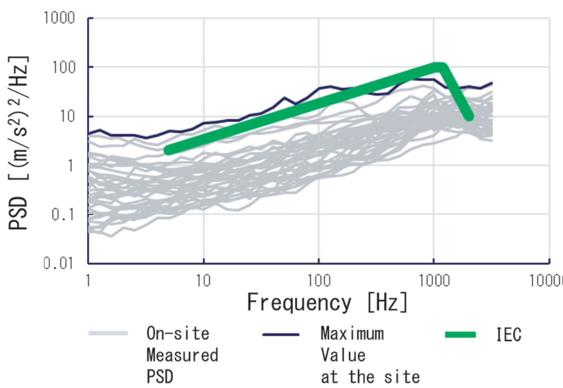

(a) Up-down direction of rails

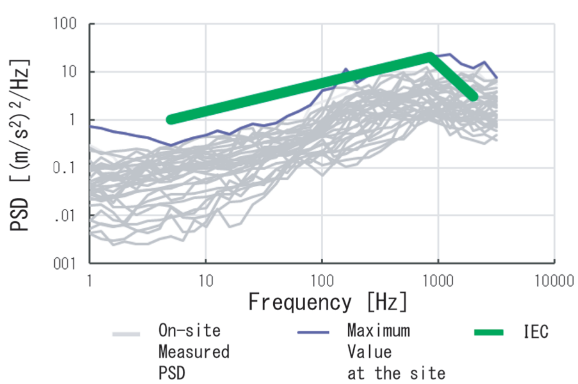

(b) Up-down direction of sleepers

Fig. 7 PSD of vibration acceleration

Acknowledgment

We would like to express our sincere gratitude to the people at the Hokkaido Railway Company, East Japan Railway Company, Central Japan Railway Company, West Japan Railway Company, Shikoku Railway Company, and Kyushu Railway Company for their generous cooperation in conducting the field surveys described in this report.

References

[1] "Parts for railway signal – Vibration test methods," Japanese Industrial Standards JIS E 3014:1976, 1976 (in Japanese).

[2] "Parts for railway signal – Vibration test methods," Japanese Industrial Standards JIS E 3014:1992, 1992 (in Japanese).

[3] "Parts for railway signal – Vibration test methods," Japanese Industrial Standards JIS E 3014:1999, 1999.

[4] Oshimi, Y., Shiomi, S., Takasaki, K. and Kamiya, T., "Investigation of the Vibrational Acceleration to Signalling Systems in the Installation Environment," *Proceedings of the 29th Railway Technology Union Symposium (J-RAIL2022)*, No. S7-4-4, pp. 348-351, 2022 (in Japanese).

[5] Isshiki, R., Oshimi, Y., Shiomi, S., Takasaki, K., Kamiya, T. and Aita, N., "Analysis of vibration received by signalling equipment for types of structures and tracks," *The papers of Technical Meeting on Transportation and Electric Railway, IEE Japan*, TER-23-036, 2023 (in Japanese).

[6] Shiomi, S., Naoya, A., Oshimi, Y., Kamiya, Y. and Isshiki, R., "Investigation on impacts received by signalling equipment connecting directly to a rail from railway vehicles passing," *The papers of Technical Meeting on TER*, TER-23-035, 2023 (in Japanese).

[7] “Rolling stock equipment – Vibration and shock tests,” Japanese Industrial Standards JIS E 4031:2013.

[8] “Parts for railway signal – Shock test methods,” Japanese Industrial Standards JIS E 3015:1992, 1992 (in Japanese).

Authors

Yoshikazu OSHIMI
Assistant Senior Researcher, Signalling System Laboratory, Signalling and Operation Technology Division
Research Areas: Point Machine, Signalling Devices

Shunsuke SHIOMI
Senior Chief Researcher, Head of Signalling System Laboratory, Signalling and Operation Technology Division
Research Areas: Point Machine, Signalling Devices

Tsuyoshi KAMIYA
Researcher, Signalling System Laboratory, Signalling and Operation Division (Former)
Research Areas: Signalling Devices

Ryuto ISSHIKI
Researcher, Signalling System Laboratory, Signalling and Operation Division (Former)
Research Areas: Signalling Devices

Experiments on Damage to Track Components due to Repeated Passage of Vehicles on Rail Gaps

Katsutoshi SHIOTA **Yuki NISHINOMIYA**
Track Structures and Components Laboratory, Track Technology Division

In railways where wireless train control systems are employed, track circuits may be removed, making it difficult to detect a broken rail in such cases. In railways without track circuits, it is assumed that vehicles repeatedly pass over rail gaps until the broken rail is detected by rail inspection or other means. Therefore, in order to evaluate damage of track components due to repeated vehicle passage, we carried out falling weight tests in a laboratory, in which impact loads equivalent to passing vehicles were applied to the broken rail to simulate damage. This test clarified the plastic deformation of the rails and functional deterioration of the rail fastenings system in response to the impact loads.

Key words: *rail broken, falling weight test, rail fastenings system, FEM*

1. Introduction

Track circuits are the main method for detecting the position of a vehicle on a railway. This method detects that a vehicle is on a particular section of track by using the fact that the current flow on the rails changes depending on whether a wheel set is on the rails or not. In addition, the track circuit also has the function of immediately detecting a rail break, because the way the current flows changes when the rail has been broken, creating a gap. In this study, a rail gap is defined as a point where the rail has been broken creating a gap. On the other hand, in recent years, wireless train position detection methods (hereinafter referred to as “wireless train control systems”) have been introduced overseas [1], and some Japanese railway operators are also introducing such systems [2]. Wireless train control systems detect the position of a train using radio equipment mounted on the train. This system allows greater flexibility in operation management compared to the section-by-section detection method using track circuits. The wireless train control system also has the advantage of reducing maintenance costs by streamlining the aboveground equipment used in current track circuits. However, if the track circuit is removed due to the introduction of a wireless control system, it will no longer possible to detect broken rails using the current method. Therefore, alternative systems for detecting broken rails, such as on-board detection methods, are being researched [3]. However, unlike track circuits that can constantly monitor rail defects, there is a possibility that vehicles may repeatedly run over a rail gap at normal operating speeds before the broken rail is detected. Previous studies have investigated the running safety of a single vehicle passing over a rail gap [4]. However, assuming a situation where vehicles repeatedly pass over the rail gap, the track components around the rail gap are repeatedly subjected to impact loads, which may reduce running safety due to the damage to these components.

Previous studies have examined the damage to track components due to impact loads caused by vehicles repeatedly passing over rail gaps. These studied rail damage caused by approximately 600 repeated loadings [5], but rail damage caused by further repeated loading and damage to other track components has not been clarified. In this study, to clarify the damage to the components such as rails and rail fastening systems caused by impact loads during repeated vehicle passage over rail gaps, we developed and carried out tests with a falling weight test device capable of simulating the impact loads of a vehicle passing over a rail gap.

2. Development of falling weight test device

2.1 Need for test device development

In this study, we assume a situation in which vehicles repeatedly pass over the rail gap for a certain period of time between the time the rail is broken and the time the rail gap is detected. As a specific example of this situation, assuming an urban/suburban railway line operating 6 trains per hour each with 10 vehicles per train (4 axles per vehicle) for 18 hours per day, 4,320 axles will pass over the rail gap in one day. Furthermore, assuming that the inspection cycle for reliable detection of rail gaps runs in a seven-day cycle carried out by foot patrols along the track, it is estimated that 30,240 axles will pass over the track during this period. It is therefore necessary to check the occurrence and progression of damage to track components under such conditions. Methods to evaluate the damage to track components at the rail gap include test runs with real vehicles, repeated calculations by numerical analysis and element tests simulating impact loads. However, assuming the number of repetitions mentioned above, running test with a real vehicle is not realistic from the viewpoint of safety, and numerical analysis is not realistic from the viewpoint of computational capacity. Therefore, element tests that apply repeated impact loads during passage through the rail gap are currently considered the most appropriate for evaluation. In addition, it is considered appropriate to use a falling weight test device capable of repeated impact loading for the element test. On the other hand, it is expected that a large test device will be required to apply an impact load simulating passage of a vehicle over the gap. In a large-scale falling weight test device, the weight is often hoisted or dropped using chains or wires to lift the weight and then release it in free fall. It is expected that achieving a load cycle count in the tens of thousands will require a long period of time. In this study, we developed a new falling weight test device that can automatically apply repeated and controlled impact loads in the order of tens of thousands to reproduce passage over the rail gap. By using a cam mechanism to lift the weight, we enabled automatic repeated loading, and by using an inverter motor, we can set shorter

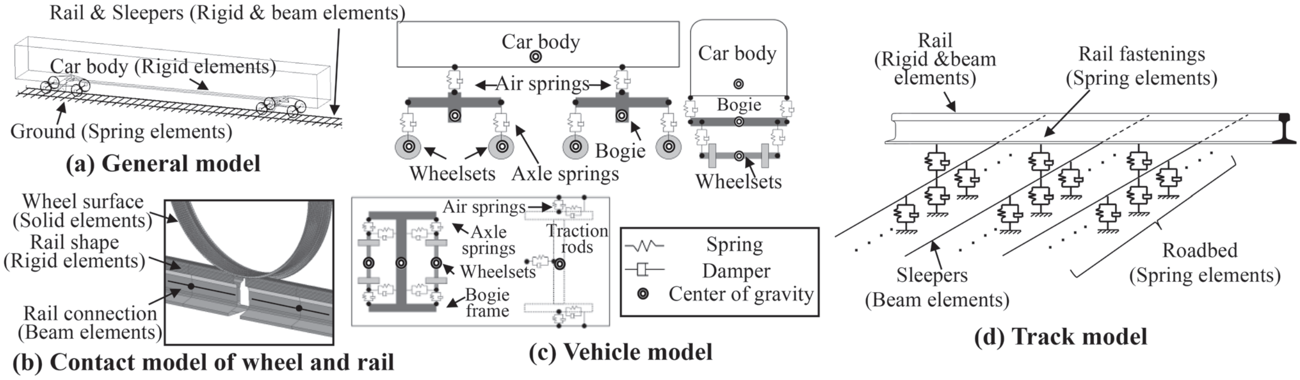

Fig. 1 Overview of analysis model

loading intervals.

2.2 Calculation of required capacity of test device by running analysis on rail gap

In order to investigate the required loads for the test device, the impact loads generated by vehicles passing over the rail gap were calculated using a dynamic FEM analysis method [6]. The analysis model is shown in Fig. 1. The track is shown in Figs. 1(a) and 1(d). The rails are modeled with beams and rigid elements, the sleepers with beam elements and the roadbed with spring and damper elements. As shown in Fig. 1(c), the vehicle model is a three-dimensional model in which the car body, bogie, and wheelset are modeled as rigid bodies, and coupled with spring and damper elements. Table 1 shows the main specifications of the track model and the vehicle model. Using this analysis model, the impact load at the time of passing over the rail gap was calculated, and this load was used as the required capacity of the falling weight test device. It is assumed that the damage to the components caused by the impact load is influenced by the value of the impact load and its duration, i.e., the impulse. Therefore, each value was calculated accordingly.

Table 2 shows the track conditions assumed in this study. In this study, we assumed a rail gap on a well-maintained ballastless track on a conventional line. We set the condition where the rail gap is located at the end of the sleeper on the receiving side, as this is where significant wheel loads are likely to occur. The “leaving side” refers to the section of rail leading up to the gap. The “receiving side” refers to where the wheel runs onto the next section of rail after the gap, as illustrated in Fig. 2, where the direction of running is left to right. The reason for setting these conditions is that when calculating the loading conditions for tests No. 1 to No. 3 of the falling weight tests described later in Chapter 3, the impact load was greatest for the condition (test No. 1) where the end of the rail gap was aligned with the edge of the sleeper on the receiving side in a straight line. Specifically, when the rail gap ends at the edge of the sleeper on the receiving side, as shown in Fig. 3, a significant height difference occurs between the leaving side rail and the receiving side rail as the wheel passes over the rail gap. This level difference is expected to cause a significant impact on the receiving rail. For the rails, of the widely used 50-60 kgN rails, we focused on the less rigid 50 kgN rail. There are many types of rail fastening systems, but we chose to use a bar-shaped spring clip type rail fastening system with a high rail fastening force. This is because, when focusing on rail damage, assuming that the spring constant of the elastic rail pad laid directly under the rail is the same, the greater the rail fastening force, the smaller the rail displacement under train loads. This is expected to reduce the dispersion effect of impact loads, making plastic deformation of the rail head more likely. The fastening interval was set at 750 mm, the largest interval among the track types

Table 1 Parameter of analysis model

(a) Track

Item	Specifications
Track gauge	1067 mm
Rail type	JIS 50 kgN Rail
Rail fastenings vertical springs	110 kN/mm
Roadbed vertical springs	3.3×10^5 N/mm

(b) Vehicle

Item	Specifications
Body mass	28.3 tonne
Mass between primary spring and secondary spring	2.2 tonne/bogie
Unsuspended mass	1.52 tonne/wheelset
Wheelbase	2.1 m
Distance between two bogies	14.15 m
Shape of wheel surface	Modified arc wheel profile (JIS)

Table 2 Condition of assumed track

Item	Specifications
Track line	Straight (Speed 100 km/h)
Track structure	Ballastless track
Fastening interval	750 mm
Rail pad vertical springs	110 MN/m
Rail gap	70 mm
Position of rail gap	End of the receiving sleeper

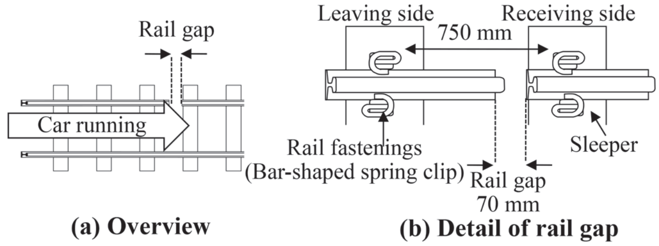

Fig. 2 Illustration of rail gap set up

used on typical conventional suburban lines.

Figure 4 shows the results of the running analysis under the conditions described above. The analysis showed that the maximum impact load acting on the rail when the wheel passed over the rail gap was 170 kN, the duration of action was 8 msec, and the impulse was 537.4 N·s. The impact load occurred only on the receiving rail. Based on these results, the components to be evaluated for damage in the falling weight test were the receiving track components. However, if the weight is dropped on to the rail end while only the track components on the receiving side are simulated, the behavior of the weight during the drop becomes unstable. This situation raises concerns about variations in the loading position and increased stress on the test device. Therefore, as shown in Fig. 5, the components on the receiving side were arranged so that they were paired around the rail gap, and the loading behavior was stabilized by dropping the weight on both rails at the same time. It was therefore decided that the falling weight test device should be capable of applying an impact load of 340 kN, which is twice 170 kN. Based on these conditions, the test device was manufactured.

2.3 Manufacturing of test device [7]

Based on the studies carried out up to the previous section, the appearance of the manufactured test device is shown in Fig. 6 and its specifications are given in Table 3. In this test device, a cam system is used to lift the weight, and an inverter motor is used to adjust the loading cycle of the weight, so that the minimum loading cycle for stable loading is 2.5 seconds per cycle. In addition, to stabilize the unstable behavior of the falling weight test onto the rail gap, the weight is guided by two guide bars. Performance verification tests were carried out on a specimen simulating the rail gap using the test device. As a result, it was confirmed that the test device can be adjusted up to 346 kN, 9 msec, and 1,557 N·s of impulse, compared to the target load of 340 kN, action time of 8 msec, and 1,360 N·s of impulse. It was also confirmed that the impact load was stable in the range of +1 to +3% when continuously operated at the minimum loading period.

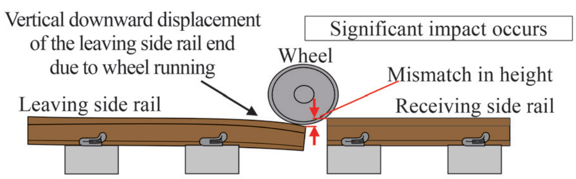

Fig. 3 Mismatch in height of the rail when the rail gap is at the receiving sleeper end

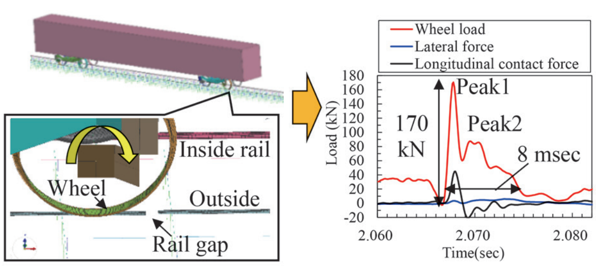

Fig. 4 Impact load generated when passing through the rail gap only on the receiving rail

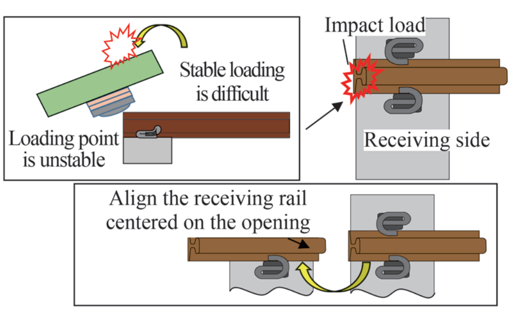

Fig. 5 Arrangement to stabilize the behavior of the weight

3. Falling weight test assuming repeated passage of vehicles over rail gap

3.1 Test conditions

Using the manufactured falling weight test device, we carried out damage verification tests on the track components, simulating the repeated passage of vehicles over the rail gap. The test conditions are given in Table 4. In this test, the rail and the rail fastening system

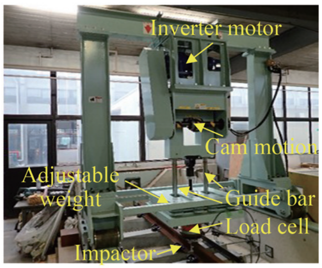

Fig. 6 Overview of test device

Table 3 Specifications of test device

Item	Specifications
Driving source	Inverter motor
Driving system	Cam mechanism
Operation system	Manual/Automatic
Manipulation system	Hand-held controller/ Control panel
Falling mass	640~1,240 kg
Falling height	25~80 mm
Falling cycle	2.5~12.5 s/times

Table 4 Test condition

Item		Specifications
Rail type		JIS 50 kgN Rail
Rail fastening system		Bar-shaped spring clip
Rail pad vertical springs		110 MN/m
Fastening interval		750 mm
Test number	1	Straight·test to confirm rail damage (rail gap begins at edge of receiving sleeper)
	2	Straight·test to confirm rail fastening system damage (rail gap is at the end of the leaving sleeper)
	3	Curve·test to confirm rail fastening system damage (rail gap begins at edge of receiving sleeper)
Test load (per rail), duration of action, impulse		Test number 1: 170 kN, 8 msec, 680 N·s
		Test number 2: 100 kN, 19 msec, 950 N·s
		Test number 3: 98 kN, 23 msec, 1,127 N·s
Loading times		100,000 times

were evaluated and three numbered tests were carried out for straight and curved running conditions. In each numbered test, the rail gap was positioned to end at the edge of the sleeper on the receiving side or begin at the edge of the sleeper on the leaving side, as shown in Fig. 7, in order to increase the load on the rail and the rail fastening system, respectively. In addition, the loading conditions for each numbered test were calculated for the impact load, duration of action, and its impulse using the rail gap running analysis method described in Section 2.2. Because of the characteristics of the test, it was difficult to match the impact load and duration of action exactly to the target values, so the load was adjusted so that the impulse was not less than the target value. The target number of load cycles was set at 100,000 cycles in order to check for component damage from further repeated impacts in addition to the repeated passage conditions described in Section 2.1. An example of specimen installation is shown in Fig. 8. In this test, the receiving track components were installed in pairs each side of the rail gap in order to stabilize the weight behavior as described in Fig. 5. For evaluation, measurements were performed on the rail and rail fastening system on the north side of the specimen, which was arranged symmetrically in a north-south direction around the rail gap, as shown in Fig. 8. The detailed conditions of each test number are described below.

3.1.1 Test No. 1 (Straight line test to confirm rail damage)

Test No. 1 was a test to confirm rail damage, under the condition that the end of the rail gap is the edge of the receiving sleeper in a straight line. This is because when the end of the rail gap is aligned with the edge of the receiving sleeper (Fig. 7(a)), there is a step difference between the leaving and receiving rails, which is considered to place a large load on the receiving rail. The assumed running speed was 100 km/h. The target test load, duration of action, and impulse were 170 kN, 8 msec, and 680 N·s.

3.1.2 Test No. 2 (Straight line test to confirm rail fastening system damage)

Test No. 2 was a test to confirm damage to the rail fastening system under the condition that the rail gap begins from the edge of the sleeper on the leaving side in a straight line. This is because, when the rail gap begins from the edge of the leaving side sleeper (Fig. 7(b)), the receiving rail acts as a cantilever beam. This is because, under these circumstances, the distance between the rail end and the rail fastening system that serves as the fulcrum becomes longer, and it is thought that a large load will be placed on the rail fastening system when the load is transferring. The assumed running speed was 100 km/h. The target test load, duration of action, and impulse were 100 kN, 19 msec, and 950 N·s.

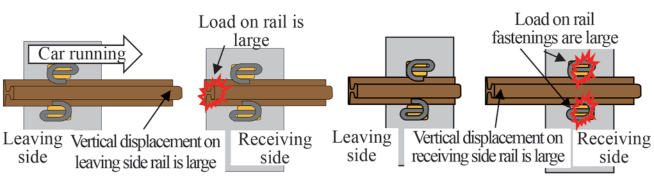

(a) Condition of high load on rails (b) Condition of high load on rail fastenings

Fig. 7 Setting test conditions according to the arrangement of rail gap

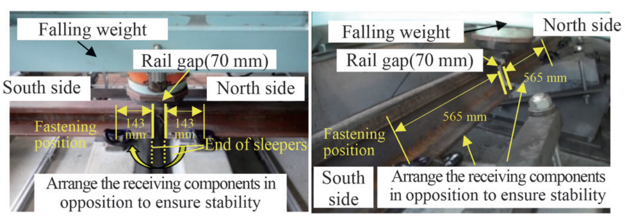

(a) Condition of high load on rails (Test No. 1) (b) Condition of high load on rail fastening system (Test No. 2)

Fig. 8 Setting example of test components

3.1.3 Test No. 3 (Curve section test to confirm rail fastening system damage)

Test No. 3 was a test to confirm damage to the rail fastening system, under the condition that the rail gap begins from the edge of the sleeper on the leaving side in a curved section. This is to check the effects of the lateral force as well as the wheel load when running in curves. The assumed curve parameters were a radius of 620 m, a cant of 50 mm, and a running speed of 90 km/h. The target test load, duration of action, and impulse were 98 kN, 23 msec, and 1,127 N·s. Due to the limitations of the test device, loads cannot be applied simultaneously from two directions, so the test load in the curved condition was the combined force of the wheel load and the lateral force, and the specimen was tilted by the angle of the combined force. It should be noted that the test to confirm rail damage in curves was not included in this study because it is difficult to simulate the contact condition between the wheel flange and the rail that occurs when running in a curve. However, based on the results of Test No. 1 described below in Section 3.2, it is thought that the state of rail damage in a curve can also be roughly estimated from the experimental estimation formula.

3.2 Straight lines test to confirm rail damage (Test No. 1) [8]

3.2.1 Test method

The test conditions and a test load example are shown in Fig. 9. Test loads were converted per single rail by dividing the value measured by the load cell by 2. To ensure that the load was applied evenly to both rails, the acceleration of each rail was measured in advance and the loading position was adjusted so that the accelerations were equal. Looking at the test load shown in Fig. 9(b), compared to the target impact load of 170 kN, duration of 8 msec and an impulse of 680 N·s, the load of the first wave was 170.5 kN, duration of 10 msec and an impulse of 852.5 N·s, which exceeded the impulse of the target load conditions. It should be noted that the second and third waves also occurred after the first wave. This is the result of the weight repeatedly bouncing up and down several times after the fall. Although it is difficult to control the rebound of the weight, the impact load of the second wave was 65.1 kN, with a duration of 11 msec and an impulse of 358.1 N·s, which was significantly lower than the target load condition's impulse. Therefore, in this study, it was not counted as a load cycle. Additionally, to confirm the amount of plastic deformation on the top surface of the rail being evaluated, the cross-sectional shape of the rail was measured. The measurement point was set at a position 5mm from the rail end in the longitudinal direction, and the vertical deflection at the center of the rail top surface was confirmed.

3.2.2 Test results

Figure 10 shows the amount of plastic deformation on the rail

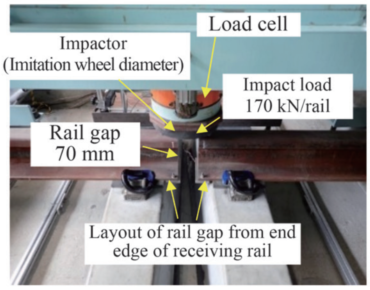

(a) Setting condition of test

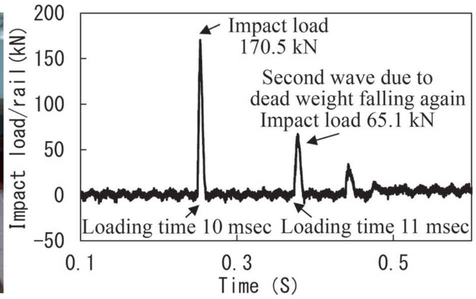

(b) Test load of test No. 1

Fig. 9 Implementation status and test load of test No. 1

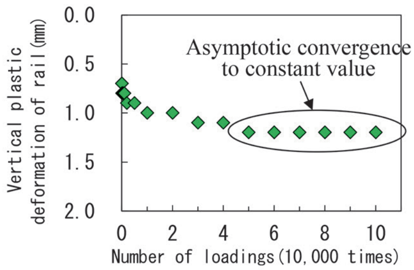

(a) Vertical plastic deformation of rail

(b) Appearance of rail after test

Fig. 10 Result of test No. 1

head surface and the condition near the rail head surface after 100,000 load cycles. The results of the cross-sectional profile measurement of the rail showed that the amount of depression of the rail head due to plastic deformation was 1.2 mm after 100,000 cycles. Considering the fact that there are reports [9] that rail steps of up to 3 mm have occurred at rail joints, the amount of deformation tested is small and is not considered to immediately cause a running safety problem. No other defects or cracks in the rail were observed. Additionally, the vertical depression of the rail head surface due to plastic deformation tended to converge to a constant value after approximately 50,000 cycles. These results confirmed that although the rail undergoes some plastic deformation due to the impact load when passing over the rail gap, the amount of deformation asymptotically converges to a constant value and does not lead to failure even after approximately 100,000 load cycles. Additionally, Urakawa et al have proposed an estimation formula based on experiments [5], as shown in Equation (1), for the maximum plastic deformation of the rail head surface due to the impact load at the rail gap.

$$Z_{pmax}=\frac{-\beta+\sqrt{\beta^2+4\alpha\dfrac{P_a}{\sigma_y}}}{2\alpha} \tag{1}$$

Z_{pmax}: Maximum plastic deformation of rail (mm), P_a: Impact load (kN), σ_y: Rail yield stress (N/mm^2) (reference value 450 N/mm^2), α, β: Geometric shape coefficient (reference value α = 121.14, β = 231.39)

By applying the impact load of 170 kN, which is the test condition, to the above experimental formula, the estimated maximum plastic deformation was 1.05 mm. This estimation agreed with the test result of 1.2 mm with an accuracy of 87.5%. This suggests that the amount of plastic deformation of the rail head due to impact loading can be estimated.

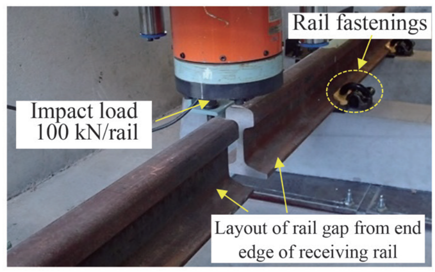

(a) Setting condition of test

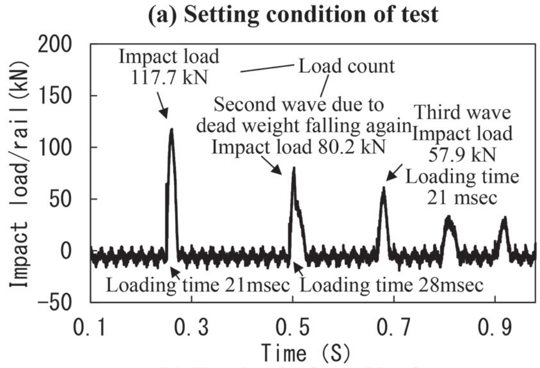

(b) Test load of test No. 2

Fig. 11 Implementation status and test load of test No. 2

3.3 Straight line test to confirm rail fastening system damage (Test No. 2) [10]

3.3.1 Test method

The test conditions and examples of test loads are shown in Fig. 11. Checking the test loads shown in Fig. 11(b), it can be seen that there are more repeated impacts compared to test No. 1. This is because the rail is in a condition similar to a cantilever beam, causing elastic bending deformation of the rail when the weight collides with it. This results in a spring-like response of the weight, leading to an increase in the number of impacts. Additionally, the value of the impact load for the first wave was 117.7 kN, 21 msec, and 1,235.9 N·s, which exceeded the target load conditions of 100 kN, 19 msec, and 950 N·s. Furthermore, the impact load, duration, and impulse of the second wave were 80.2 kN, 28 msec, and 1,122.8 N·s, respectively. Since the impulse of the second wave also exceeded the target load conditions, it was counted as a load cycle. However, the impact load, duration, and impulse of the third wave were 57.9 kN, 21 msec, and 608.0 N·s, respectively, which were lower than the target load conditions. Therefore, the third wave and subsequent waves were not counted as load cycles. In this test, to verify the functionality of the rail fastening system after repeated impact loads, the fastening force of the rail fastening system was measured after the test was completed.

3.3.2 Test results

The appearance of the rail fastening system after 100,000 load cycles is shown in Fig. 12. As a result of the test, no visible damage to the rail fastening system was observed. However, it was confirmed that the clip constituting the rail fastening system had plastically deformed upward by approximately 1.6 mm compared to an unused clip. This is because the receiving rail was in a condition similar to a cantilever beam, with impact loads applied to the rail end. As a result, the clips of the rail fastening system, which act as fulcrums, were repeatedly subjected to an upward vertical force exceeding the rail fastening force. After the test, the rail fastening force was 21.2 kN for the two clips, with an average fastening force of 10.6 kN per clip. The result represents a reduction of 11.7% compared to the nominal rail fastening force of 12.0 kN for the spring-type rail fastening system used in this test. Regarding the performance of the rail fastening system with reduced rail fastening force, a performance verification test was previously carried out on a similar rail fastening system. In this test, the rail fastening force per clip was reduced to 9.3 kN, and the train equivalent load was repeatedly applied 1,000,000 times. The result reported that no abnormalities were observed in the rail fastening system after the test [11]. As the rail gap was not the subject of the previous study, the results of the previous study do not directly correspond to the results of the falling weight test carried out this time. However, taking into account the results of the previous study, it is believed that the functional degradation of the rail fastening system in this test does not significantly reduce the holding function of the rail.

3.4 Curve section test to confirm rail fastening system damage (Test No. 3) [12]

3.4.1 Test method

The test conditions and examples of test loads are shown in Fig. 13. In this test, to simulate the wheel load and lateral force during the curve passage, the specimen was inclined as shown in Fig. 13(a), and the resultant force of the wheel load and lateral force were set as the impact load. Checking the test loads shown in Fig. 13(b), repeated impacts occurred after the first wave, similar to previous tests. Additionally, the value of the impact load for the first wave was 102.9 kN, 27 msec, and 1,389.2 N·s, which exceeded the target load conditions of 98 kN, 23 msec, and 1,127 N·s. Furthermore, the impact load, duration, and impulse of the second wave were 47.7 kN, 35 msec, and 834.8 N·s, respectively. Since these values were lower than the target load conditions, the second wave was not counted as a cycle. To verify the functionality of the rail fastening system after repeated impact loads, the fastening force of the rail fastening system was measured at the end of the test, similar to Test No. 2.

3.4.2 Test results

The insulator, which is a resin component of the rail fastening system, was damaged after 55,000 loading cycles. The appearance of the rail fastening system after 55,000 loading cycles is shown in Fig. 14. No deformation was observed in the damage process up to approximately 30,000 cycles. However, as shown in Fig. 15(a), the insulator, which is a resin component of the rail fastening system on the outer side of the track, began to crack at around 32,000 cycles, and was finally damaged at 55,000 cycles. The reason for this is that the receiving rail was in a cantilever beam-like condition, with the

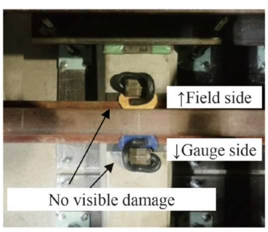

(a) Overview of rail fastening system

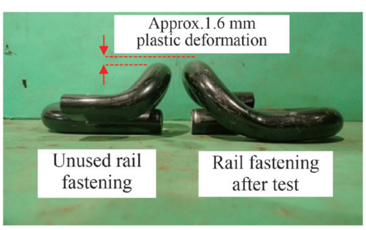

(b) Plastic deformation of rail fastening system

Fig. 12 Result of test No. 2

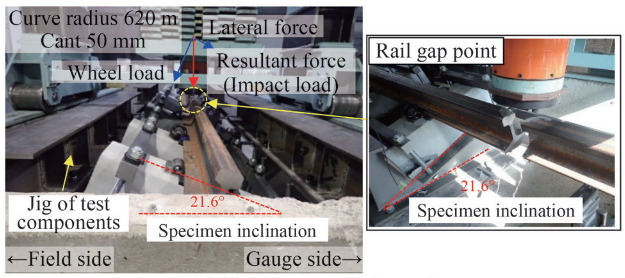

(a) Setting condition of test

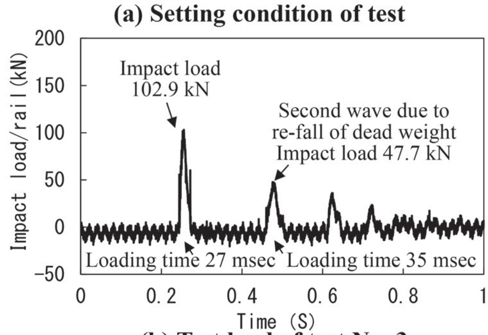

(b) Test load of test No. 3

Fig. 13 Implementation status and test load of test No. 3

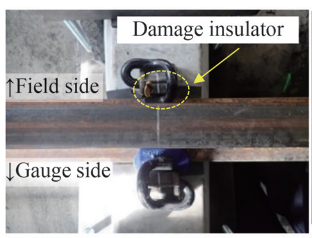

(a) Overview of rail fastenings

(b) Damage of insulator

Fig. 14 Appearance of rail fastenings after test No. 3

impact lateral force from passing through a curve acting on the rail end. As a result, the rail fastening system, acting as a fulcrum, experienced a lateral impact load. The load is transmitted to the rail, insulator, and the shoulder part that fixes the clip. Among these, the insulator, being a resin component, has the lowest strength, which likely led to the cracks and damage. Since the behavior of the falling weight was unstable, the test was terminated after 55,000 loading cycles.

The rail fastening force of the rail fastening system was then measured after the test. It should be noted that when the insulator is damaged, the deflection of the clip decreases, resulting in a reduction in the rail fastening force. Therefore, to confirm the reduction in rail fastening force due to the plastic deformation of the clip itself, excluding the effects of damaged insulators, the rail fastening force was measured using new insulators. As a result of the measurement, the rail fastening force per clip was 11.2 kN, which is a reduction of 6.7% compared to the nominal rail fastening force of 12.0 kN. However, as mentioned in Section 3.3, this reduction is not considered to significantly decrease the rail holding function. Next, considering the damage to the insulator, we examined the rail fastening force in the condition where one side of the insulator was missing. However, in the condition where one side of the insulator is missing, it is not possible to conduct a stable rail fastening force measurement test. Therefore, using the analytical model [13] shown in Fig. 16, the rail fastening force was calculated for the condition where one side of the insulator was missing. The analytical model represents the components as three-dimensional solid elements. Additionally, the clip is modeled as an elastoplastic material, and its stress-strain characteristics are determined by performing tensile tests on material specimens cut from the straight section of the clip. The rail and insulator are modeled as linear elastic bodies, while the rail pad is modeled as a nonlinear elastic body. The elastic modulus is set to obtain the nominal spring constant. In this analysis, we removed one side of the insulator from the analytical model, which was initially fastened with insulators on both sides, and calculated the rail fastening force in this condition. The physical properties used in the analysis are shown in Table 5.

As a result of the analysis, the rail fastening force of the clip on the side without the insulator was 3.5 kN. On the other hand, the rail fastening force of the clip on the side with the insulator was 12.0 kN, and the combined fastening force of the two clips on both sides was 15.5 kN. This is approximately equivalent to the rail fastening force of a typical plate spring type rail fastening systems [14]. Therefore, even after the insulator is damaged, although the rail fastening condition is incomplete, the rail holding function is considered to be maintained. Based on the above results, it was confirmed that the strength of the insulator, a resin component of the rail fastening system, is crucial against the impact load assumed from the repeated passage of vehicles at the rail gap in curved sections.

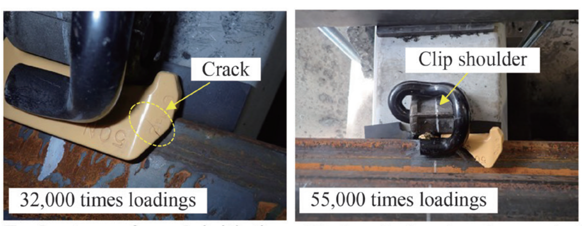

(a) Early stage of crack initiation (b) Just before insulator missing

Fig. 15 Transition of insulator damage

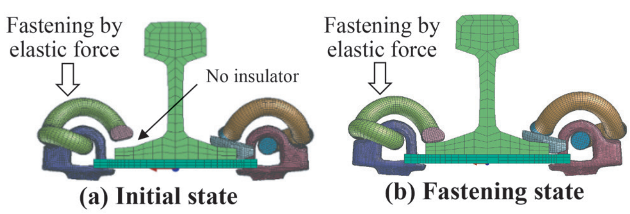

(a) Initial state (b) Fastening state

Fig. 16 Overview of analysis model

3.5 Discussion

Based on the results reported in the previous sections, the damage to the track components during the repeated passage of vehicles at the rail gap was clarified through experimental investigation. Specifically, in the straight section, it was confirmed that the rail and rail fastening system experienced approximately 1.5 mm of plastic deformation at the rail head and approximately 1.6 mm of plastic deformation in the clip due to the impact load of passing over the rail gap, but no significant damage was observed. Therefore, under the conditions examined in this study, it is considered that there are no strength problems with the rail and rail fastening system during the repeated passage of vehicles in the straight section. In the curved section, it was found that the insulator, a resin component of the rail fastening system, could be damaged due to the lateral force when passing over a rail gap. However, it was confirmed that immediate damage does not occur, and no problems were observed up to approximately 30,000 cycles. Therefore, under the conditions examined in this study, it is considered that the strength problems of the rail fastening system in the curved section are minimal for repeated passages up to approximately 30,000 cycles. It should be noted that these results are based on the limited conditions examined in this study. However, for other different track structures, it is considered possible to clarify the conditions using numerical analysis based on the load conditions and test results of this study.

4. Conclusion

In this study, to obtain basic insights into the damage to track components by the repeated passage of vehicles over rail gaps on ballastless track, a falling weight test device capable of simulating the impact load of a railway vehicle passing over a rail gap was fabricated. Furthermore, repeated falling weight tests were carried out to confirm the damage to track components. The main results are as follows:

(1) By using the fabricated falling weight test device, it became possible to repeatedly apply the rail gap impact load to track components.

(2) As a result of the repeated falling weight tests simulating the

Table 5 Material properties

Parts	Material model	Young's modulus (N/mm^2)	Poisson ratio
Rail	Elastic body	2.06×10^5	0.3
Insulator	Elastic body	3.00×10^3	0.35
Shoulder/ Baseplate	Nonlinear elastic body	-	-
Rail pad	Elastic-plastic body	Non-linear value setting based on experiments	
Clip	Elastic-plastic body		

conditions where the rail is subjected to a load in a straight section, the plastic deformation at the rail head was approximately 1.2 mm after 100,000 cycles of repeated loading. Considering that the rail joint has a misalignment of approximately 3 mm due to the drop of the rail, this amount of deformation was small.

(3) As a result of the repeated falling weight tests simulating the conditions under which the rail fastening system is loaded in a straight section, it was confirmed that no significant external damage to the rail fastening system was observed after 100,000 cycles of repeated loading. Additionally, as a functional check of the rail fastening system after the test, the rail fastening force was measured. The results showed that although the rail fastening force was reduced by 11.7% due to repeated impact loads, the rail fastening function was maintained.

(4) As a result of repeated falling weight tests under conditions simulating the load of a passing railway vehicle on a rail fastening system in a curved section, the insulator, which is a resin component, was damaged after approximately 55,000 repetitions. However, since no problems were observed up to approximately 30,000 repetitions, it was confirmed that the rail fastening system does not cause any immediate problems.

References

[1] Bayissa,WL. and Dhanasekar, M., "High speed detection of broken rails, rail cracks and surface faults," *CRC for Rail Innovation (An Australian Government Initiative)*, 2011.

[2] Baba, Y., Tateishi, Y., Mori, K., Aoyagi, S., Takeshi, K., Saito, S., Suzuki, Y. and Watanabe, T., "Radio Train Control System (ATACS)," *JR East Technical Review*, No. 3, pp. 54-62, 2004.

[3] Hosoda, M., Aizawa, H. and Yamamoto, R., "Rail broken detection system from vehicle as an alternative to track circuits," *RTRI Report*, Vol. 36, No. 3, pp. 17-22, 2022 (in Japanese).

[4] Shiota, K. and Nishinomiya, Y., "Systematic evaluation of running safety on broken rail considering track and vehicle conditions," *Journal of railway engineering*, Vol. 26, pp. 225-232, 2022 (in Japanese).

[5] Urakawa, F., Ota, S., Shimizu, S. and Nishinomiya, Y., "Grasp of the characteristics of the plastic deformation development of the rail occurring on rail gaps by means of repeated drop weight test," *J-RAIL2018*, 1504, 2018 (in Japanese).

[6] Nishinomiya, Y., Kataoka, H. and Hiraide, S., "Expansion of the application range of the continuous welded rail in the slab track," *RTRI Report*, Vol. 29, No. 8, pp. 11-16, 2015 (in Japanese).

[7] Yasuda, S., Shiota, K. and Nishinomiya, Y., "Development of a dead weight drop test equipment capable of simulation repeated impact loads when passing through broken rail," *The journal of Japan Railway Civil Engineering Association*, Vol. 60, No. 6, pp. 54-57, 2022 (in Japanese).

[8] Nakano, T., Nishinomiya, Y., Shiota, K. and Yasuda, S., "Evaluate of the plastic deformation of the rail occurring on rail gaps by means of repeated drop weight test," *Proceedings of the 76th Annual Conference of the Japan Society of Civil Engineers*, VI-317, 2021 (in Japanese).

[9] Funayama, S., Onodera, T. and Nagai, Y., "Efforts to Develop Rail Grinding Methods for Eliminating Misalignment at Joints," *Proceedings of the 58th Annual Conference of the Japan Society of Civil Engineers*, IV-075, 2003 (in Japanese).

[10] Koketsu, T., Nishinomiya, Y., Shiota, K. and Yasuda, S., "Evaluation of impact load on the durability of rail fastening device when passing through rail damage points in straight sections," *Proceedings of the 77th Annual Conference of the Japan Society of Civil Engineers*, VI-413, 2022 (in Japanese).

[11] Deshimaru, T., Motono, T., Kataoka, H. and Wakatsuki, O., "Laying standards of wire spring clip fastening system in the curved section," *RTRI Report*, Vol. 26, No .2, pp. 37-40, 2012 (in Japanese).

[12] Yasuda, S., Nishinomiya, Y., Shiota, K. and Koketsu, T., "Evaluation of impact load on the durability of rail fastening device when passing through rail damage points in curve sections," *Proceedings of the 77th Annual Conference of the Japan Society of Civil Engineers*, VI-414, 2022 (in Japanese).

[13] Nishinomiya, Y., "A method for simulating stress of round bar rail clips using nonlinear elastic-plastic dynamic explicit FEA," *Proc. of the 12th Int. Conf. on Railway Engineering 2013*, 2013.

[14] Tabuchi, T., Abe, N. and Wakatsuki, O., "Development of rail fastening device for new type of ballast-less track," *Proceedings of the 58th Annual Conference of the Japan Society of Civil Engineers*, IV-081, 2003 (in Japanese).

Authors

Katsutoshi SHIOTA
Assistant Senior Researcher, Track Structures and Components Laboratory, Track Technology Division
Research Areas: Turnout, Railway Vehicle Dynamics Simulation

Yuki NISHINOMIYA, Ph.D.
Senior Researcher, Track Structures and Components Laboratory, Track Technology Division
Research Areas: Continuous Welded Rail, Railway Vehicle Dynamics Simulation

Low-strength Stabilization Method for Reducing of Settlement in Fouled Ballast

Takahiro KAGEYAMA **Takahisa NAKAMURA**
Track Structures & Geotechnology Laboratory, Track Technology Division

Masaru HOJO **Fumika TAJIMA**
Track Structures & Geotechnology Laboratory, Track Technology Division

As ballast on railway tracks is compacted and fragmented, settlement of the track tends to occur even after tamping, which leads to a need for more frequent maintenance. The basic measure to reduce maintenance frequency of replacing old ballast with new ballast, is costly. This calls for a low-cost method to reduce ballast settlement without need for ballast replacement. Therefore, we developed a low-strength stabilization method for reducing settlement without replacing ballast. This study confirms the effectiveness of the developed method for reducing settlement through laboratory tests. We conducted field tests on a commercial line to verify the effectiveness of this method in reducing settlement.

Key words: *low strength stabilization, cyclic triaxial compression test, full-scale test, test construction, fouled ballast*

1. Introduction

Repeated train loads on ballasted tracks causes settlement. Sections of track with significant settlement, identified during regular inspections, need tamping using portable tampers. If the ballast does not undergo progressive crushing and granulation, then the ballast settlement after tamping is small, thus resulting in low maintenance frequency. However, if ballast is progressively crushed and granulated ("fouled ballast") by cyclic train loads and tamping [1, 2], then ballast settlement is likely to occur even after tamping, which consequently increases the maintenance frequency. Therefore, ballast is generally replaced to reduce maintenance frequency. However, the high cost of replacing ballast calls for low-cost settlement control methods that suppress the settlement of fouled ballast. Previously developed methods that improve the strength of fouled ballast and suppress the settlement of ballasted tracks include the granulation method, which fills fouled ballast with grout material and then crushes and granulates it after solidification to increase drainage and strength [3]. Then there is the polymer-stabilization method, which stabilizes fouled ballast using an aqueous biodegradable polyvinyl alcohol ("PVA") polymer solution and a reaction accelerator to increase strength [4].

However, the granulation method requires the removal of sleepers, mixing of grout, and crushing of the grout-filled layer, which challenges workability. The polymer-stabilization method, on the other hand, requires an aqueous PVA polymer solution that contains a significant amount of water. This reduces the strength of the fouled ballast immediately after it has been added, rendering it susceptible to initial settlement.

Therefore, we developed a low-strength stabilization method [5, 6, 7] that uses a mixture of ultra-fast hardening cement and a polymer solidification material ("stabilizing material"). This method is easy to implement, suppresses the settlement of fouled ballast, and allows normal tamping to be conducted even after hardening.

This study reports on cyclic triaxial compression and cyclic loading tests using a full-scale track model, and test implementation on a commercial line. These tests were conducted to confirm the settlement-suppression effect of the low-strength stabilization method.

2. Overview and implementation procedure of low-strength stabilization method

The low-strength stabilization method suppresses track settlement by the addition of stabilizing material during tamping using a portable tamper and stabilizing the fouled ballast. Stabilizing material is added at eight locations per sleeper (Fig. 1). The features of this method are as follows:

(1) Applicable using a portable tamper, tamping machine, and backhoe tamper.
(2) Suppresses ballast settlement immediately after application. This means that implementation of the method [does not have to rely on nighttime track closures but] can be completed within daytime track work windows.
(3) Allows tamping to be performed using portable tamper even after application.

The stabilizing material is a 1:1 (by weight) mixture of two types of materials (Fig. 2): ultra-fast hardening cement and a polymer solidification material. The low-strength stabilization method does not require replacement of ballast or the disposal of generated ballast. Therefore, its application incurs only approximately 10% of the cost of ballast replacement.

The procedure for the low-strength stabilization method is as follows:

1) Excavate an area to the depth of the sleeper bottom at the tamping position (Fig. 3(a)).
2) Add 500 g (standard addition amount) of stabilizing material to each tamping position (eight positions per sleeper) (Fig. 3(b)).

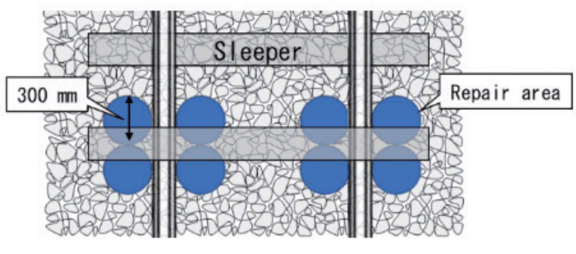

Fig. 1 Overhead view of repair area of low-strength stabilization method

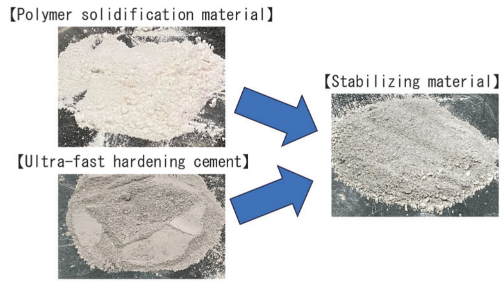

Fig. 2 Stabilizing material for low-strength stabilization method

Fig. 3 Implementation of low-strength stabilization method [7]

3) Backfill using ballast, perform tamping, and stabilize the fouled ballast (Fig. 3(c)).

Even when a tamping machine is used, the stabilizing material is added to the excavated area as per the abovementioned procedure. However, as described later in Section 5.2, even when the stabilizing material was dispersed on the ballast surface during tamping work, a settlement-suppression effect was observed in tests. Considering workability, this therefore suggests when tamping work alone is being carried out, it is also effective to simply spread the stabilizing material on the ballast surface.

Additionally, the area where tamping can be performed using a portable tamper was assumed to be a cylinder with a diameter of 300 mm and a height of 150 mm (Fig. 4), and the added amount of stabilizing material A_S (g) was determined using (1).

$$A_s = \frac{V \rho_d R_s}{100} \tag{1}$$

where V is the cylinder volume (cm^3), ρ_d the dry density of fouled ballast (2.05 g/cm^3), and R_s the proportion of added stabilizing material (2%). In this study, R_s was determined based on the results of presented in Sections 4 and 5.

Additionally, we examined whether tamping can be conducted after adding stabilizing material using a portable tamper to tamp the fouled ballast in a circular soil tank (diameter 300 mm) that had been stabilized using four times the standard added amount of stabilizing material (additional amount of 8%). Tamping was conducted three months after air curing, i.e., when the strength was assumed to have developed sufficiently, and ballast tamping was confirmed to be feasible.

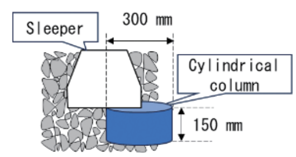

Fig. 4 Location of stabilizing material application

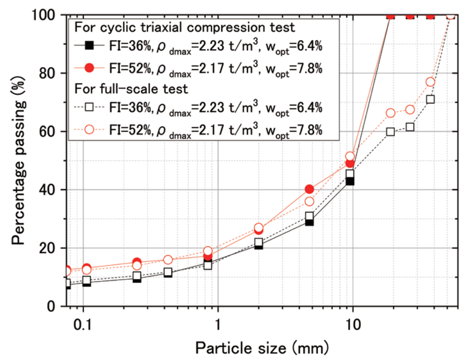

Fig. 5 Sample particle-size distribution

3. Examination by cyclic triaxial compression test

Cyclic triaxial compression tests were conducted to examine the added amount of stabilizing material to the fouled ballast. The fouled ballast used for the test ("sample") had a fouling index of ballast "*FI*" (sum of passing mass percentages at 0.075 mm sieve and 4.75 mm sieve) [8] of 36% (Fig. 5). Additionally, Fig. 5 shows the maximum dry density ρ_{dmax} and optimal moisture content was obtained from a compaction test performed using the E method specified in JIS A 1210. When the *FI* is 20% or higher, the ballast is evaluated as "fouled," which signifies that settlement is likely to increase [7]. The samples were prepared by mixing new ballast with cobble stone and kaolin clay such that the particle-size distribution would be similar to that of the ballast obtained on-site. In triaxial compression tests, the specimens used were cylindrical, with a diameter of 100 mm and height of 200 mm (which complies with JGS 0524 (Method for consolidated-drained triaxial compression test on soils)), and the peak particle size of the sample was adjusted by considering the specimen dimensions and maximum particle size. The sample was prepared by mixing a sample with a moisture content of 8% (saturation degree Sr = 68%) with the added amount of stabilizing material shown in Table 1, which shows the relationship between the permanent vertical strain and the number of loadings. Subsequently, the sample was divided into five portions and placed in a cylindrical mold to be compacted to the target compaction degree Dc = 92% [9]. The moisture content was set to the wetter side of the optimal moisture content by approximately 2%, which was the condition for obtaining a significant amount of settlement. The added amount of stabilizing material is shown herein in mass% relative to the dry sample (Table 1).

The test involved conducting isotropic consolidation at a negative pressure of 20 kPa at first, followed by cyclically loading the sample with a haversine wave. The loading conditions were 5,000 loads, a loading frequency of 0.5 Hz, and a confining pressure of 20 kPa. The vertical-stress amplitude was determined by setting the load distribution rate of the rails for a train load of 160 kN to 0.4 [10] and then dividing it by the base area of the sleeper to be used in the full-scale test in the next section. Here, the train load of 160 kN was determined based on the actual axle loads: 90 kN [11] for conventional railways and 110 kN [12] for Shinkansen. For Shinkansen, a dynamic load factor accounting for high-speed impact [10] was applied, whereas for conventional railways, the load was adjusted to reflect the impact factor at rail joints [10]. In the next section, tests in case of *FI*=36% were conducted using PC sleepers (3PR specified in JIS E 1201), which is the bottom area of the sleeper of 0.48 m², installed on conventional lines. And tests in case of *FI*=52% were conducted using PC sleepers (3H specified in JIS E 1201), which is the bottom area of the sleeper of 0.79 m², installed on Shinkansen lines. Therefore, the vertical stress amplitude in case of *FI*=36% was set to 133 kPa and the vertical stress amplitude in case of *FI*=36% was set to 88.6 kPa. The curing time for this method was set to 2 hours after accounting for the time between nighttime work and the first train.

Figure 6 shows that the permanent vertical strain was reduced to approximately 1/8 by adding at least 0.2% of stabilizing material as compared with the case without any measures implemented.

4. Examination of settlement-suppression effect by full-scale test

Cyclic loading tests were conducted on a full-scale track model to examine the appropriate added amount of stabilizing material during actual construction. The test cases used a full-scale model with PC sleeper (3PR) in case of *FI*=36% (Case 1) and PC sleeper (3H) in case of *FI*=52% (Case 2), and the same ballast material as in the cyclic triaxial compression test. The full-scale track model was a ballasted track with one sleeper. Figure 5 shows the particle-size distribution of the ballast. The loading conditions were 300,000 loading cycles, a loading frequency of 5 Hz, a minimum load of 5 kN, and a maximum load of 85 kN. Figure 7 shows the test conditions. The construction procedure for the low-strength stabilization method is as presented in Section 2. Additionally, a cyclic loading test was conducted separately for the new ballast using one PC sleeper (3PR) under the same conditions as this test.

Table 1 Added amount of stabilizing material

FI	added amount of stabilizing material
36%	0% (without stabilizing), 0.02%, 0.2%, 2%
52%	0% (without stabilizing), 0.2%, 0.3%, 3%

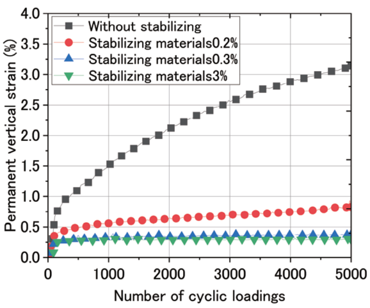

(a) *FI*=36%

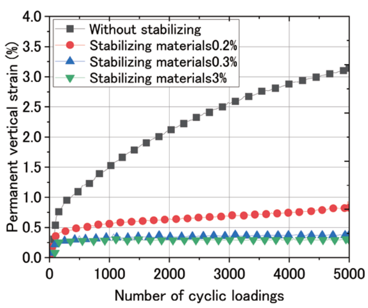

(b) *FI*=52%

Fig. 6 Shifts in vertical strain

Figure 8(a) shows the amount of sleeper settlement in Case 1. In the case without any measures implemented, settlement progressed rapidly from the start of loading and continued to increase gradually, with approximately 32 mm of settlement accumulated after 300,000 cyclic loadings. By contrast, in the cyclic triaxial compression test, the addition of 0.2% stabilizing material, which provided the settlement-suppression effect, resulted in a settlement amount of approximately 26 mm after 300,000 loadings, which corresponded to a reduction by approximately 20% as compared to the case without measures implemented. The less prominent settlement-suppression effect in the cyclic triaxial compression test is attributable to the inability of the stabilizing material to mix uniformly with the ballast when it is mixed with the ballast using a portable tamper in actual construction. Therefore, we considered the variation in the on-site strength and added 2% stabilizing material, i.e., 10 times of the 0.2% stabilizing material. Results showed that the settlement amount after 300,000 loadings was approximately 5.6 mm, which was approximately 1/6 of the amount for the cases without measures implemented. In fact, this amount is similar to the settlement amount yielded when using the new ballast.

5. Tests on a commercial line

5.1 Tests using portable tamper

Tests using portable tamper were conducted in a straight section with an annual passing tonnage of 17 million tons (Fig. 9). The *FI* of the ballast was 24%, significant amount of settlement was indicated and the amount of maintenance required had increased in this area. Excavation was manually conducted for this intervention (Fig. 9(a)), and 2% stabilizing material was added to 15 sleepers before and after the joint where mud pumping had occurred.

Figure 10 shows the longitudinal level irregularity (10 m-chord versine) before and after construction. The maximum longitudinal level irregularity after two months of normal tamping was approximately -11 mm. Meanwhile, the longitudinal level irregularity after 16 months of the intervention using the low-strength stabilization method was approximately -5 mm. The longitudinal level irregularity within the intervention area after 16 months of the intervention using the low-strength stabilization method was reduced to approximately half of what it was before, and a greater settlement-suppression effect compared to conventional tamping was confirmed.

The increase in longitudinal sectional irregularity directly below the joint was approximately -7 mm between one week and 16 months after intervention. Meanwhile, a maximum longitudinal level irregularity of approximately -6 mm was recorded after 16 months of intervention outside the boundary of the intervention area (horizontal position of approximately 7 m). This is attributable to the fact that the overlift amount within the intervention area was relatively large (i.e., approximately 10 mm) and that the intervention area was relatively larger compared to the area outside it.

5.2 Test using tamping machine

A test was conducted using a tamping machine in a straight section with an annual passing tonnage of 5.2 million tons. In this

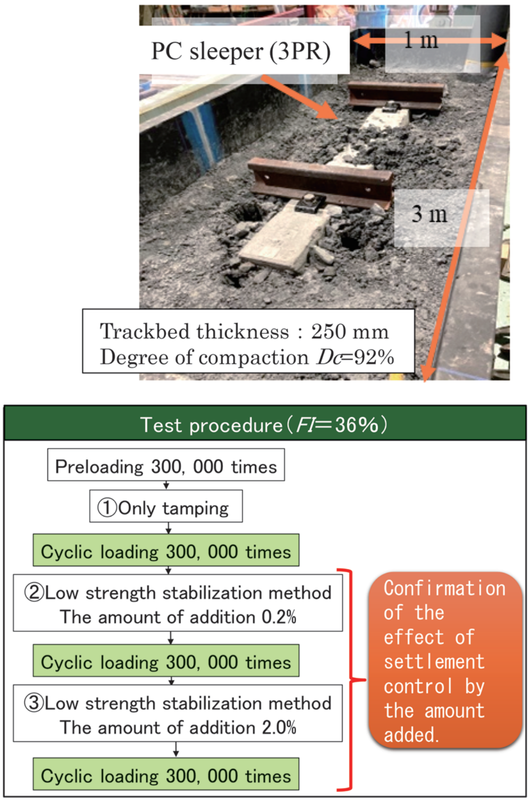

(a) ***FI*=36%**

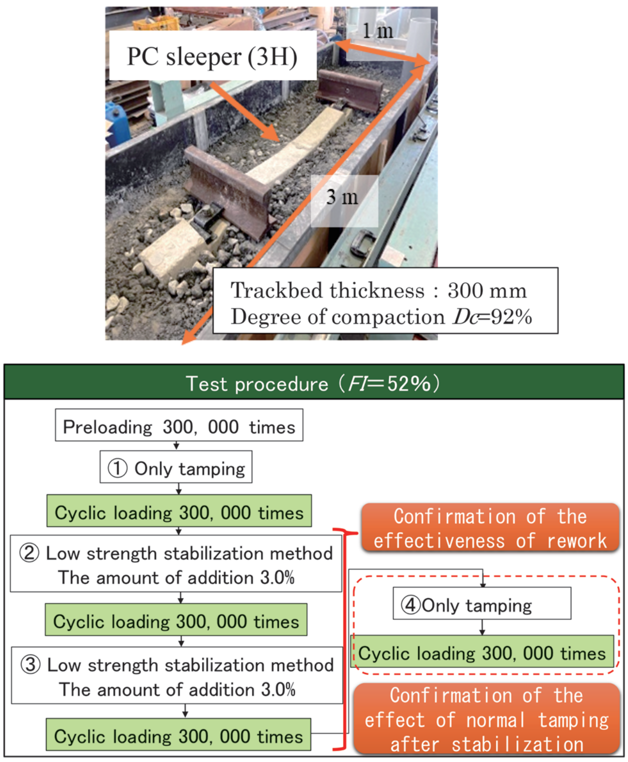

(b) ***FI*=52%**

Fig. 7 Test conditions for full-scale test

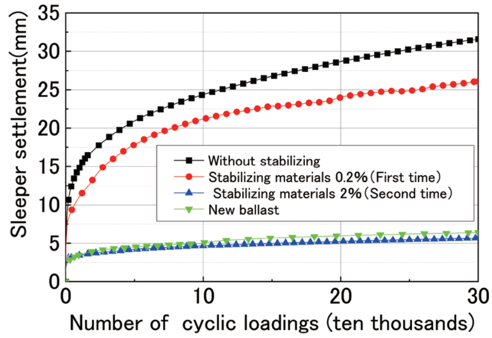

(a) ***FI*=36%**

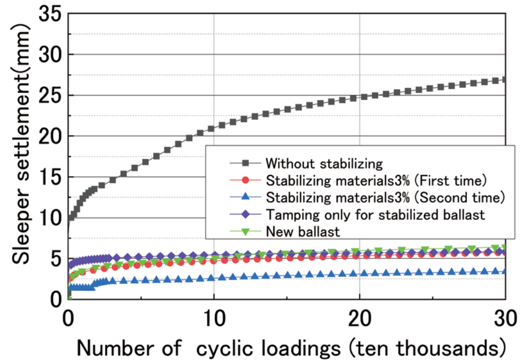

(b) ***FI*=52%**

Fig. 8 Settlement in full-scale test

intervention, 2% stabilizing material was added to six sleepers before and after the joint where mud pumping had occurred. The *FI* of the ballast in this area was 46.5% and a significant amount of maintenance was required.

In this test, no excavation was conducted, and the stabilizing material was dispersed on the ballast surface. In the normal tamping using tamping machine, the tamping tool is opened wide and inserted, whereas the ballast is forcibly pushed from the outside of the sleeper directly below it. Therefore, even if the stabilizing material is dispersed around the sleeper, the stabilizing material might not be sufficiently mixed with the ballast directly below the sleeper. Therefore, we eased the mixing of the stabilizing material with the ballast below the sleeper by narrowing the tamping tool on tamping machine in advance to make it fit along the sleeper and then inserting it into the tamping position, as well as pushing the stabilizing material down to the sleeper bottom (Fig. 11). Finally, we opened the tamping tool and performed tamping in the same manner as in the normal tamping machine construction.

Figure 12 shows the longitudinal level irregularity before and after construction. The maximum longitudinal level irregularity after three months of normal tamping machine repair was approximately -20 mm. Meanwhile, the longitudinal level irregularity after eight months of the intervention using this method was approximately -3 mm, which was approximately 1/7 of the displacement before the intervention.

Additionally, we confirmed that only a trace amount of settlement had progressed between four and eight months after the intervention and that a good track condition was maintained.

(a) Digging

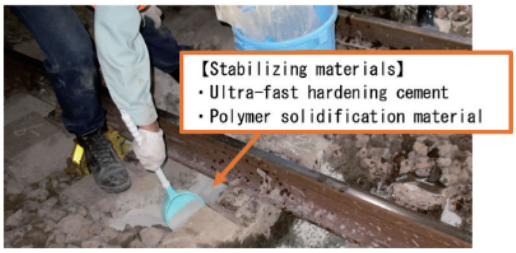

(b) Addition of stabilizing material

(c) Tamping

Fig. 9 Test situation (portable tamper) [5]

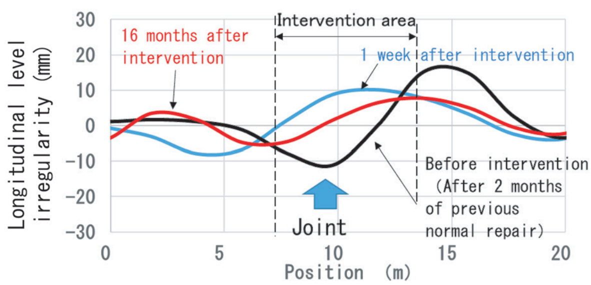

Fig. 10 Longitudinal level irregularity before and after test (portable tamper)

6. Conclusions

We developed a low-strength stabilization method for fouled ballast that suppresses settlement by mixing a stabilizing material composed of ultra-fast hardening cement and a polymer solidification material during tamping. We confirmed the settlement-suppression effect by conducting cyclic triaxial compression and cyclic loading tests using a full-scale track model. Furthermore, we conducted tests using the method on a commercial line to verify the settlement-suppression effect. The main findings obtained are as follows:

a) The fouled ballast with an *FI* of 20% or more was stabilized using stabilizing material, and a cyclic triaxial compression test was conducted. The settlement amount under *FI*=36%, which involved the addition of at least 0.2% stabilizing material, was approximately 1/8 of that for the case without any measures implemented.

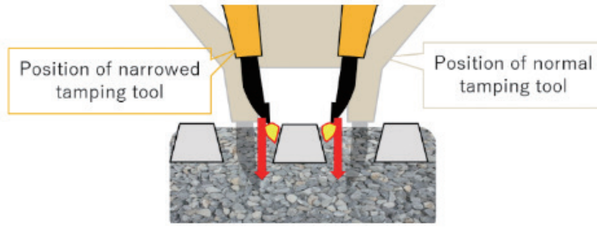

Fig. 11 Tool positions of sleeper and tamping machine

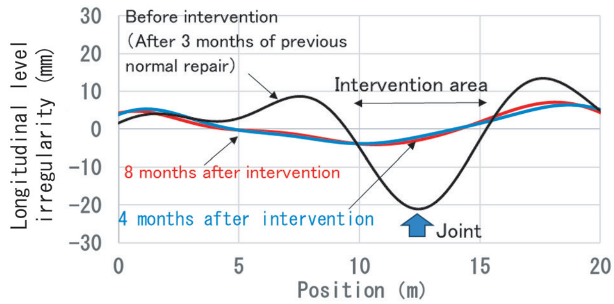

Fig. 12 Longitudinal level irregularity before and after testing (tamping machine) [5]

b) The fouled ballast with an *FI* of 20% or more was stabilized using stabilizing material, and a full-scale test was conducted. The result of the cyclic triaxial compression test showed that by adding 0.2% stabilizing material by cyclic triaxial compression test, which yielded the settlement-suppression effect, settlement was reduced by approximately 20% compared when no measures were implemented. The settlement-suppression effect was speculated to have been weakened because of variations in strength caused by the use of a portable tamper.

c) A test was conducted in an on-site fouled ballast with an *FI* of 20% or more, in which 2% stabilizing material was added using a portable tamper. The results showed that the longitudinal level irregularity within the intervention area after 16 months of the intervention reduced to approximately half the longitudinal level irregularity after two months of normal tamping. Additionally, a greater settlement-suppression effect was achieved compared with conventional tamping.

d) A test was conducted in an on-site fouled ballast with an *FI* of 20% or more, in which 2% stabilizing material was added using a tamping machine. The results showed that the longitudinal level irregularity within the intervention area after eight months of the intervention reduced to approximately 1/7 of the longitudinal level irregularity after three months of normal tamping. Additionally, a greater settlement-suppression effect was achieved compared with conventional tamping.

Acknowledgment

We would like to express our gratitude to the West Japan Railway Company and the Shikoku Railway Company for their cooperation in this test construction.

References

[1] Nakamura, T., Momoya, Y., and Kijiya, I., "Clarification of Mechanism of Ballast Crushing and Grain Refining Progress and Proposal of Remaining Life Prediction Method," *RTRI Report*, Vol. 35, No. 4, pp. 35-40, April 2021 (in Japanese).

[2] Jose, P. and André, D., "Railway ballast degradation," presented at *15th Swiss Transport Research Conference*, Ascona, Switzerland, April 15-17, 2015, pp. 1-26.

[3] Nakamura, T., Momoya, Y., and Kijiya, I., "Performance Recovery of Fouled Ballast Without Ballast Replacement," *RRR*, Vol. 76, No. 7, pp. 16-19, July 2019 (in Japanese).

[4] Nakamura, T., Kijiya, I., and Ijichi, T., "Countermeasure Preventing Settlement Using Biodegradable Polymers in Ballasted Track with High Mixture Raio of Fine Particles," *The journal of Japan Railway Civil Engineering Association*, Vol. 55, No. 6, pp. 26-29, June 2017 (in Japanese).

[5] Kageyama, T. and Nakamura, T., "Low-Strength Stabilization Method for Preventing Settlement in Fouled Ballast," *The journal of Japan Railway Civil Engineering Association*, Vol. 60, No. 8, pp. 619-622, August 2022 (in Japanese).

[6] Kageyama, T., Nakamura, T., Kijiya, I., Momoya, Y., Akagi, H., and Saito, R., "Development of low-strength stabilization method for fouled ballasted tracks," *Transportation Geotechnics*, Vol. 34, 100765, May 2022.

[7] Kageyama, T. and Nakamura, T., "Evaluation Method for Ballast Replacement in Railway Ballasted Tracks Damaged by Heavy Rainfall," *The journal of Japan Railway Civil Engineering Association*, Vol. 61, No. 8, pp. 619-622, August 2023 (in Japanese).

[8] Selig, E. T., "Ballast for heavy duty track," *Track Technology: Proceedings of a Conference organized by the Institute of Engineers (ICE) and held at the University of Nottingham, 11-13 July 1984*, pp. 245-252, 1985.

[9] Aoyagi, T., Ishikawa, T., Matsuya, S., Nakamura, T. and Kijiya, I., "Evaluation of Influence of Fine Particles and Moisture Content on Cyclic Deformation Characteristics of Railway Ballast," presented at *53rd Annual Meeting of the Japan National Conference on Geotechnical Engineering*, Aichi, Japan, July 12-14, 2018, pp. 1185-1186 (in Japanese).

[10] Railway Technical Research Institute, *Design Standards for Railway Structures (soil structure)*, Maruzen Publishing Co., Ltd., Tokyo, Japan, p. 612, 2013 (in Japanese).

[11] Japan Transport Engineering Company, https://www.j-trec.co.jp/company/070/04/jtr04_088-093.pdf (Reference date : April 4, 2024).

[12] SHINSEI Publishing Editorial Department, *Complete Illustrated Guide to the Mechanism of Shinkansen, Revised Edition*, SHINSEI Publishing, p. 21, 2010 (in Japanese).

Authors

Takahiro KAGEYAMA, Ph.D.
Researcher, Track Structures & Geotechnology Laboratory, Track Technology Division
Research Areas: Ballasted Track

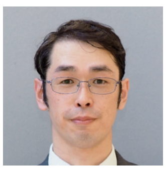

Takahisa NAKAMURA, Ph.D.
Senior Chief Researcher, Track Structures & Geotechnology Laboratory, Track Technology Division
Research Areas: Ballasted Track

Masaru HOJO
Researcher, Track Structures & Geotechnology Laboratory, Track Technology Division
Research Areas: Ballasted Track, Ballastless Track

Fumika TAJIMA
Researcher, Track Structures & Geotechnology Laboratory, Track Technology Division
Research Areas: Ballasted Track

Increase in Tangential Force by Ceramic Particles under Low Adhesion Conditions

Shinya FUKAGAI
Frictional Materials Laboratory, Materials Technology Division

Takemasa FURUYA
Traction Systems Laboratory, Vehicle Technology Division

Ryo TAKANO
Tess Co., Ltd

Railway wheel spinning and sliding caused by leaves on the line in autumn affect operational safety and regularity. This paper reports on results of braking tests using a vehicle equipped with apparatus for applying ceramic particles to rails to enhance adhesion. To ensure uniform conditions along the rails and minimize differences between test trials, low adhesion conditions were simulated by applying paper tape to the top of the rail. The tangential coefficient at the beginning of the wheel slide increased with the amount of ceramic particles applied. The larger the area of holes made by the particles in the paper tape, the higher the tangential force during sliding. These findings will be useful in designing new adhesion enhancers and evaluating their performance.

Key words: *slippery rail, adhesion, ceramic particle, sanding*

This paper is published in Wear Vol 530-531 (2023) 205001 "Penetration of contaminated film on rails by ceramic particles and increase of traction force," © 2023 Elsevier B.V., doi.org/10.1016/j.wear.2023.205001.

1. Introduction

Railway wheel spinning due to low adhesion with rails can cause train delays or cancellations. Sliding while braking can result in overrunning, which is a safety concern. Furthermore, spinning and sliding can cause damage to components, for example rail burns and wheel flats.

The application of sand or other hard particles from vehicles is typically used to mitigate low wheel/rail adhesion. In Japan, sand particles of a few millimetres in diameter have been applied to the rails using a principle similar to that of gravitational force since the era of old steam locomotives. However, during high-speed running of the vehicle, the proportion of sand actually landing on the wheel–rail interface was low because most of it was blown away by wind, or bounced off the rail surface as it fell during high speed running. [1]. In Japan, another process was developed to overcome the problems of using sand. This process employed hard ceramic particles (e.g., alumina) with a diameter of approximately 0.3-0.4 mm spread in small quantities (e.g., 30 g/min) using compressed air [1]. This technology has been widely used in Japan since the 1990s for conventional locomotives and diesel trains, as well as for high-speed trains such as the Shinkansen. This method has also been applied to trains on Taiwan's high-speed rail network [2, 3]. Furthermore, low-pressure injection systems have been developed for vehicles without compressors and are now installed on many conventional rail vehicles in addition to vehicles without compressors [4]. These particle applications are not only used in high-speed railways but also widely employed across Japan's conventional railways network, particularly in sections with steep gradients. Figure 1 shows a photograph of the particle applicator. The hard particles are primarily composed of ceramic particles, such as alumina, with a diameter of approximately 0.3–0.4 mm, which is significantly smaller than natural sand used in older sanding devices where particles have a diameter of several millimeters.

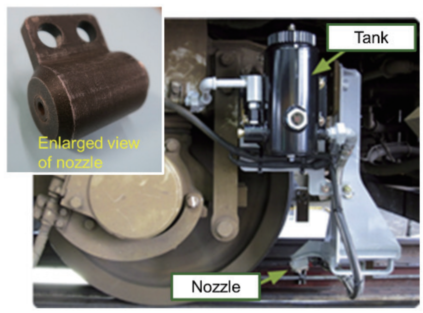

Fig. 1 Photograph of particle applicator.

Low adhesion can be caused by several factors. On high-speed railways, which operate mainly on viaduct tracks, water films caused by rain and condensation lead to low adhesion. These films are typically of the order of 1 μm or less [5], and a slight increase in roughness can be considered to contribute to improving adhesion. However, the thick films that form on rails in mountainous sections of the track can be a more serious problem in the autumn. Leaves blown onto lines by passing trains, are crushed by rails and wheels, and stick to the railhead surface. Moisture from morning dew causes repeated reactions between the leaves and rail, resulting in the gradual formation of a tough film. The thickness of this film has been reported to be of the order of several tens of micrometers [6], and particles significantly thicker than water film may be present. These conditions call for suitable adhesion enhancers.

One paper offers a review of the studies which have been carried out on materials applied to the wheel/rail interfaces to recover adhesion and methods used to apply these materials [7]. For example, Lewis et al. investigate the effects of different hose type, mounting angle, and nozzle on the amount of material fed to the interface using full-scale rigs [8]. Ban et al. investigate the effect of hard particle size on wheel/rail friction using a full-scale friction machine

[9]. They conduct tests under low adhesion conditions using paper tapes simulating the leaf layer and reported a higher tangential force with larger particles than with smaller particles. Skipper et al. investigate the effects of three different sand types under dry, wet, and leaf extract-contaminated conditions using a high-pressure torsion test [10]. The results of their study show that under low adhesion conditions, adhesion increased with particle size. In addition, when contaminated with leaf extract, larger particles are more likely to cause breakage of the leaf film [11]. Arias-Cuevas et al. investigate the effect of sand particle size on wheel–rail adhesion using a wide range of particles with particle sizes varying from a few hundred micrometers to a few millimeters [12, 13]. Their results of field tests show that the coefficient of friction decreases with increase in particle size. The reason for this is not only that particles are more likely to be trapped at the wheel/rail interface, but also that extremely fine sand can be incorporated into the contaminant and lose [13].

As mentioned above, although the differences between the properties and effects of different adhesion enhancers have been investigated from various perspectives, many aspects remain unknown. In this study, the effects of differences in the amount of adhesion enhancer and particle size were investigated using a simple, uniform film of paper tape simulating a thick contaminant, such as leaves on the line. In the tests, an actual vehicle was driven on a test track, and braking tests were performed while the adhesion enhancer was fed from an onboard injection system. Paper tape was stuck to the surface of the rails to recreate low adhesion and a uniform film. After the test, the condition of the paper tape was observed to determine its effect on the friction properties.

2. Methodology

2.1 Test vehicle

Figure 2 shows a photograph of the test train. Tests were conducted on a test track at the Railway Technical Research Institute (RTRI). The test vehicles were the R291 series (two vehicles) owned by RTRI. The second bogie, one of the four bogies in the traveling direction, was equipped with motors.

Figure 3 shows a schematic diagram of the mounting positions of the test equipment on the test train. An apparatus for applying ceramic particles between the wheel and rail was installed in front of the bogie with motors.

Figure 4 shows the photographs of the test devices mounted on the second bogie. The nozzles for injecting the ceramic particles were mounted at an angle to allow them to inject the ceramic particles into the wheel/rail contact interface (Fig. 4(a)). A photoelectric sensor (Fig. 4(b)) was used to confirm that the vehicle was in the test section. Two water spray nozzles (Fig. 4(c)) were mounted on the rear axle of the bogie to clean the wheel tread outside the test section. Photoelectric sensors were installed to project light vertically and detect the light reflected from the targets (reflectors) placed on the track in the test section.

2.2 Test conditions

Figure 5 shows the test site for the test train. Paper tape was stuck to the top of the rail to ensure uniform conditions along the rail and minimize differences between test trials (50 mm wide × 0.14 mm thick). The use of paper tape on rails to recreate low adhesion conditions during tests on actual tracks has been reported by the Rail Safety and Standards Board in the UK [14]. The actual thickness of the leaf layers was reported to be between 5–100 μm [6, 15], and the test conditions in this study were made to be slightly more severe compared with these values. However, the present study focuses on the effect of the quantity and size of the applied particles on adhesion. In order to emphasize these parameters, other parameters have to be as uniform as possible. Therefore, in this study, paper tape was used for simplicity, as has been done by other researchers in the past.

The test train was operated using only the electric brake of the powered bogie. The test train in this study used a special program that increased the braking force linearly after braking was initiated. This made it possible to calculate the train's acceleration and deceleration using the motor current, motor torque, and vehicle dynamic model. When the braking force increases, there comes a point where the wheels start to slide. The program is designed to release the brakes when deceleration falls below a certain threshold for a specific period of time.

Owing to the low conductivity of the paper tape applied to the

Fig. 2 Photograph of the test train.

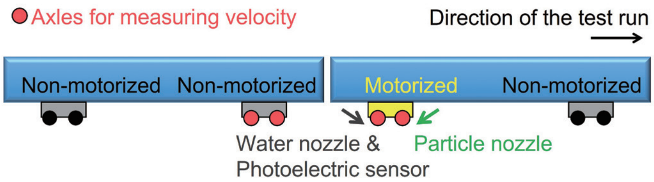

Fig. 3 Schematic diagram of mounting position of test devices on test train

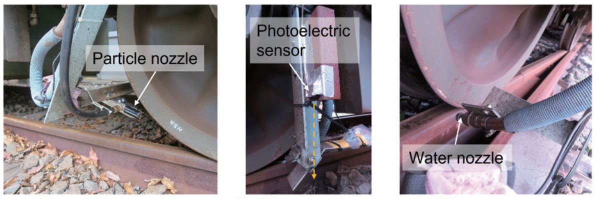

(a) Nozzle for applying ceramic particles (b) Photoelectric sensor to detect the vehicle location (c) Water nozzle to clean the wheel tread

Fig. 4 Photographs of test devices mounted on test train.

Fig. 5 Photograph of test site for the test train

rail, arcing could occur between the wheel and rail because of interruptions in the return current path when the train ran on the rail covered by the tape. Therefore, in this study, the characteristics of the R291 test train which can be operated in battery mode were utilized to prevent the return current from flowing from the wheel to rails. The contact pressure calculated based on the design geometry of the wheel and rail was approximately 650 MPa.

The tangential force F_t on the outer circumference of the wheel was calculated by the following equation:

$$F_t = \frac{T_m \alpha}{r \eta_g} \eta_i \tag{1}$$

where T_m is the motor torque, α is the gear ratio, r is the wheel radius, η_g is the gear efficiency, and η_i is the inverter efficiency. T_m was calculated by multiplying the measured motor current by a factor obtained from the calibration tests. The tangential force coefficient was defined as F_t/F_n, which was value by dividing the tangential force F_t by the static load F_n of the wheelset. Table 1 lists the test conditions used in this study.

The ceramic material used was alumina with two different particle sizes. Figure 6 shows photographs of the ceramic particles.

Figure 7 shows an example of the volume-based size distribution of the ceramic particles. Measurements were performed using a laser diffraction and scattering particle size analyzer (MicrotracBEL, SYNC-ST01). Three trials were conducted for each type of particle and the size distribution of the ceramic particles was obtained. Consequently, the average particle diameters of three trials were 383 μm and 487 μm (median diameter) for the regular and large ceramic particles, respectively. The coefficient of uniformity was 1.64 for regular particles and 1.98 for large particles, indicating that the large particles have a wider distribution of particle sizes compared with the regular particles. Note that the calculation of the coefficient of uniformity was made under the assumption of uniform density, based on the volume-based particle size distribution.

Table 1 Test conditions

Parameter	Value
Initial speed (target)	30 km/h
Injection pressure	500 kPa
Amount of ceramic particles applied (target)	60, 130, 200 g/min
Average diameter of ceramic particles (Median diameter)	383 μm (regular size); 487 μm (large size)

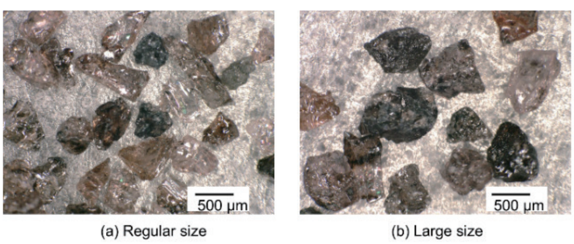

Fig. 6 Photographs of ceramic particles: (a) regular size normally used in applicator, (b) large size

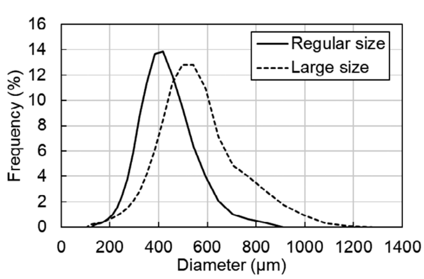

Fig. 7 Example of the results of measuring the size distribution of ceramic particles (volume-based)

2.3 Test procedure

Figure 8 shows a schematic diagram of the test procedure. Prior to the test, several conditioning runs were conducted to remove surface rust. The following steps (i)–(v) were repeated during the test.

(i) The test vehicle begins to travel and accelerate to a target speed (30 km/h).

(ii) Application of ceramic particles and braking are conducted before the motorized bogie enters the low-adhesion zone. At this time, only the electric brakes of the motorized bogie are operated (the braking force increases gradually and linearly).

(iii) F_t/F_n is obtained when sliding is detected in the low adhesion zone.

(iv) The test is considered as completed when the motorized bogie passes through the low adhesion zone.

(v) The paper tape is removed from the rails. The top of the head is then ground and cleaned using a rail grinder. Since a grinder with a dust collection function is used, little dust is generated. However, the presence of dust is checked and cleaned. The wheels are cleaned using a water spray outside the test zone when the vehicle comes back.

At the end of the test, the tape was removed and placed on a transparent polyethylene terephthalate film for storage. The film was placed on an LED panel where light was projected from below and it was photographed from above, to examine holes created in the tape by the application of ceramic particles. Figure 9 shows the locations of the paper tape samples collected for analysis. To mini-

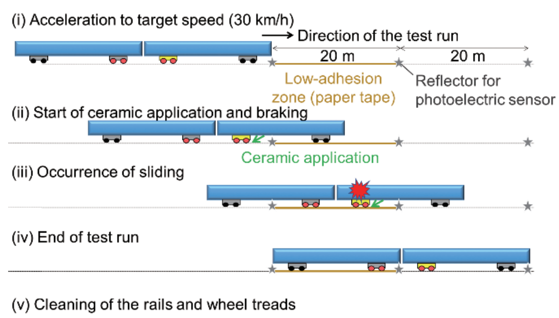

Fig. 8 Schematic diagram of test procedure

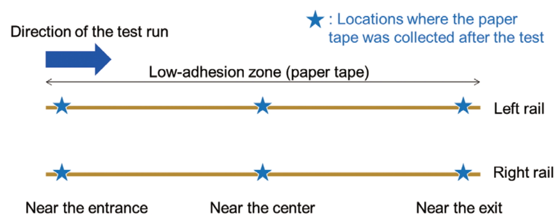

Fig. 9 Locations of paper tape samples collected for analysis

mize the effects of changes of the injection and vehicle running conditions, and the rail geometry on the creation of hole, to the extent possible, during each test the samples were taken from a total of six points on the left and right rails at three locations, namely, near the entrance, center, and exit of the test zone. The length of each sample taken at the six sampling locations was approximately 280 mm, and the total length of samples collected per test was over 1.5 m.

All photographs were trimmed to sizes of (1) 45 × 45 mm, (2) 45 × 90 mm, or (3) 45 × 135 mm in the sleeper and longitudinal directions. The length in the sleeper direction was 45 mm, because the width of the paper tape was 50 mm and was not strictly parallel to the camera when photographed. For the longitudinal direction, (3) was selected when there were no particular problems to minimize the influence of the distribution bias, sizes (2) or (1) were selected for paper tapes that tore when removed from the rail.

3. Results of experiments

3.1 Change in tangential force coefficient during the test

Figure 10 shows an example of the changes in each measured parameter during the test. The bottom line represents the values measured using a photoelectric sensor. The data between the first and second peaks from the left were obtained when the motorized bogie traveled in the low adhesion zone which was simulated by paper tape. The second line from the bottom (dotted line) shows the operating status of the particle applicator, with the higher and lower values representing the operating (ON) and non-operating (OFF) states, respectively. The application of ceramic particles and the braking action occurred before the motorized bogie entered the low-adhesion zone. F_t/F_n began to increase approximately 2 s before the motorized bogie entered the low adhesion zone and peaked at the middle of the test zone. A difference was observed in the velocity change between the non-motorized and motorized axles at the peak F_t/F_n. Only the motorized axle slid, since braking force was not imposed on the non-motorized axle. As mentioned in section 2.2, the braking force was programmed to decrease when deceleration fell below a threshold value for a certain period of time. Therefore, the tangential force decreased and the velocity difference reduced, so that F_t/F_n peaked. The peak of F_t/F_n is the tangential coefficient at just before the start of the slide and will be hereafter referred to as the $(F_t/F_n)_{peak}$.

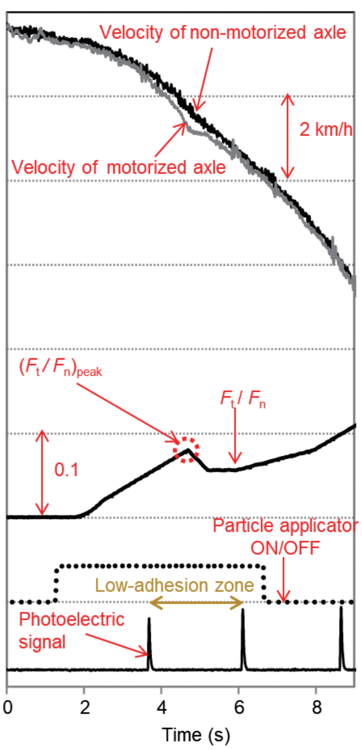

Fig. 10 Example of change in each measured item during the test.

3.2 Relationship between amount of ceramic particles applied and $(F_t/F_n)_{peak}$

Figure 11 illustrates the relationship between the amount of ceramic particles applied to the wheel-rail interface per minute and the $(F_t/F_n)_{peak}$. For both particle sizes, the $(F_t/F_n)_{peak}$ increased with the amount of ceramic particles applied. For a large particle, the $(F_t/F_n)_{peak}$ tends to be higher. On the other hand, for regular particles, the adhesion increased linearly with the number of ceramic particles applied. However, for the large particles, the increase in the amount of ceramic particles was not linear with respect to the amount of ceramic particles applied per minute.

3.3 Relationship between amount of ceramic particles applied and number of holes made

Figure 12 shows examples of the photographed rail surfaces after the test: (a) before removing the paper tape and (b) after removing the paper tape. It is noted that the two locations are not the same. The tiny white particles scattered on the rail shown in Fig.12(a) are assumed to be crushed ceramic particles. This is because ceramic particles are white when crushed. The white particles shown in Fig.12(b) can be seen more clearly, with many particles having penetrated the paper tape. At the time of manufacture, the thickness of the paper tape was 0.14 mm. However, when the thickness was measured after the test, using an electromagnetic film thickness gauge (Elcometer, 456 Coating Thickness Gauge), the thickness was approximately 0.09 mm, indicating that the thickness had decreased due to contact between the wheel and the rail.

Figure 13 shows photographs of the paper tapes obtained after the tests, which were binarized for visual clarity. The paper tapes obtained from the tests in which (a) regular particles were injected

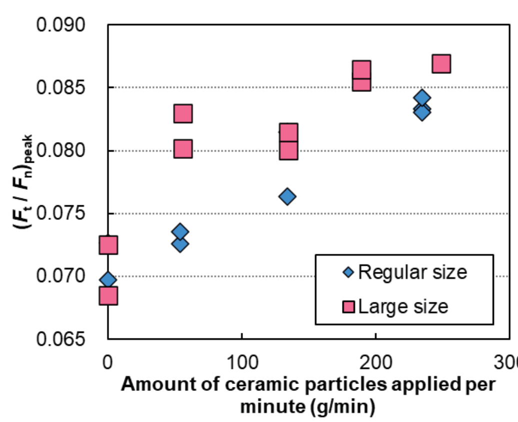

Fig. 11 Relationship between amount of ceramic particles applied per minute and $(F_t/F_n)_{peak}$

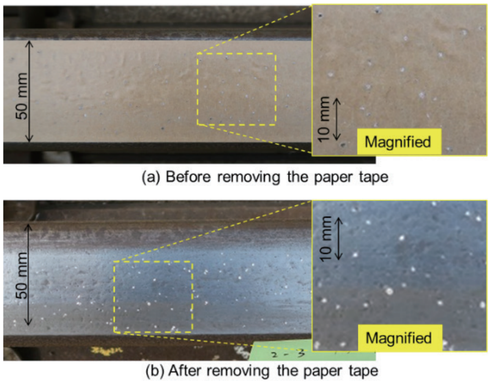

Fig. 12 Examples of the rail surface after testing with large particles (each of the two photos is taken at different location).

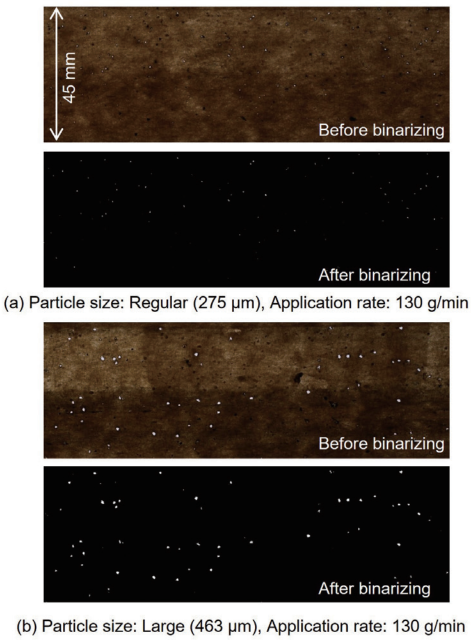

Fig. 13 Photographs (binarized for visual clarity) of paper tapes obtained after the tests

and (b) large particles were injected, are shown together for comparison. Numerous holes were observed in both cases. The holes shown in (b) are clearly larger than those shown in (a). It is assumed that this is due to the holes created in the tape by the compression of the particles applied between the wheel and rail.

Figure 14 shows the relationship between the amount of ceramic particles applied per minute and the number of holes made per meter of paper tape. The number of holes per meter of the paper tape was obtained by counting the number of holes within a specified range (e.g., 45 × 135 mm), based on binarized data, and extending it to a length of 1,000 mm. Six paper tapes were obtained near the entrance, as well as at the center and exit of both the left and right rails of the low adhesion zone to determine the number of holes. Average values per meter were obtained and plotted. For the regular particles, the number of holes increased linearly with the amount of ceramic particles applied, whereas for the large particles, the number of holes increased nonlinearly. This difference can be attributed to the presence of smaller particles, which are more likely to be homogeneously dispersed between the wheel and rail.

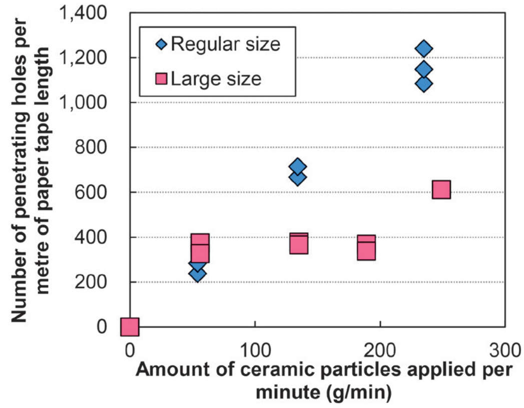

Fig. 14 Relationship between amount of ceramic particles applied per minute and number of holes made per meter of paper tape.

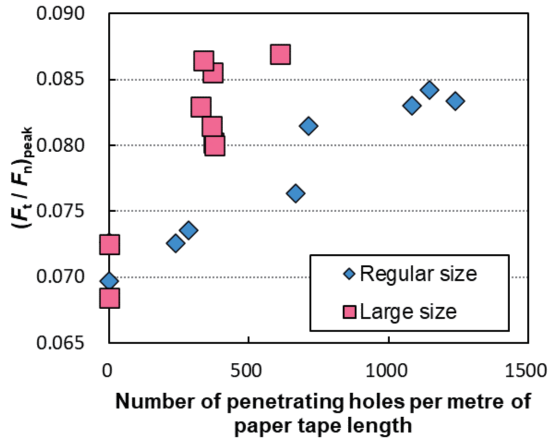

Fig. 15 Relationship between number of penetrating holes per meter of paper tape length and $(F_t/F_n)_{peak}$.

3.4 Relationship between number of holes per meter length of paper tape and $(F_t/F_n)_{peak}$

Figure 15 shows the relationship between the number of holes per meter of the paper tape and the $(F_t/F_n)_{peak}$. For the regular particles, the $(F_t/F_n)_{peak}$ tended to increase linearly with the number of holes per meter of the paper tape. A similar trend of the $(F_t/F_n)_{peak}$ increasing with the number of holes was observed for the large particles, although not as clearly as that for the regular particles.

4. Discussion

In Figs 11 and 14, the $(F_t/F_n)_{peak}$ and number of holes increase with the amount of particles applied respectively, suggesting a possible correlation between them. Figure 11 shows a good linear relationship between the $(F_t/F_n)_{peak}$ and the amount of regular particles. On the other hand, the same figure shows large enough deviation from the linear relationship for the large particles: $(F_t/F_n)_{peak}$ in particular rises when the amount of ceramic is applied at 60 g/min. A similar trend to this was observed in the relationship between the feed rate of the ceramic particles and the number of holes, as shown in Fig. 14. Regular particles are relatively small and numerous and can be distributed uniformly across the wheel-rail interface, resulting in a linear relationship between the number of holes in the tape and the amount applied. In contrast, large particles may be relatively nonuniform, resulting in an irregularly large number of holes in the tape, such as at 60 g/min. Another factor that may contribute to this variation is the difference in the uniformity of the particle size distribution. From the size distribution of particles in Fig. 7, it can be seen that the size distribution in large particles is wider than that in regular particles. Also, the coefficient of uniformity of large particles was larger than regular particles (regular particles: 1.64 and large particles: 1.98). These can result in increased variability in particle distribution within the contact area between wheel and rail.

Figure 15 indicates that the tendency for $(F_t/F_n)_{peak}$ to increase with the number of holes in the tape is steeper for large particles than that for regular particles. The reasons for this difference in effect depending on particle size are discussed below. Figure 13 shows that the holes formed on the paper tape when larger particles are applied are larger than those formed on the paper tape when regular particles are applied. Figure 16 shows the relationship between the approximate hole area and $(F_t/F_n)_{peak}$. Assuming that the increase in tangential force when ceramic particles are crushed at the wheel rail interface is proportional to the projected area of the particles, the hole area was determined by multiplying the number of holes made by the projected area per particle (the area was calculated using the mean radius on the basis of the assumption of the particles as spherical particles). The method of simply reading the sum of the white areas from the binarized data was not chosen. This is because that the tape could have been torn during penetration, and subsequent enlargement of the hole could have occurred when it was removed from the rail.

We compare the relationship between the number of holes and the $(F_t/F_n)_{peak}$ shown in Fig. 15 with the relationship between the penetrated area per meter and the $(F_t/F_n)_{peak}$ shown in Fig. 16. It was found that the relationship in Fig.16 more than the relationship in Fig.15 is closer to a linear relationship regardless of the size of the particles. This could mean that the ceramic particles that penetrated the paper tape film mainly transmitted the tangential forces between the wheel and rail. The effect of hard particles on increasing the $(F_t/F_n)_{peak}$ could be due to several factors such as roughening of the wheel or rail and cleaning of the surface. However, Fig. 16 also suggests that the penetration of ceramic particles through the low adhesion coating is one of the factors that increase the tangential force between the wheel and rail. Therefore, efficiently breaking through the low adhesion coating is considered an effective approach to increasing the $(F_t/F_n)_{peak}$. Figure 17 shows the ratio of the number of tape-penetrating ceramic particles to the number of regular and large particles applied respectively. The number of particles applied was determined by dividing the overall weight by the average weight of one particle. The average weight per particle was obtained by dividing the weight of dozens of particles by the number of particles counted actually. The values are the averages of test results, and the error bars indicate the maximum and minimum values. This suggests that the large particles may have penetrated the paper tape used in this test more easily than regular particles. Related to the trend described in the above, Skipper et al. investigate the effect of particle characteristics on adhesion and surface conditions with high pressure torsion testing [16]. They suggest that small particles could lead to a reduction in leaf-cleaning efficiency due to the reduced area acting on leaves.

As shown in Fig. 16, traction performance depends on the area of holes made in the paper tape, and large particles tend to have larger hole areas than regular particles. As shown in Fig. 13, there was a clear difference in the size of the holes formed in the paper tape between the regular particles and large particles. It is possible that the alumina particles, which are incompressible, were crushed, remained on the rail, and penetrated the paper tape due to the pressure created between the wheel and rail. Considering the difference in diameter of approximately 0.4 mm and 0.5 mm, it may seem like a small difference, but simple calculations show that the projected area increases with the square of the diameter (radius) of the particle. It is estimated that the projected area per particle of large particle is approximately 1.5 times to that of a regular particle. Furthermore, the volume increases in proportion to the cube of the sphere's diameter, so that the difference in lateral spreading during compression may become even greater. In addition, the particle size has a certain degree of spread, so the effect of particle size on penetrating the paper tape may be even greater than the average size. However, as mentioned above, it cannot be simply said that the only increase in the particle size increases the tangential force. This is because large particles may lead to uneven action at the interface. In the future, more systematic studies are required to examine the relationship between film thickness and particle size, as well as particle behavior during compression.

The experimental data here demonstrates the importance of applying particles with properties that resist film thickness, which inhibits metal contact between the wheel and rail, in order to in-

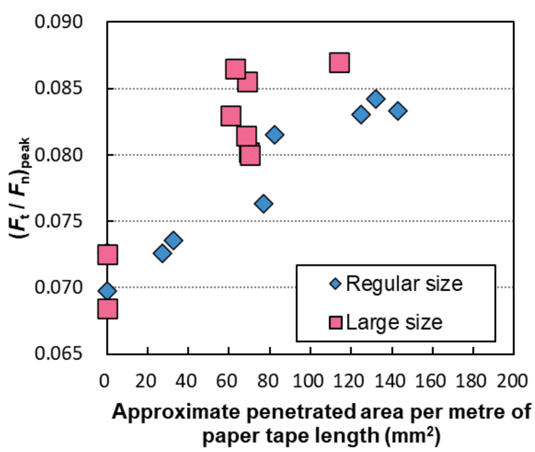

Fig. 16 Relationship between approximate penetrated area per meter of paper tape and $(F_t/F_n)_{peak}$.

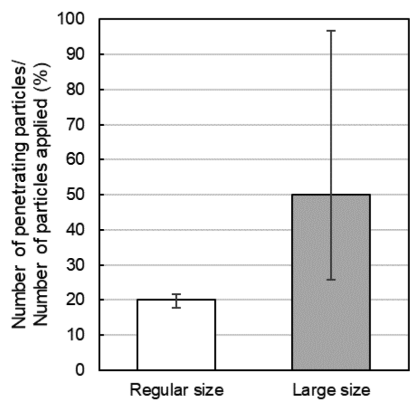

Fig. 17 The ratio of the number of tape-penetrating ceramic particles to the number of regular and large particles applied respectively. The error bars indicate the maximum and minimum ranges.

crease the tangential force. These findings will be useful not only in designing new adhesion enhancers, but also in evaluating their relative performance. This is because measuring traction requires a significant amount of effort, whereas observing films is relatively easy.

5. Conclusions

This study investigated the tangential force during braking with the application of an adhesion enhancer. A vehicle equipped with an apparatus for applying ceramic particles as adhesion enhancers was used for the tests. Low-adhesion conditions due to thick films formed by leaves on the line in autumn were simulated to recreate a simple but uniform film using paper tape. The following conclusions were drawn from the test results:

1. The larger the amount of ceramic particles applied, the higher the tangential coefficient at the beginning of the wheel slide. For regular size ceramic particles (mean particle size of 0.4 mm), the tangential force increased linearly with flow rate. For large particles (mean particle size of 0.5 mm), the tangential force tended to deviate from linearity, when a small amount (60 g/min) of large ceramic particles was applied, compared with regular particles, due to the increased tangential force.
2. A linear relationship was observed between the number of holes formed through the paper tape after the test and the tangential coefficient at the beginning of the wheel slide.
3. It was assumed that the product of the number of holes formed in the paper tape and the projected area per particle could be used to estimate the penetrated area of the paper tape. The relationship between the approximate penetrated area and the tangential coefficient at the beginning of the wheel slide was closer to a linear relationship regardless of the size of the particles.
4. In the presence of a thick film on the rail, it could be important to ensure that hard particles, such as adhesion enhancers, penetrate the film sufficiently.

References

[1] Ohno, K., Ban, T., Obara, T. and Kawaguchi, K., "Adhesion improvement with jetting ceramics particles in high speed running," *Quarterly Report of RTRI*, Vol. 35, pp. 218-220, 1994.
[2] RSSB, "Sand alternatives to boost adhesion (S316) v2.0," 2019.
[3] Ohno, K., Matsuoka, K. and Watanabe, K., "Slip prevention particle injection device," EP1182109A1, 2002.
[4] Ohno, K., Gushima, K. and Honda, K., "Sanding device, especially for railway vehicles," EP1407952A1, 2004.
[5] Chen, H., Ban, T., Ishida, M. and Nakahara, S., "Influential factors on adhesion between wheel and rail under wet conditions," *Quarterly Report of RTRI*, Vol.53, pp. 223-230, 2012.
[6] Fulford, C. R., "Review of low adhesion research," *RSSB Report*, CRF04002., 2004.
[7] Skipper, W. A., Chalisey, A. and Lewis, R., "A review of railway sanding system research: adhesion restoration and leaf layer removal," *Tribology-Materials Surfaces & Interfaces*, Vol. 12, pp. 237-251, 2018.
[8] Lewis, S. R., Riley, S., Fletcher, D. I. and Lewis, R., "Optimisation of a railway sanding system for optimal grain entrainment into the wheel–rail contact," *Proc. Inst. Mech. Eng. Part F J. Rail Rapid Transit*, Vol. 232, pp. 43-62, 2018.
[9] Ban, T., Fukagai, S., Takano, R. and Ohno, K., "Investigation of the Adhesion Promoting Materials (APM) for Wheel Slip Prevention in Autumn," *Proceedings of the conference J-Rail-2014*, 2014 (in Japanese).
[10] Skipper, W. A., Chalisey, A. and Lewis, R., "Particle characterisation of rail sand for understanding tribological behaviour," *Proc. 11th Int. Conf. Contact Mech. Wear Rail/wheel Syst. C. 2018*, pp. 886-895, 2018.
[11] Skipper, W. A., Nadimi, S., Chalisey, A. and Lewis, R., "Particle characterisation of rail sands for understanding tribological behaviour," *Wear*, Vol. 432-433, No. 7, p. 202960, 2019.
[12] Arias-Cuevas, O., Li, Z. and Lewis, R., "A laboratory investigation on the influence of the particle size and slip during sanding on the adhesion and wear in the wheel-rail contact," *Wear*, Vol. 271, No. 1-2, pp. 14-24, 2011.
[13] Arias-Cuevas, O. and Li, Z., "Field investigations into the adhesion recovery in leaf-contaminated wheel-rail contacts with locomotive sanders," *Proc. Inst. Mech. Eng. Part F J. Rail Rapid Transit*, Vol. 225, No. 5, pp. 443-456, 2011.
[14] Purcell, L. and Lightroller, A., "Trial of Sander Configurations and Sand Laying Rates (T1107)," *RSSB Report*, No. 2, 2018.
[15] Poole, W., "Characteristics of Railhead Leaf Contamination. Summary Report.," *RSSB Report*, 2007.
[16] Skipper, W. A., Nadimi, S., Watson, M., Chalisey, A. and Lewis, R., "Quantifying the effect of particle characteristics on wheel/rail adhesion & damage through high pressure torsion testing," *Tribol. Int.*, Vol. 179, No. 9, p. 108190, 2023.

Authors

Shinya FUKAGAI, Ph.D.
Senior Researcher, Frictional Materials Laboratory, Materials Technology Division
Research Areas: Friction Management between the Wheel and Rail, Tribology

Takemasa FURUYA, Ph.D.
Assistant Senior Researcher, Traction Systems Laboratory, Vehicle Technology Division
Research Areas: Traction Control Systems, Power Conversion Systems

Ryo TAKANO
General Manager/Technical Manager, TESS Co., LTD

Method for Energy-efficient Timetable Rescheduling for Small-scale Delays

Aiko KUNISAKI **Yoko TAKEUCHI**
Transport Operation Systems Laboratory, Signalling and Operation Systems Technology Division

We proposed a method for energy-efficient timetable rescheduling for small-scale delays using mathematical optimization. In the developed algorithm, the timetable rescheduling is converted for reducing the powering energy and increasing the regenerative energy. We considered passenger convenience under the condition that the total time from the starting station to the terminal station of each train did not change. This paper describes the details of the method for energy-efficient timetable rescheduling and reports the results of a case study using actual railway line data.

Key words: *energy efficiency, small-scale delay, powering energy, regenerative energy, passenger convenience, mathematical optimization*

1. Introduction

These days, the energy issues are attracting a great deal of attention because of concerns about the stability of fossil fuel supplies and increase in global energy consumption. In addition, global environmental issues have led companies in various industrial sectors to work towards the Sustainable Development Goals (SDGs) and achieve carbon neutrality. Over recent decades, Japanese railways, for example, have introduced ground equipment such as energy storage systems and regenerative inverters [1], energy-efficient rolling stock [2] and energy-efficient transport operations [3] to save energy.

There are two major approaches to saving energy in transport operations: the first is through train-driving strategy, to minimize energy consumption during train operation [4]. The second focuses on timetabling, to optimize the running time to minimize powering energy [5, 6]. However, these studies assume that trains can run according to the planned timetable, and do not assume train delays.

Therefore, we proposed a method for energy-efficient timetable rescheduling, in the event of small-scale delays of a few minutes and the need to stop trains at stations [7]. Energy-efficient timetable rescheduling is achieved with a short calculation time of about one minute, based on current timetable rescheduling which adjusts operating intervals caused by train delays. Currently, timetables are usually rescheduled without considering energy conservation ("basic timetable rescheduling"). Consequently, an energy-efficient rescheduled timetable created in the light of each specific delay situation contributes to more energy-efficient train operation. The proposed energy-efficient timetable rescheduling is a method for adjusting the arrival and departure times using mathematical optimization, so that powering energy can be reduced by running slowly and regenerative power interchange can be promoted by coordinating the timing of powering and braking.

In this paper, we report the details of the method for energy-efficient timetable rescheduling and present the results of a case study on actual railway line data. In the case study, we simulated the energy-efficient timetable rescheduling using the Train Operation Power Simulator [8] developed by RTRI and calculated the energy-saving effect.

2. Method for creating energy-efficient timetable rescheduling

2.1 Basic concept of energy-efficient timetable rescheduling

In general, extending the running time can reduce the maximum speed of a train by shortening the powering time, thereby reducing the energy consumption for train operation. In addition, if the regenerative power can be interchanged to a nearby powering train, the energy supplied from the substation can be reduced. Focusing on these two points, we will reduce the energy consumption for train operation by running at low speeds and by coordinating the timing of powering and braking.

When creating energy-efficient rescheduled timetables, the calculation time is aimed at less than one minute in order to update timetable rescheduling according to the delay situation.

Figure 1 illustrates the energy-efficient timetable rescheduling process. The timetable targets the event of a small-scale delay (from dotted line (planning timetable) to solid red line (when small delays occur)), as shown in Fig. 1(a). Then, as shown in Fig. 1(b), trains are sometimes required to have extended stopping time at stations (from dotted line to blue and green solid line) in order to prevent spikes in passenger numbers and also to avoid having trains slow down or come to a stop between stations. This is basic timetable rescheduling.

In this paper we focus on the extended stopping time at station ("suspension time"), in the black dotted circle in Fig. 1(b). As shown in the dotted red and purple circles in Fig. 1(c), the suspension time is allocated to the running time and the stopping time for energy efficient, by reducing the powering energy with running slowly to the next station and by effective use of regenerative power with coordinating the timing of powering and braking. This is the proposed energy-efficient timetable rescheduling.

The terms used in this paper describes: "powering energy" is the energy supplied by the overhead contact line minus the auxiliary energy; "auxiliary energy" is the energy used for purposes other than train running, such as lighting and air conditioning; "regenerative energy" is the energy returned to the overhead contact line by the braking train; and "energy consumption" is the value of powering energy minus the regenerative energy, adding the auxiliary energy. The Train Operation Power Simulator [8] consists of a feeding circuit calculation component, rolling stock calculation component and speed profile calculation component, and enables highly accurate calculation of various energies.

2.2 Passenger convenience

In general, there is a trade-off between energy consumption to operate trains and passenger convenience, so it is necessary to find a balance between the two.

As shown in Fig. 1, the number of trains, the stations where

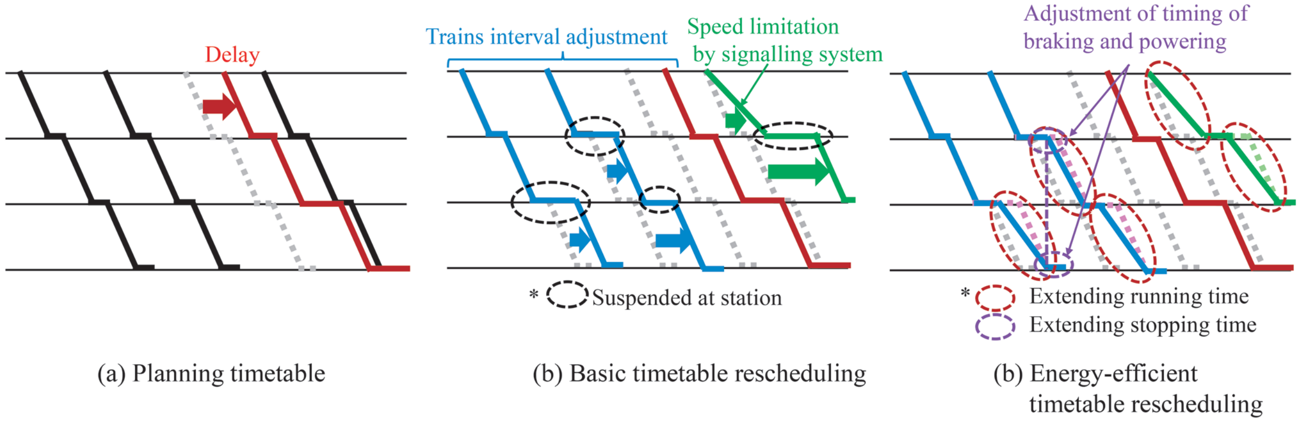

Fig. 1　An example of creating the energy-efficient timetable rescheduling

each train stops, and the number of cars in trainsets are not changed from the planned timetable, so the impact on passengers is kept to a minimum.

Passenger convenience was considered on the condition that the total time from departure to arrival of each train does not change from the basic timetable rescheduling.

In large stations with a large number of passengers or stations with connections to other lines, it may be more desirable to maintain the stopping time at the station rather than aim to improve energy efficiency. For such stations, the arrival and departure times or stopping time can be set to be the same as the basic timetable rescheduling.

2.3 Algorithm for powering energy reduction

Powering energy can be reduced by extending the running time and operating at lower speeds. The extent of this reduction varies depending on the trains and the sections between stations, as it is influenced by factors such as distance, gradients, curves, and other conditions. Therefore, a mathematical optimization algorithm was developed to determine the running time of each train and the sections between stations in order to minimize the total powering energy.

First, we plot the amount of powering energy as a function of the extended running time for each train and section between stations as shown in Fig. 2 ("WT plot"). As shown in Fig. 2, the decrease in powering energy tends to saturate as a function of the extended running time. Therefore, rather than extending the running time of a specific train or section between stations by a large margin, it would be more energy efficient to gradually extend the running time of multiple trains or sections between stations.

Next, based on the basic timetable rescheduling, under the condition that the total time from the departure to the arrival of each train does not change, running time of sections between stations and stopping time at stations of each train are determined with the optimization calculation that minimizes the sum of powering energy. The running and stopping time should be values in multiples of the unit time (e.g., 5 seconds) for creating the train timetable. The formulation of this powering energy reduction algorithm is described in Chapter 3.

2.4 Algorithm for effective use of regenerative power

We developed the algorithm that promotes regenerative power interchange by coordinating the timing of powering and braking. First, we defined the "Regenerating-powering overlap index" as the

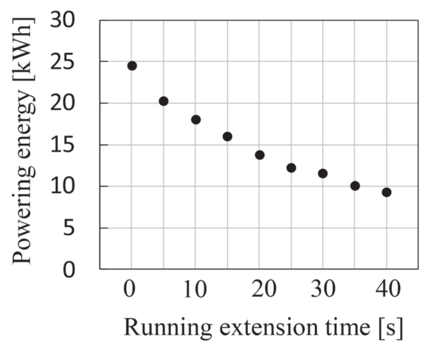

Fig. 2　An example of WT plot

overlap time between braking and powering times of two trains, as shown in Fig. 3. Figure 3(a) shows the timetable with color-coded driving operation. Figure 3(b) shows the Regenerating-power overlap indexes between braking of train 3 and powering of train 2, train 1, zooming in on the blue hatched area of Fig. 3(a).

Considering the Regenerating-powering overlap index there are five possible cases of overlapping relationship between braking time (represented as o_{start}~o_{end}) and powering time (represented as c_{start}~c_{end}), as shown in Fig. 4. An example of Regenerating-powering overlap indexes between train 3 and train 2, and between train 3 and train 1 in Fig. 3(b) are equivalent to Case (3) and Case (2) in Fig. 4, respectively.

When the braking time and powering time do not overlap, the Regenerating-powering overlap index (represented as z) is equal to 0. Otherwise, the Regenerating-powering overlap index is $z_{end} - z_{start}$, where $z_{end} = \min\{o_{end}, c_{end}\}$ and $z_{start} = \max\{o_{start}, c_{start}\}$. So, the Regenerating-powering overlap index z is expressed by (1).

$$z = \max\{0, z_{end} - z_{start}\} \tag{1}$$

When considering the Regenerating-powering overlap index, there is a concern that the calculation time will increase if all combinations for one braking train with other all trains are considered. In addition, even if the timing of powering and braking are adjusted for combinations of one braking train with multiple powering trains, the number of powering trains which can actually interchange regenerative power are limited by distance between trains and voltage conditions of the overhead contact lines. Therefore, powering and braking trains are paired in blocks delimited by distance and time as shown in Fig. 5. In a DC feeding system, the regenerative power interchange generally occurs only between a braking train and its nearby powering train. We divided the area by substations ("substation block," or

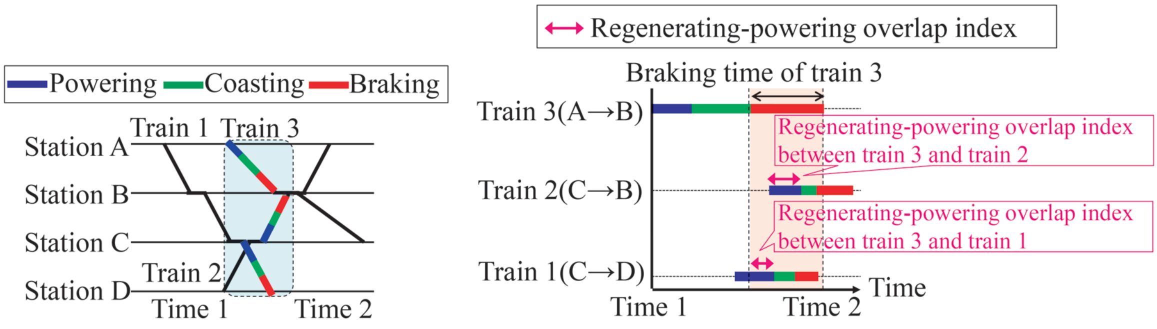

(a) Timetable (b) Status of driving operation

Fig. 3 Definition of the regenerating-powering overlap index

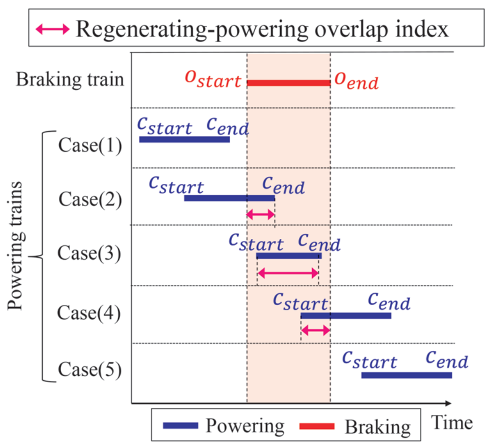

Fig. 4 Divided cases of braking train and powering trains

distance separation, as shown in Fig. 5), and pair trains between stations in the same substation block. In addition, we limit pairings of trains between stations to those braking and powering within a certain period of time (time separation as shown in Fig. 5).

The running time and stopping time of each train at and section between stations are determined with the optimization calculation to maximize the sum of the Regenerating-powering overlap indexes. The formulation of this effective use of regenerative power algorithm is described in Chapter 3.

Note that the speed profile changes as the running time is extended, and the powering and braking times also change. It is necessary to prepare powering and braking time data for each extended running time.

2.5 Compatibility between reducing powering energy and effective use of regenerative power

Figure 6 shows an example of the effect of adjustments to make effective use of regenerative power during powering. As shown in Fig. 6, the arrival and departure times of train 3 is adjustable and the arrival and departure times of trains 1 and 2 are fixed. In order to increase the sum of the Regenerating-powering overlap indexes in Fig. 6(a), the running time of train 3 from station A to station B is shortened as shown in Fig. 6(b). As a result, the sum of the Regenerating-powering overlap indexes will increase, and so will powering energy. Therefore, it is necessary to make the powering energy reduction algorithm and effective use of regenerative power algorithm as compatible as possible.

We introduce a weight parameter, W [kWh/s], to adjust the balance between reducing powering energy and effective use of regenerative energy. The weight parameter, W, represents the expected value of the regenerative energy per second of the Regenerating-powering overlap index, and the value obtained by the sum of the Regenerating-powering overlap indexes multiplied by the weight parameter is considered to have a positive correlation with the regenerative energy. So, based on the algorithms proposed in Sections 2.3 and 2.4, the objective function was set to maximize the sum of the total reduction in powering energy and the total Regenerating-powering overlap indexes multiplied by W, to balance reducing powering energy and effective use of regenerative power. If W increases, increasing the total Regenerating-powering overlap indexes will be preferred over total reduction in powering energy. It is possible to maximize energy efficiency by adjusting W to balance reduction in powering energy and effective use of regenerative power.

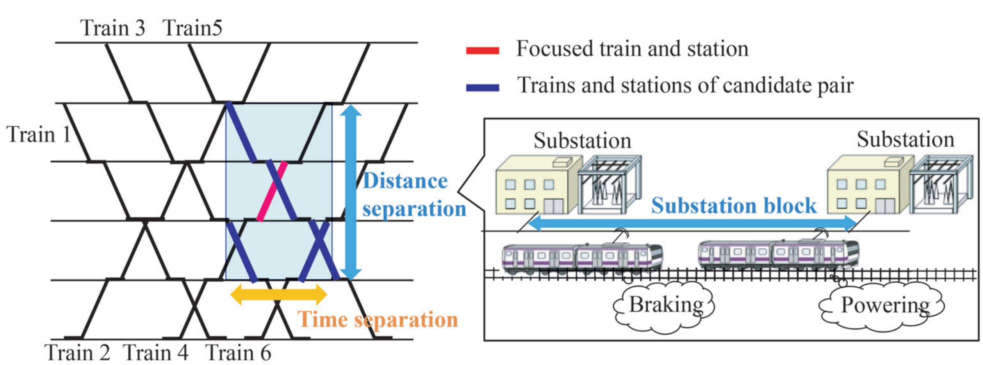

Fig. 5 Candidate pair for timing alignment between powering and braking trains

3. Formulation as a mathematical optimization problem

The algorithms described in sections 2.3 and 2.4 are combined and formulated as a mathematical optimization problem to allow balancing between powering energy reduction and effective use of regenerative power. This chapter describes the formulation with details of the objective function and an overview of the constraints. Table 1, 2 and 3 show the set, constant, variable notation for the

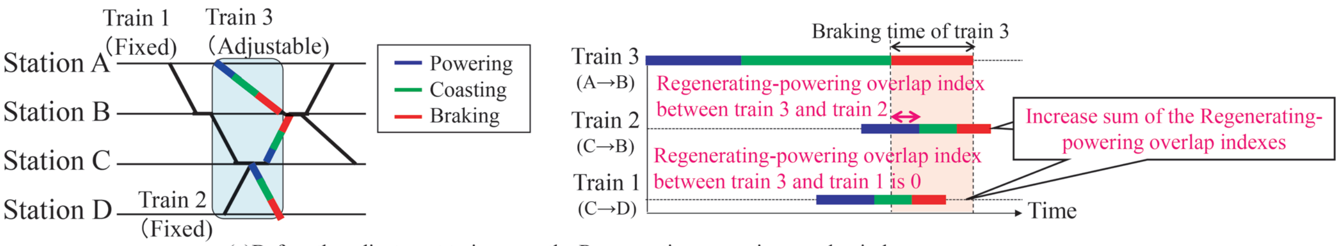

(a)Before the adjustment to increase the Regenerating-powering overlap index

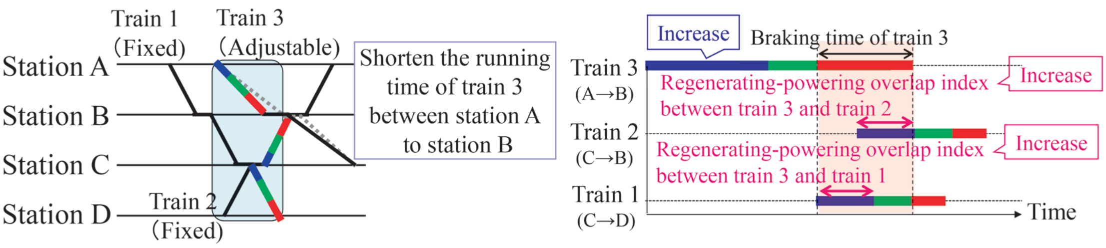

(b)After the adjustment to increase the Regenerating-powering overlap index

Fig. 6 Difficulty of balancing between reducing powering energy and effective use of regenerative power

Table 1 Set notation

Set	Explanation
$\mathcal{A}^{adjust}$	A set of trains of adjusting the running time and stopping time (Represent the element as a^{adjust})
$\mathcal{S}^{adjust}(a^{adjust})$	A set of adjusting sections between stations of adjusting train a^{adjust} (Represent the element as s^{adjust})
$\mathcal{D}(a^{adjust}, s^{adjust})$	A set of candidates for the running extension time of sections between stations s^{adjust} for train a^{adjust} (Reperesent the element as Δd) The extension time is a multiple of the unit time for creating the timetable
$\mathcal{M}(a^{adjust}, s^{adjust})$	A set of candidates for the stopping extension time of sections between stations s^{adjust} for train a^{adjust} (Repere-sent the element as Δm) The extension time is a multiple of the unit time for creating the timetable
$\mathcal{B}^{power}(a^{adjust}, s^{adjust})$	A set of powering trains which considers the Regenerating-powering overlap index when train a^{adjust} is braking between stations s^{adjust} (Represent the element as b^{power})
$\mathcal{S}^{power}(a^{adjust}, s^{adjust}, b^{power})$	A set of sections between stations of train $b^{power} \in B^{power}(a^{adjust}, s^{adjust})$ which considers the Regenerating-power-ing overlap index when train a^{adjust} is braking between stations s^{adjust} (Represent the element as s^{power})

Table 2 Constant notation

Set	Explanation
$\Delta e(a^{adjust}, s^{adjust}, \Delta d)$	The reduction of the powering energy [kWh] when the running time of section between stations s^{adjust} of train a^{adjust} is extended by Δd

Table 3 Variable notation

Variable	Explanation
$x(a^{adjust}, s^{adjust}, \Delta d)$	A variable that is 1 if the running extension time of train a^{adjust} between stations s^{adjust} is Δd, and 0 otherwise
$y(a^{adjust}, s^{adjust}, \Delta m)$	A variable that is 1 if the stopping extension time of train a^{adjust} between stations s^{adjust} is Δm, and 0 otherwise
$z(a^{adjust}, s^{adjust}, b^{power}, s^{power})$	A non-negative variable representing the Regenerating-powering overlap index for braking train a^{adjust} be-tween stations s^{adjust} and powering train b^{power} between stations s^{power}
W	The weight parameter [kWh/s] for adjusting the balance between reducing powering energy and effective use of regenerative power

$$\text{Max} \sum_{a^{adjust}} \sum_{s^{adjust}} \sum_{\Delta d} \left(\Delta e\left(a^{adjust}, s^{adjust}, \Delta d\right) \times x\left(a^{adjust}, s^{adjust}, \Delta d\right)\right) + W \times \sum_{a^{adjust}} \sum_{s^{adjust}} \sum_{b^{power}} \sum_{s^{power}} z\left(a^{adjust}, s^{adjust}, b^{power}, s^{power}\right) \quad (2)$$

formulation. Based on these formulations, calculations were performed using the mathematical optimization solver Gurobi Optimizer (ver. 9.5.1).

Objective function is maximizing the sum of the total powering energy reduction and the total Regenerating-powering overlap indexes multiplied by W, as represented by (2).

The following constraints were considered.

(a) Redistribute the suspension time of the basic rescheduled timetable to the running time and stopping time of the energy-efficient rescheduled timetable.

(b) The departure time of the energy-efficient rescheduled timetable should not be earlier than the planning timetable.

4. A case study using actual railway line data

We report the results of a case study applying the method to actual railway line data to create an energy-efficient rescheduled timetable, as described in Chapters 2 and 3.

4.1 Calculation conditions

The target railway line has 38 stations and is approximately 69 km long. The target train timetable covers one hour during an evening rush hour with 62 trains and 612 trips between stations. Auxiliary power is set according to the ambient temperature of equivalent to 15°C. The planning timetable of the case study is shown in Fig. 7(a). Based on the actual data of past delays, the initial delay of the first train was set to 290 seconds and is indicated by the red line in Fig. 7(a). Figure 7 shows only the area that includes the stations to be adjusted due to the delay.

Figure 7(b) shows the basic timetable rescheduling created by calculating the delay propagation for each train, specifying the required headway time, minimum stopping time at each station and the running operation at the planned running time, and assuming that trains have extended stopping time at stations. The trains whose stopping time at stations are extended are indicated by the bold lines in Fig. 7(b). The four trains that preceded the first delayed train were assumed to have had extended stopping time at stations to prevent spikes in passenger numbers, and the three trains that followed the first delayed train were assumed to have had extended stopping time at stations to avoid trains slowing down or stopping between stations. By adjusting the 7 trains and 50 trips between stations that had extended stopping time, an energy-efficient rescheduled timetable was created. The suspension time for each train ranged from 30 to 195 seconds, and the total suspension time for all trains was 745 seconds.

The data on the relationship between the extended running time and the reduction of powering energy for each train and section between stations (WT plot) used in the powering energy reduction algorithm is prepared using the Train Operation Power Simulator [8]. The data on the powering and braking time of the extended running time, used in the effective use of regenerative power algorithm is also the same.

We describe the calculation conditions for creating an energy-efficient rescheduled timetable. Candidate extended running times (Δd in chapter 3) and candidate extended stopping times (Δm in chapter 3) are set to 5, 10, 15, ..., 40 seconds for all trains. The weight parameter W for adjusting the balance between powering energy reduction and effective use of regenerative power was varied to 0, 0.05, 0.1, 0.15, 0.2, 0.25 kWh/s.

4.2 The energy-efficient timetable rescheduling created by the proposed method

The energy-efficient timetable rescheduling was created using the calculation conditions described in section 4.1. To confirm the running extension time by the powering energy reduction algorithm, the energy-efficient timetable rescheduling created with W set to 0 is shown in Fig. 7(c). It can be seen that the suspension time in the basic timetable rescheduling as shown in Fig. 7(b) is allocated to running extension time in the energy-efficient timetable rescheduling as shown in Fig. 7(c) as indicated by the red dotted circles, which can be seen more clearly in the enlarged images in the lower right-hand part of the figures.

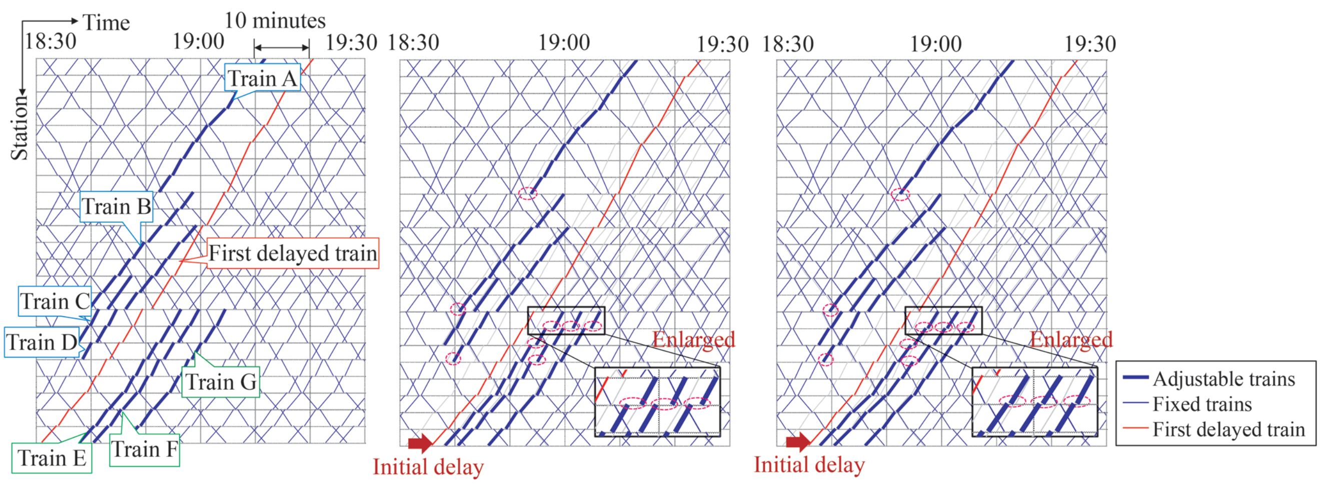

(a) Planning timetable (b) Basic timetable rescheduling (c) Energy-efficient timetable rescheduling

Fig. 7 Created energy-efficient timetable rescheduling

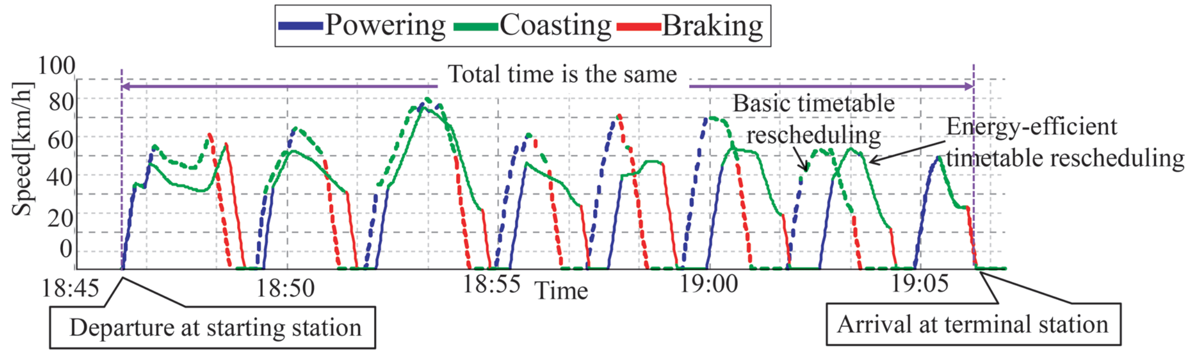

Fig. 8 Comparison of the train performance curve of train G(W = 0)

4.3 Estimation of the energy-saving effect by simulation

The basic timetable rescheduling and energy-efficient timetable rescheduling were simulated with the Train Operation Power Simulator [8], and various kinds of energies were estimated for one hour (from 18:30 to 19:30 as shown in Fig. 7).

First, the speed profiles of train G with *W* set to 0 is shown in Fig. 8, comparing the basic timetable rescheduling (dotted line) and the energy-efficient timetable rescheduling (solid line). Figure 8 shows that the total time does not change, and that the powering energy is efficiently reduced by reducing the powering time and the maximum speed.

Next, the powering and regenerative energy of adjusted trains and between stations (7 trains and 50 between stations) for each *W* is shown in Fig. 9. Increasing the value of *W* means that increasing regenerative energy is preferred over decreasing the powering energy. It is confirmed that as the value of *W* increases, regenerative energy increases and powering energy also increases, as shown Fig. 9. In other words, by adjusting the weight parameter *W*, the balance between reducing powering energy and effective use of regenerative power can be adjusted.

In addition, the energy-saving effect for each *W* calculated based on the energy consumption of the entire one-hour timetable is shown in Fig. 10. Those energy-saving effects were calculated by comparing this with the energy consumption of the basic timetable rescheduling. Under the calculation conditions of this case study, there is almost no difference between the energy-saving effects due to the value of *W*, the maximum and minimum energy-saving effects were 2.2% and 1.9%, respectively.

Table 4 shows the calculation time for creating the energy-efficient timetable rescheduling. The calculation time was within the target of 1 minute when *W* was set in the range of 0 to 0.1 kWh/s.

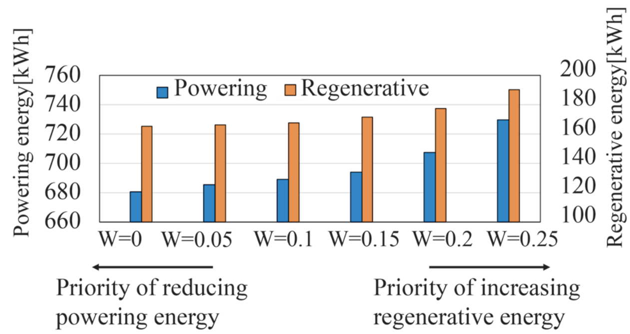

Fig. 9 Comparison of powering and regenerative energies

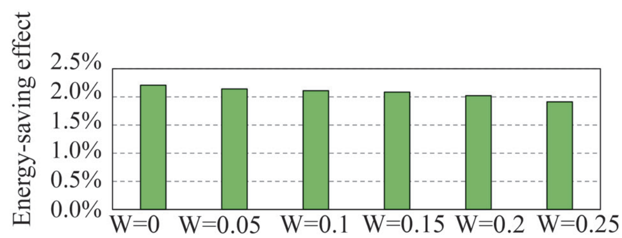

Fig. 10 Energy-saving effect

Table 4 Calculation time taken to create the energy-efficient timetable rescheduling

W[kWh/s]	0	0.05	0.1	0.15	0.2	0.25
Calculation time [s]	0.1	13.0	59.9	101.2	459.8	479.7

5. Conclusion

In this study, we proposed a method for timetable rescheduling that can achieve energy-saving effects in the event of small-scale delays lasting a few minutes, creating a need for trains to have extended stopping time at stations. By adjusting the arrival and departure times of each train at stations, we achieved a balance between reducing powering energy and effective use of regenerative power, while taking passenger convenience into consideration.

As a result of a case study, it was confirmed that an energy-efficient timetable rescheduling could be created within one minute and that an energy-saving effect of up to 2.2% could be achieved.

In the future, we plan to apply the developed method to timetable planning and to create an energy-efficient timetable that balances the reduction of powering energy and the effective use of regenerative power.

Acknowledgment

This study is financially supported in part by the Japanese Ministry of Land, Infrastructure, Transport and Tourism.

References

[1] Ito, T., "The state of energy-saving measures in the field of ground power equipment," *2018 IEE-Japan Industry Applications Society Conference*, 5-S1-2, 2018 (in Japanese).

[2] Tomikawa, H., Wakabayashi, Y. and Shinomiya, T., "The current trend of Energy Saving Technology in Railway Rolling Stock," *2018 IEE-Japan Industry Applications Society Conference*, 5-S1-3, 2018 (in Japanese).
[3] Watanabe, S. and Miyatake, M., "Recent Studies of Energy-Efficient Operation and Scheduling in Electric Railway," *2018 IEE-Japan Industry Applications Society Conference*, 5-S1-4, 2018 (in Japanese).
[4] Takeuchi, Y., Taguchi, A., Ogawa, T. and Morimoto, H., "Minimization of Total Train Operation Energy based on Brake Pattern Selection with Simplified Feeder Circuit Model," *Technical Meeting on "Transportation and Electric Railway" and "Linear Drives," I.E.E. Japan*, VT-20-077/TER-20-073, 2020 (in Japanese).
[5] Miyatake, M., "Theoretical Study on Energy-saving Operation and Scheduling of Railways," *Technical Meeting on "Transportation and Electric Railway" and "Intelligent Transport Systems," I.E.E. Japan*, TER-11-68/ITS-11-43, 2011 (in Japanese).
[6] Akashi, D., Nakano, J., Sato, T., Miyatake, M., Watanabe, S., Takeuchi, Y. and Ogawa, T., "Generation of Energy-Efficient Train Scheduling for a Model Line and Its Evaluation Using Train Operation Power Simulator," *2020 Annual Meeting Record I.E.E. Japan, I.E.E. Japan*, 5-205, pp. 337-339, 2020 (in Japanese).
[7] Kunisaki, A. and Takeuchi, Y., "Examination of Timing Alignment between Powering and Braking in Energy-Saving Reschedule Diagram Creation Method for Small Delays," *Technical Meeting on "Transportation and Electric Railway" and "Micromachine and Sensor System," I.E.E. Japan*, TER-23-038/MSS-23-004, 2023 (in Japanese).
[8] Ogawa, T., Takeuchi, Y., Morimoto, H., Kageyama, M. and Minobe, S., "Estimation Method of Energy Consumption Using Train Operation Power Simulator," *IEEJ Transactions on Industry Applications, I.E.E. Japan*, Vol. 141, No. 5, pp. 374-387, 2021 (in Japanese).

Authors

Aiko KUNISAKI
Assistant Senior Researcher, Transport Operation Systems Laboratory, Signalling and Operation Systems Technology Division
Research Areas: Energy-efficient of Transport Operation, Mathematical Optimization

Yoko TAKEUCHI
Senior Chief Researcher, Head of Transport Operation Systems Laboratory, Signalling and Operation Systems Technology Division
Research Areas: Train Operation Simulation, Energy Simulation and Control, Mathematical Optimization

Estimation of Price Elasticity of Demand for Higher-class Car Travel on Commuter Trains

Ryosuke MATSUMOTO
Data Analytics Laboratory, Information and Communication Technology Division

Higher-class Car (seat upgrade) fares on local trains affect not only demand for higher-class travel, but also ordinary class demand on the same trains. It is therefore important to estimate the impact of price changes on the demand for Higher-class Cars, especially during weekdays' commuting time when overcrowding is at a high level. This research focuses on the two-stage pricing structure of Higher-class Car fares where prices jump by 210 JPY when the travel distance exceeds 50 km in the Tokyo area. Then, this research estimates the price elasticity using regression discontinuity design. The estimation results show that the elasticity is significantly larger than one, which means that the price sensitivity to demand is at a high level. Pricing decisions should be made carefully based on the estimation results of price elasticity and current overcrowding levels in Ordinary and Higher-class Cars.

Key words: *Higher-class Car, Green Car, price elasticity, regression discontinuity design, natural experiment*

1. Introduction

The spread of Covid-19 has promoted the introduction of new ways of working, such as teleworking and staggered commuting times, and has reduced the number of passengers on local trains in urban areas. On the other hand, West Japan Railway Company (JR West) expanded the routes covered by its Higher-class Car (seat upgrade), "A Seat," for local trains in the Osaka area in October 2023. In addition, East Japan Railway Company (JR-EAST) plans to expand the routes covered by its Higher-class Car, "Green Car," to local trains in the Tokyo area in the spring of 2025 [1]. Therefore, the demand for seat upgrades is expected to continue even after the Covid-19 pandemic. Note that "Green Car" is the name for the Higher-class Car used by the JR Group throughout Japan, not only on local trains but also on Shinkansen and other trains, while the "Green Car" in this article refers to the Green Car attached to local trains operated by JR East. Figure 1 shows the exterior and interior of the Green Car and Ordinary Car on the JR-EAST Joban Line.

The pricing of seat upgrades is important both in terms of passenger satisfaction and railway operator revenue. For example, if the fare for the seat upgrades is reduced from the current level, passengers in Ordinary Cars will shift to higher-class cars. This in turn will reduce the comfort (in terms of quieter, non-crowded space) of the seat upgrades. On the other hand, if the fare for the seat upgrades increases, more passengers will opt to travel in ordinary class, causing overcrowding in Ordinary Cars. This shows how upgrade comfort levels and the level of crowding in the Ordinary Cars affect each other. Furthermore, changes in railway operator revenue depend on the relative size of the change in fares and the change in demand. It is therefore necessary to quantify the impact on demand of fare changes for seat upgrades in order to set appropriate fares. The impact of such fares on demand can be quantified using the indicator of price elasticity of demand. This index expresses the sensitivity of demand to price changes, and can be interpreted as a value that shows by approximately what percentage demand will decrease (increase) when the price increases (decreases) by 1%.

It is important to consider appropriate pricing based on the price elasticity of demand. However, Green Cars fares, the oldest type of seat upgrade, has been set at the same level as in the past, except for minor adjustments when the consumption tax was increased (in 2019, 2014 and 1997). Therefore, there is no guarantee that the current fare is appropriate. Note that Green Car fares was revised on March 16, 2024, but the goal is to promote a "more comprehensible fare system" and "IC and ticketless" [2].

There is no previous research that has estimated the price elasticity of demand for seat upgrades. There are a few previous studies that have estimated the price elasticity of demand for train fares in Japan [3, 4, 5], etc., but these use aggregated data, using for example, individual train lines. Therefore, all of the previous studies have room for more detailed analysis. Nevertheless, it is difficult to estimate the price elasticity of demand for rail because unlike air fares, rail fares do not fluctuate on a daily basis and are instead largely fixed.

An ideal way to estimate the price elasticity of demand for seat upgrades is to conduct a field experiment in which Green Car fares are randomly changed on a route-by-route or day-to-day basis. Figure 2 illustrates the results of such a field experiment in which more and less expensive fares were randomly changed on a daily

Fig. 1 JR-EAST Green Car and Ordinary Car, Left: Exterior of Green Car and Ordinary Car, Center: Interior of Green Car, Right: Interior of Ordinary Car (Photographed by the author with prior permission from JR-EAST)

basis for each route. The longer the distance traveled by train, the more likely the passenger is to choose a seat upgrade. With two pricing patterns like this, two curves can be obtained for the distance traveled on the train and the probability of choosing the seat upgrade. By quantifying the relationship between the difference in the two types of fares and the difference in the probability of choosing a seat upgrade, the price elasticity of demand can be estimated. However, conducting this type of field experiment is extremely difficult.

This study aims to estimate the price elasticity of demand for seat upgrades by identifying situations as if an experiment had been conducted, without actually conducting a field experiment. This study focuses on morning commuter trains in the Tokyo area, as these are the most crowded. As we will discuss in Section 3.3, it is common in Japan for employers to pay for their employees' commuter passes, since travel allowances are non-taxable up to a certain limit. Therefore, when estimating the price elasticity of demand for Green Cars for commuting, it is not necessary to consider the Regular fare, and I only need to quantify the impact on higher-class travel of changes in Green Car fares.

2. Method

2.1 Method approach

Green Car fares jump at a certain fare-calculation distance boundary. This study analyzes the Green Car fare jump before and after the boundary, considering it as a social experiment that changes the Green Car fare. Figure 3 depicts an illustration of how to estimate the price elasticity of demand for Green Car travel based on the boundary.

This section explains the approach adopted for analyzing 2015 Green Car fares, because the analysis uses data from 2015. As shown in the upper part of Fig. 3, the first Green Car fare is 770 JPY (7.0 USD; 1 USD = 110 JPY) up to 50 km of the fare-calculation distance, but then jumps to 980 JPY (8.9 USD) at 51 km. This means that the fare jumps by 210 JPY (1.9 USD), even though the distance traveled is almost the same. Therefore, as shown in the lower part of Fig. 3, the probability of choosing Green Car travel should gradually increase as the fare-calculation distance increases up to 50 km, while the probability of choosing Green Car should drop at the 51 km boundary, where Green Car fare jumps by 210 JPY (1.9 USD). By quantifying the relationship between Green Car fares and the probability of choosing Green Cars, I estimate the impact of changes in Green Car fares on demand for Green Cars, i.e., the price elasticity of demand for Green Cars. Note that the fare-calculation distance is defined to the first decimal place for each station, however, unless otherwise specified, the fare-calculation distance in this article refers to the whole number rounded up to the first decimal place. This is because Green Car fares and other train fares are calculated based on the whole number of kilometers rounded up to the first decimal place. It should also be noted that Green Car fares in 2015 differ depending on whether a ticket is purchased on the train or in advance, the advance fare being cheaper. In this study, I assume that commuters purchase their Green Car ticket in advance, so the above shows the advance fares.

This method of quantifying causal relationships using jumps in levels before and after the boundary is known as a regression discontinuity design (hereafter, RDD). As mentioned above, there are very few examples of quantifying the impact of train fares on demand, because of the difficulty of conducting field experiments and the fact that railway fares do not vary from day to day. RDD-based analysis is expected to produce results with the same level of accuracy as field experiments when the conditions described in Section 2.2 are satisfied.

2.2 Overview of RDD and its application to this study

RDD is a method for estimating some effect by focusing on the event that the value of a certain continuous variable z is assigned to a separate group depending on whether it is lower or higher than a specific boundary value, and measuring the jump in the target variable y before and after that boundary. The condition for obtaining valid results using RDD is that no other variables other than the target variable y jump at the above-mentioned boundaries.

In this study, the continuous variable z above is the fare-calculation distance, and the dependent variable y is the probability of choosing a Green Car. By focusing on the fact that Green Car fares is either 770 JPY (7.0 USD) or 980 JPY (8.9 USD) depending on whether the fare-calculation distance is less than or more than 51 km, I estimate the price elasticity of demand for Green Cars by measuring the jump in the probability of choosing y around 51 km. The condition for obtaining a reasonable result here is that the variables other than the probability of choosing Green Cars y (time variables and attribute variables) do not jump around the fare-calculation distance of around 51 km. The advantage of RDD is that it can estimate causal relationships using a simple model with only continuous variables z and the jumping variables as explanatory variables.

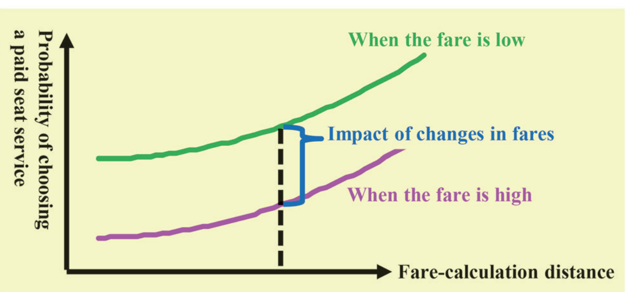

Fig. 2 Visualization of the field experiment

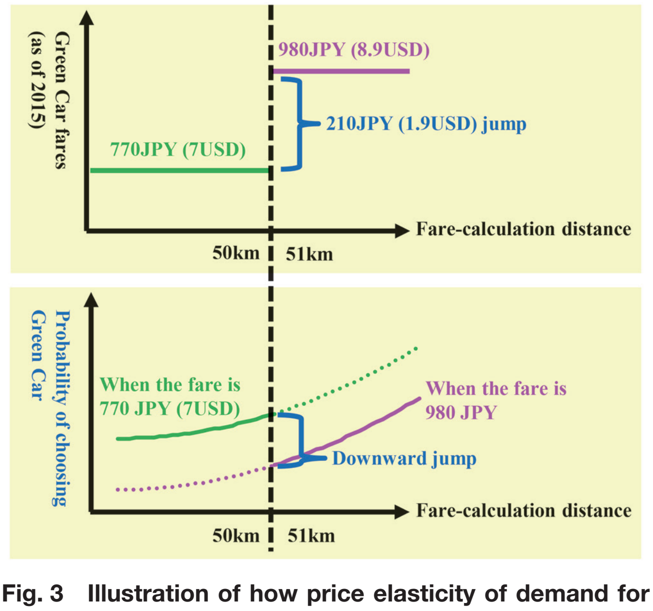

Fig. 3 Illustration of how price elasticity of demand for Green Car is estimated

Note that while the results estimated using RDD provide highly reliable results (internal validity) around the boundary, there is always the question of how applicable they are outside the boundary (external validity).

2.3 RDD model in this study

This study employs a binomial logit model to formulate whether each passenger uses a Green Car or not. The binomial logit model is a statistical model commonly used to formalize choice behavior with two options. Equations (1) and (2) show the RDD model employed in this study.

$$y_i^* = \alpha + \beta z_i + \gamma d_i + \varepsilon_i \tag{1}$$

$$y_i = \begin{cases} 1 \left(\text{if } y_i^* > 0 \right) \\ 0 \left(\text{if } y_i^* \leq 0 \right) \end{cases} \tag{2}$$

The subscript i indicates an individual, and the objective variable y_i^* is the latent variable (utility) for choosing a Green Car. The explanatory variable z_i indicates the fare-calculation distance (before rounding to the first decimal place) that individual i traveled within the Green Car service area, and di is a dummy variable that takes the values 1 or 0, i.e. 1 when the fare-calculation distance is 51 km or more, and 0 when it is less than 51 km. By assuming that the error term ε_i follows an independent and identical Gumbel distribution, this model becomes a binomial logit model. The constant term is represented by α, while β and γ are parameters indicating the weight of each explanatory variable. As shown in (2), the dependent variable y_i takes the value of 1 or 0, where 1 indicates that individual i uses a Green Car and 0 indicates that it does not. In this study, the γ coefficient for di is the most important parameter because it represents the jump in demand for Green Cars.

The theoretical value of the probability of choosing a Green Car, $\Pr(y_i = 1)$, can be calculated with the estimated value of y^* as shown in (3).

$$\Pr\left(y_i = 1\right) = \frac{\exp\left(\widehat{y^*}\right)}{1 + \exp\left(\widehat{y^*}\right)} \tag{3}$$

The price elasticity η in this study can be expressed as in (4), using (3) and Green Car fares $p(d_i)$ depending on whether the fare-calculation distance is less than or more than 51 km.

$$\eta = -\frac{\Pr\left(y_i = 1 | d_i = 1, z_i = 50.1\right) - \Pr\left(y_i = 1 | d_i = 0, z_i = 50.0\right)}{\left\{\Pr\left(y_i = 1 | d_i = 1, z_i = 50.1\right) + \Pr\left(y_i = 1 | d_i = 0, z_i = 50.0\right)\right\}/2} \div \frac{p\left(d_i = 1\right) - p\left(d_i = 0\right)}{\left\{p\left(d_i = 1\right) + p\left(d_i = 0\right)\right\}/2} \tag{4}$$

$p(d_i = 0)$ is 770 JPY (7.0 USD), and $p(d_i = 1)$ is 980 JPY (8.9 USD). The first fraction term in (4) represents the rate of change in the probability of choosing a Green Car, and the second fraction term represents the rate of change in Green Car fares. The denominator used to calculate these rates of change is the midpoint between the pre- and post-change values, following Mankiw (2012) [6]. To calculate the probability of choosing a Green Car, I use the minimum fare-calculation distance ($d_i = 1$, $z_i = 50.1$) where Green Car fares is 980 JPY (8.9 USD) and the maximum fare-calculation distance ($d_i = 0$, $z_i = 50.0$) where Green Car fares is 770 JPY (7.0 USD), as the basis. Note that the price elasticity η is defined by multiplying by -1, so the estimated value should be positive.

Price elasticity η can be interpreted as the percentage decrease (increase) in demand when the price increases (decreases) by 1% in the vicinity of the fare-calculation distance of 51 km.

As already mentioned in Section 2.2, the condition for accurately estimating the price elasticity is that the variables other than the probability of choosing a Green Car do not jump. I will check this in Section 3.3.

3. Data

3.1 Overview of the Metropolitan Transportation Census

In this study, I use individual cross section data from the Metropolitan Transportation Census for the Tokyo area in 2015 (the latest year for which data are available before the Covid-19 pandemic).

The Metropolitan Transportation Census is conducted every five years by the Ministry of Land, Infrastructure, Transport and Tourism (MLIT) to understand the actual use of railways and buses, and the target areas are the Tokyo, Nagoya and Osaka areas. The Metropolitan Transportation Census is made up of several surveys, but the main data used in this study is the individual cross section data for the Tokyo area of the "Survey of Commuters Using Railway Season Tickets, Ordinary Tickets, etc." The survey was conducted over three days from Tuesday, November 17th to Thursday, November 19th, 2015.

Passengers who receive the survey form describe and provide details of their first to third railway trips of the day. Here, 'a trip' refers to a series of movements between an origin (e.g. home) and a destination (e.g. workplace). The passengers describe the purpose of each trip, the origin and destination points, the lines used, the stations where they get on and off, the type of train used, and the departure and arrival times, etc. They also describe the time they start work and provide personal attributes such as gender and age. Note that respondents select train type from the following four options: each station stop, rapid, extra-fee service, and Shinkansen. 'Extra-fee' train service included Green Car travel, express trains, and special commuter liners. Therefore, when respondents selected 'Extra-fee' train service, for journeys in sections where several possible fee-paying train services were running side by side, it is necessary to distinguish local train Green Cars from other trains based on information such as the station where the respondent got on and off, and the time of day.

3.2 Analysis target sample

The analysis targets commuters who hold a commuter pass and whose purpose of the trip is commuting, and whose work starts between 8:00 and 10:00.

To formulate the choice between Ordinary Cars and Green Cars, the analysis targets lines where Green Cars are always attached to local trains. As of 2015, there were 9 lines (based on the line classification of the Metropolitan Transportation Census) where Green Cars are always attached to local trains. Basically, passengers need to pay Green Car fares once per train, but they can transfer to another train without paying the fare again as long as they do not exit the ticket gate. For this reason, the fare-calculation distance for each passenger's trip within the Green Car operating area is substituted for the model's explanatory variable z_i.

Even on sections where Green Cars are in operation, passengers who have the potential to bias the results must be excluded from the analysis. Even on sections where Green Cars operate, bias occurs at ODs where limited express trains or similar trains stop. For this reason, ODs where express trains or similar trains stop during the morning commuting hours are excluded from the analysis, based on the boarding and alighting stations within the Green Car operating area.

Table 1 shows the descriptive statistics for the samples analyzed. The fare-calculation distance is between 1 and 70 km, and the sample size is 17,136. Unknown responses are excluded from the calculation of descriptive statistics.

3.3 Checking the conditions for the RDD

As already mentioned in Section 2.1, the condition for the RDD to be established is that the variables other than the probability of choosing the Green Car do not jump around the fare-calculation distance of 51 km. Figure 4 (a) to (f) show the average values and approximate curves (quadratic approximation) by fare-calculation distance for variables other than the probability of choosing a Green Car.

First, I interpret the time variables. The (a) starting time and (b) arrival time tend not to depend on the fare-calculation distance. The (c) departure time and (d) boarding time tend to be earlier as the fare-calculation distance increases. The reason for this is assumed to be that the longer the fare-calculation distance, the longer the commuting time, and so the need to leave earlier and get on earlier.

Secondly, I interpret the individual attribute variables. (e) The female ratio is the average of the female dummy, i.e. the ratio of women by fare-calculation distance. The female ratio tends to be lower for longer fare-calculation distances. The reason for this is assumed to be that women are more likely to be in part-time employment, and therefore have less incentive to spend time commuting than those in full-time employment. (f) Age tends to increase with longer fare-calculation distances. This is assumed to be due to the tendency for people to own houses as they get older. More specifically, they have an incentive to live in the suburbs where land prices are low in order to own a house, and the cost of moving becomes higher once they own a house.

The price of a commuter pass increases by 1 km of fare-calculation distance. However, I suppose that this is not an issue for analysis since the cost of commuter passes is generally paid for by the company in Japan. This is because there is a tax-free allowance of 100,000 JPY (909.1 USD) per month for commuting expenses in Japan (as of 2015). There are Green Passes that allow you to use the Green Car every day, but employers are generally not expected to pay for Green Car fares. Therefore, Green Passes are not taken into account in the analysis. Furthermore, around the fare-calculation distance of 51 km, a Standard Green Car fare is generally cheaper than a Green Pass. There are two types of Green Pass: one-month and three-month. The three-month pass is cheaper per day. Assuming you use the three-month pass for 20 days a month, the fare is 1,564 JPY/day (14.2 USD/day) for a fare-calculation distance of 50 km, and 2,052 JPY/day (18.7 USD/day) for a fare-calculation distance of 51 km (as of 2015) [7] Therefore, there should be no problem with the analysis assuming that the Green Passes are not used very much.

Based on the above considerations, no jumps were observed at a fare-calculation distance of around 51 km. Therefore, the dummy variable parameter γ in the RDD model shown in Section 2.2 is assumed to indicate the change in utility due to changes in the fare of Green Cars.

4. Results of the analysis

4.1 Estimation results for the model parameters and the price elasticity

In this study, I estimate the parameters for three fare-calculation distances: (1) 1 to 70 km, (2) 11 to 70 km, and (3) 21 to 70 km, and calculate the price elasticity based on each of them. The reason for estimating the parameters for several fare-calculation distances is to check the robustness of the results. Note that the glm function (generalized linear model) of the statistical analysis software R (64-bit) version 3.6.1 was used to estimate the parameters using the maximum likelihood method.

Table 2 shows the results of the parameter estimation for the model and the price elasticity of demand for Green Cars. Fig. 5 depicts the relationship between the fare-calculation distance and the probability of choosing a Green Car for each estimated parameter.

4.2 Interpretation

In all cases (1) to (3), γ is estimated to be statistically significant and negative, and the price elasticity is greater than 1. Therefore, the demand for Green Cars drops around the fare-calculation distance

Table1 Descriptive statistics

Variables	Unit	Mean	Standard deviation	Min	Median	Max
z_i: Fare-calculation distance	km	25.3	13.7	1.1	24.7	69.7
d_i: Dummy of 51 km or more	-	5.9%	0.24	0	0	1
y_i: Dummy of Green Car choice	-	1.1%	0.10	0	0	1
Work start time	h:mm	8:56	0:25	8:00	9:00	10:00
Departure time	h:mm	7:11	0:42	4:00	7:10	9:53
Boarding time	h:mm	7:28	0:42	4:44	7:28	9:42
Alighting time	h:mm	8:17	0:38	5:25	8:17	10:00
Arrival time	h:mm	8:29	0:37	5:55	8:30	10:00
Female ratio※)	-	29.2%	0.45	0	0	1
Age	year	49.7	10.6	18	50	97

※) Descriptive statistics for a dummy variable that takes the value 1 if the passenger is female and 0 if the passenger is male.

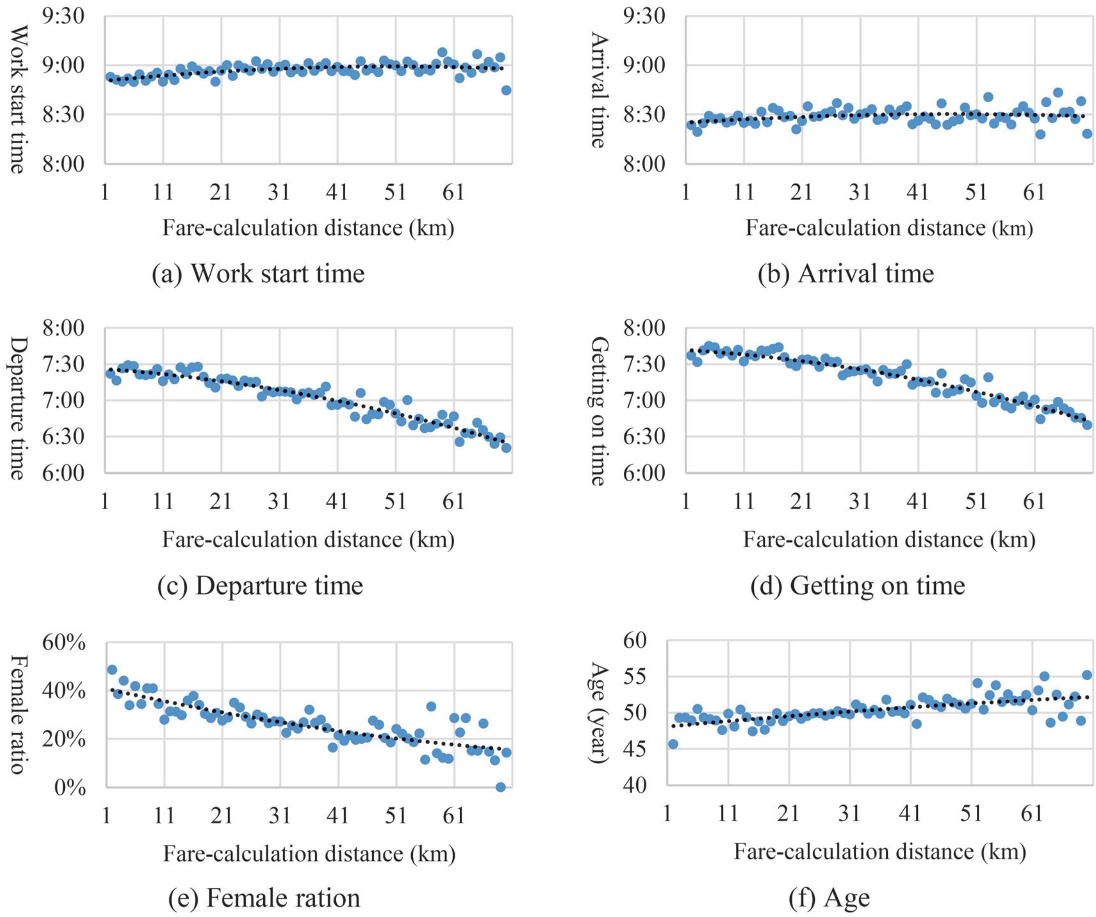

Fig. 4 Average values for time variables and personal attributes by fare-calculation distance

of 51 km, where Green Car fares jump by 210 JPY (1.9 USD). The price elasticity is also statistically significant and exceeds 1. Price elasticity exceeding 1 means that the rate of change in demand due to a change in price exceeds the rate of change in price, that is, the sensitivity of demand to price is high. Furthermore, a price elasticity value greater than 1 means that a reduction in price will increase demand by more than the rate of reduction in price, i.e. a reduction in price will increase revenue.

From the above, it can be interpreted that the demand for Green Cars is highly sensitive to fares, and that when Green Car fares is reduced, the demand for Green Cars increases by more than the percentage reduction in fares, resulting in an increase in fare revenue. This suggests that changes in Green Car fares can contribute to an increase in revenue for railway operators without large-scale investment in facilities such as quadruple tracks or additional vehicles. However, as already mentioned in Chapter 1, excessively low fares for Green Cars will lead to overcrowding and make it impossible to provide the kind of comfort in terms of space and quietness expected with the upgrade. Therefore, to set appropriate fares for Green Cars, careful consideration based on the estimated price elasticity and a comparison of the current level of congestion in Ordinary Cars and Green Cars is necessary. Note that since these values have been estimated from jumps in price at around 51km in fare-calculation distance, additional research is needed to determine whether the above interpretation can be extended to commuters other than those around 51 km.

The probability of choosing a Green Car at a fare-calculation distance of 51 km ($d_i = 1$) was estimated to be between 1.5% and 1.8%, a difference of 0.3 points. The probability of choosing a Green Car at a fare-calculation distance of 50 km ($d_i = 0$) was estimated to be between 3.5% and 4.3%, a difference of 0.8 points, and the range was wider. The price elasticity was estimated to be between 2.761 and 4.013, with a somewhat wider range of 1.252 points. In addition, because the number of samples for fare-calculation distances of 51 km or more is small (5.9% of the total), the average probability of choosing a Green Car by fare-calculation distance is somewhat scattered. In order to solve these issues and obtain more stable estimation results, I need to ensure a sufficient sample size by using data from Metropolitan Transportation Censuses for years other than 2015, as well as data other than Metropolitan Transportation Census data.

5. Conclusions

5.1 Summary of this study

In this study, I have estimated the price elasticity of demand for Green Cars in the weekday morning commute by applying RDD, focusing on the jump in Green Car fares at the fare-calculation distance of 51 km. The analysis result shows that the estimated price elasticity of demand for Green Cars exceeds 1 with statistical significance. This suggests that the demand for Green Cars is highly sensitive to fares, and that a reduction in Green Car fares will increase the demand for Green Cars by more than the percentage reduction in fares and increase the railway operators' revenue. The appropriate

Table 2　Estimation results of the parameters and the price elasticity

Parameters	Corresponding terms		(1)			(2)			(3)		
α	1	Constant	-6.582	(-26.52)	***	-6.382	(-23.49)	***	-5.886	(-16.91)	***
β	z_i	Fare-calculation distance	0.070	(9.57)	***	0.064	(8.09)	***	0.051	(5.18)	***
γ	d_i	Dummy of 51 km or more	-1.086	(-3.75)	***	-0.970	(-3.25)	***	-0.712	(-2.20)	**
Log-likelihood			-941.2			-923.0			-850.2		
McFadden's pseudo-R-squared			0.058			0.041			0.019		
Target of fare-calculation distance			1~70 km			11~70 km			21~60 km		
Sample size			17,136			14,717			10,811		
$\Pr(y_i = 1 \mid d_i = 0)$	Probability of Green Car choice at $d_i = 0$		4.3%			4.1%			3.5%		
$\Pr(y_i = 1 \mid d_i = 1)$	Probability of Green Car choice at $d_i = 1$		1.5%			1.6%			1.8%		
η	Price elasticity		4.013			3.647			2.761		

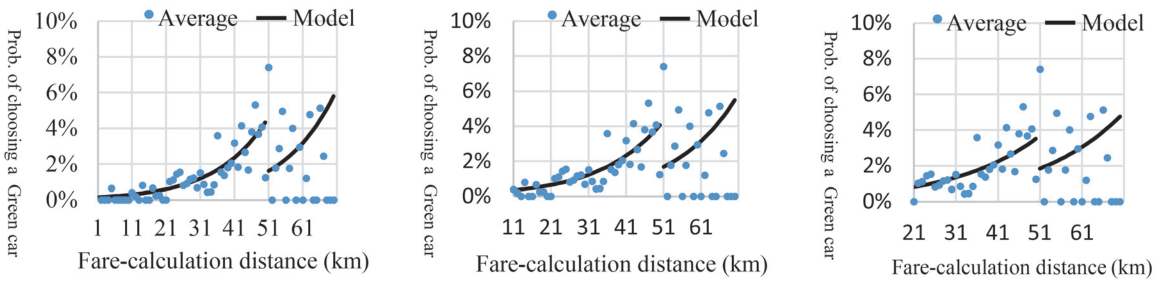

(1) Fare-calculation distance 1~70 km　(2) Fare-calculation distance 11~70 km　(3) Fare-calculation distance 21~70 km

Fig. 5　Average and theoretical values of the probability of choosing a Green Car, by fare-calculation distance

price for Green Cars during the weekday morning commute needs to be carefully considered, comparing the current level of overcrowding in Ordinary Cars and Green Cars with the estimated price elasticity. I hope that the results of this research will be used in discussions on the appropriate fare setting for seat upgrades, including Green Cars, and the number of vehicles to be introduced.

In conclusion, although there are still issues to be addressed, such as the fact that the price elasticity was estimated over a somewhat wide range of values, I have established a basic method for estimating the price elasticity of demand for railways by applying RDD to railways for the first time.

5.2 Future work

Due to the limitations of the data sample used in this study, I focused on the weekday morning commute and estimated the price elasticity of demand for Green Cars by combining data from several lines. However, the actual price elasticity is expected to differ depending on the time of day, such as weekdays and holidays, morning and evening commutes, and off-peak hours and also depending on lines. Therefore, future work should involve using data from other years of the Metropolitan Transportation Census and other data on actual usage to eliminate the problem of data constraints and estimate price elasticity that differs by time of day and route. This will make it possible to consider more flexible fare systems, such as a system where the fare is higher during peak hours and lower during off-peak hours, or a system where the fare differs depending on the route.

Furthermore, the goal of future research is not only to estimate the price elasticity of demand for Green Cars, but also to expand it to the construction of a fare setting method for Green Cars that achieves an appropriate level of crowding from the perspective of both passenger satisfaction and operator revenue.

Finally, this paper is a slightly modified version of a paper [8] that was published in *The Japanese Journal of Transportation Economics*, No. 63.

References

[1] East Japan Railway Company, "中央線快速・青梅線でグリーン車サービスを開始します," *JR East News*, September 10, 2024 (in Japanese).

[2] East Japan Railway Company, "首都圏の普通列車グリーン車の料金体系を見直します," *JR East News*, December 15, 2023 (in Japanese).

[3] Kaneko, Y., Fukuda, A., Koda, J. and Chiwaki, Y., "Analysis of the Railway Fare Elasticity in the Tokyo Metropolitan Area," *Infrastructure Planning Review*, Vol. 21, pp. 175-181, 2004 (in Japanese).

[4] Aoki, M., Suda, M. and Hayakawa, S., "Estimation and Comparative Analysis of Passenger Demand between Public-Private Railways and Private Railways in Japan," *The Japanese Journal of Transportation Economics*, No. 49, pp. 161-170, 2006 (in Japanese).

[5] Fujita, T., "A Study on Railway Demand in Local Areas: Empirical Analysis by Panel Data," *The Japanese Journal of Transportation Economics*, No. 62, pp. 45-52, 2019 (in Japanese).

[6] Mankiw, N. G., *Principles of Economics (6th Edition)*, Cengage

Learning, 2012.
[7] Central Japan Railway Company, “旅客営業規則　別表第2号,” (as of November 22, 2017) (in Japanese).
[8] Matsumoto, R., “Estimation of the Price Elasticity of Local Train Green-Car Demand -Based on Regression Discontinuity Design-,” *The Japanese Journal of Transportation Economics*, No. 63, pp. 71-78, 2020 (in Japanese).

Author

Ryosuke MATSUMOTO
Assistant Senior Researcher, Data Analytics Laboratory, Information and Communication Technology Division
Research Areas: Transport Economics, Spatial Economics, Applied Econometrics

Concrete Creep Strain Estimation Formula and Design Values of Concrete by Considering the Strength Development

Ken WATANABE **Mami NAKAMURA**
Concrete Structures Laboratory, Structures Technology Division

This paper presents an estimation of creep coefficients to investigate design values of creep coefficients for different types of cement. A formula for estimating compressive strength during loading, which is used to calculate the creep strain used in estimating the creep strain coefficient, was formulated based on the existing formula for estimating compressive strength. First, the design values of creep coefficients for effective prestress calculations are presented. The values were calculated assuming cement types and standard conditions for prestressed concrete (PC) bridges. Then the authors confirm the effect of the creep coefficients on the verification of simple PC girder.

Key words: *concrete, prestressing force, creep factor, design values*

1. Introduction

In recent years, there has been an increase in the use of concrete admixtures to address on the one hand concerns about the difficulty of obtaining high quality aggregate, and on the other to ensure the durability of structures. In particular, concrete with low water-cement ratio has been used in PC structures to ensure relatively high design compressive strength. As a result, the total alkali content of concrete increases. Consequently, there is growing interest in materials which can be used in response to this, such as the use of concrete mixed with fly ash or blast-furnace slag powder.

The 2004 edition of the Design Standard and Commentary for Railway Structures (Concrete Structures) (hereafter "the 2004 Railway Standard") [1] and the 2017 edition of the JSCE Standard Specifications for Concrete (Design Edition) (hereafter "the 2017 JSCE Standard") [2] provide formulas for calculating creep strain per unit stress. These formulas were formulated mainly for ordinary Portland cement, and their applicability to mixed cements has not been clarified.

This paper reports on the formulas and design values of creep coefficients taking account into cement types. In estimating the creep coefficient, a compressive strength estimation equation for loading was formulated based on the existing compressive strength estimation equation to be used in calculating the creep strain. Then, design values of creep coefficients for effective prestress calculations are presented. These were calculated assuming the type of cement and standard conditions of PC bridges. Finally, the influence of the increase or decrease of the design values on the verification of simple PC girders is confirmed.

2. Application of creep strain formula to mixed cement concrete

2.1 Application of the creep strain calculation equation to mixed cement concrete

Equation (1) shows the creep strain calculation equation in the 2004 Railway Standard [1] and the 2017 JSCE Standard [2].

$$\varepsilon'_{cc}(t,t')/\sigma'_{cp}=\frac{4W(1-RH/100)+350}{12+f'_c(t')}\cdot\log_e(t-t'+1) \quad (1)$$

where, $\varepsilon'_{cc}(t,t')/\sigma'_{cp}$: creep strain per unit stress ($\times10^{-6}$/(N/mm^2)) at age t (days) for concrete first loaded at age t' (days), W: unit water content of concrete (kg/m^3), RH: relative humidity (%), t' and t: effective ages of concrete at and during loading (days), $f'_c(t')$: effective age of concrete at loading t' (days).

Equation (1) is mainly applicable to ordinary Portland cement (hereinafter "N") and has been applied mutatis mutandis to early strength Portland cement (hereinafter "H"). Therefore, based on previous reports [3][4], the differences in creep properties of different cement types, such as blast-furnace cement (Class B) (hereinafter "BB") and fly ash cement (Class B) (hereinafter "FB"), were investigated. Figure 1 shows the experimental values of unit creep strain [5]. The values in Fig. 1 are normalized by a function of $f'_c(t')$ in order to take into account the difference in the compressive strength $f'_c(t')$ and Young's modulus at the time of loading among the specimens. The unit water volume W is 175 kg/m^3 and the relative humidity RH is 60%. Although variations were observed between test cases, no clear trend was observed by admixture replacement ratio. Therefore, it is considered that (1) can be applied to mixed cements by appropriately considering $f'_c(t')$.

2.2 Compressive strength estimation formula for loading

Equation (2) expresses the compressive strength of concrete using N, H, BB and FB at the age of t days. The equation refers to the compressive strength estimation equation used for verification against temperature cracking which appears in the 2007 JSCE Standard Specification for Concrete [Design Edition] (hereinafter referred to as the 2007 JSCE Standard [6]). Equation (2) expresses the compressive strength estimation equation for the verification of temperature cracking. It is noted that the equation refers to the compressive strength estimation equation for the verification of temperature cracking in the Standard Specifications for Concrete [Design Chapter] of the Japan Society of Civil Engineers (JSCE) enacted in 2007 (hereinafter the "2007 JSCE Specifications") [6].

$$f'_c(t)=\frac{t}{a+bt}d(28)f'_c(28) \quad (2)$$

where a, b: constants, $d(28)$: rate of increase of compressive strength at 91 days of age relative to 28 days of age, $f'_c(28)$: compressive strength of concrete at 28 days of age (N/mm^2).

The values of the constants a, b, and $d(28)$ in (2) were deter-

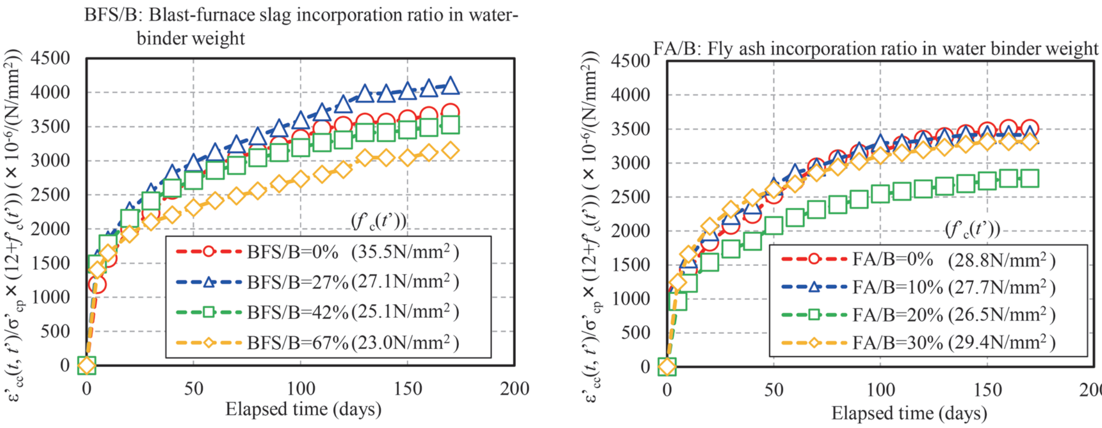

(a) Blast-furnace slag [3] **(b) Fly ash(FB) [4]**

Fig. 1 Effect of admixture mixing ratio on unit creep strain [5]

Table 1 Coefficients used in equation (2) [5]

Type of cement	a	b	$d(28)$	$f'_c(28)$
Ordinary Portland Cement	4.5	0.95	1.11	$-20+30(C/W)$
Early strength Portland cement	1.7	0.98	1.04	$-15+30(C/W)$
Blast-furnace cement Class B	6.2	0.93	1.15	$-10+25(C/W)$
Fly ash cement Class B	6.2	0.93	1.15	$-25+30(C/W)$

mined so that they can be expressed with the same degree of accuracy as the compressive strength estimation equations [2][7] in the 2017 JSCE Standard, Part 6: Verification against Temperature Cracking. Table 1 shows the values of the constants a, b, and $d(28)$ determined with reference to the results of the least-squares method and the estimating equations in the 2007 JSCE Specifications [6]. Figure 2 shows the calculated values by (2). From Fig. 2, the differences in strength development for each cement type can be confirmed. Figure 3 shows a comparison of the calculated values with the previously published experimental data [7] to [11]. Figure 3 shows experimental data of compressive strength measured at several ages between 1 and 91 days of age. As shown in Fig. 3, although FB is replaced by N with fly ash by 15% to 22% [5] the calculated values generally evaluate the actual strength. The calculated values exceeded the actual strength in some experimental data with W/B=40%-50% for FB and W/B=30%-40%-50% for BB, and the difference was slightly larger in some data. However, the variation in the prediction accuracy of the previous compressive strength estimation equation for N shown in Fig. 3(a) was comparable to the variation in the prediction accuracy of the previous equation.

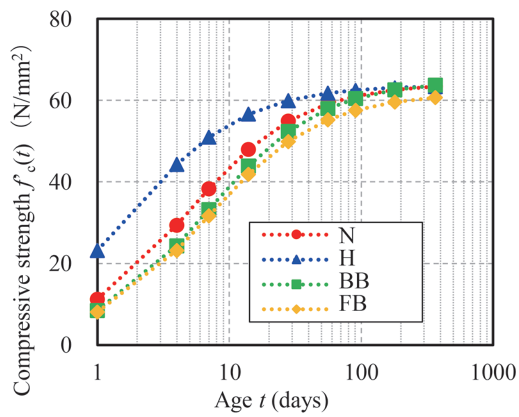

Fig. 2 Strength development of concrete calculated by Equation (2)

2.3 Effects of kind of cement on creep strain and creep coefficient

Figure 4 shows the creep strain per unit stress for the same W/B and age at start of loading. The trend in the increase in unit creep strain is dependent on cement type. Figure 5 shows the creep coefficients calculated from (1) and (2). Here, the creep coefficient was calculated from the compressive strength at loading, based on the relationship between compressive strength and Young's modulus, to obtain Young's modulus at loading, E_{ct}, and then calculated by (3).

$$\varphi(t,t')=(\varepsilon'_{cc}(t,t')/\sigma'_{cp})\cdot E_{ct} \tag{3}$$

where $\varphi(t,t')$: creep coefficient at age t (days) of concrete first loaded at age t' (days), $\varepsilon'_{cc}(t,t')/\sigma'_{cp}$: creep strain per unit stress at age t (days) of concrete first loaded at age t E_{ct}: Young's modulus of concrete (N/mm^2) at the effective age of t' (days) at the time of loading.

The difference in creep coefficients at the same age of the cement type is due to the difference in strength development shown in Fig. 2. In the construction of PC structures, the compressive strength at the introduction of prestress is generally controlled and the creep modulus is calculated by (3). If the compressive strength at the time of prestressing is the same, the creep coefficient is expected to be about the same regardless of the type of cement.

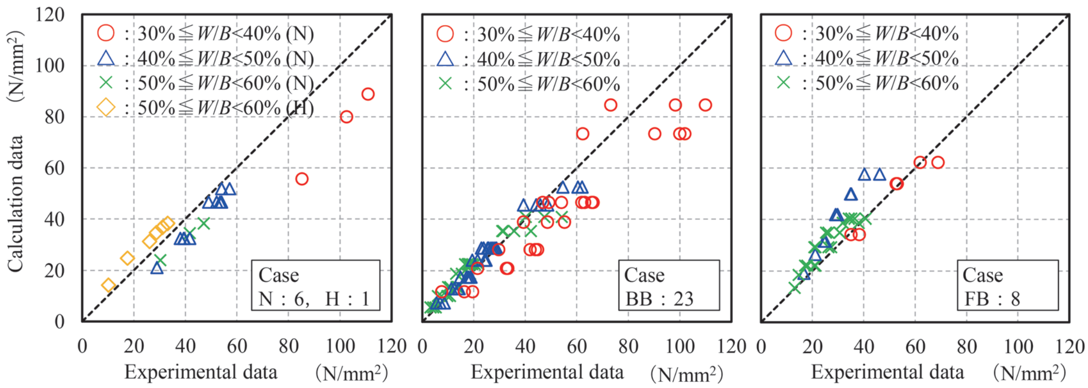

(a) N [7], H [8] (b) BB [7] (c) FB [9] [10] [11]

Fig. 3 Comparison of compressive strength between previously published experimental [5] data and calculation data

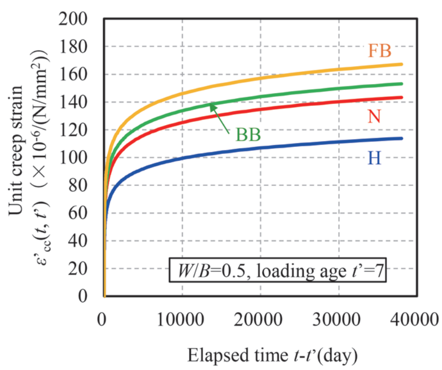

Fig. 4 Unit creep strain and cement type

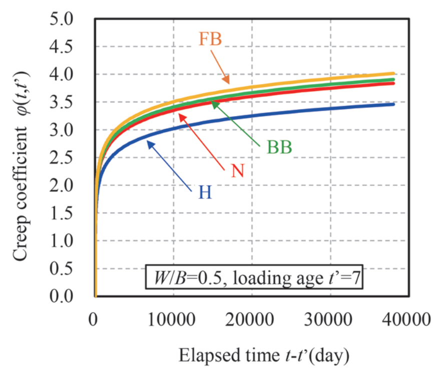

Fig. 5 Creep factor and cement type

3. Review of design values for calculating creep coefficients

3.1 Review of design values for prestress force calculation

In conjunction with the review of (2), the design values of the creep coefficient were also reviewed. The design values were determined assuming a prestressed concrete structure under standard conditions. The relative humidity of the top and bottom surfaces of the girder was calculated as the top (dry repeatedly) and bottom (always dry) surfaces of the member since the calculation of long-term deflection of a PC girder requires appropriate consideration of the relative humidity of the top and bottom surfaces of the girder. However, when the effects of creep are modeled in terms of forces, such as the variation of the prestressing force of a girder, the effects due to the difference in creep coefficients between the top and bottom surfaces are small. Therefore, the creep coefficient was calculated as the average value of the cross section as the design value of the creep coefficient used in the prestressing force calculation.

The design values of the creep coefficient were considered as follows. Equation (1) is constructed based on the creep test results of concrete specimens. In the construction of (1), the creep coefficient can be calculated by arbitrarily setting the age of the material at which loading begins, t'. However, creep tests generally do not set the initial loading age to 28 days or 3 months, and there is room for further study on the accuracy of the prediction equation when the loading age increases. In (1) and (2), for example, φ = 2.7 when loading age t' = 28 days. As shown in Table 2, the design value for 28 days of material age in the 2004 Railway Standard is φ = 1.5, which is about 1.8 times larger than the value in the 2004 Railway Standard.

The design values of the 2004 Railway Standard have been used in the construction of PC and PRC girders, and no problems have been reported, at least in terms of the calculation of the amount of prestress reduction. Therefore, it was decided to use the design values, rather than the prediction formulas, to be consistent with the 2004 Railway Standard. In other words, it is necessary to examine the accuracy of the design values together with the equation for calculating not only the creep coefficient but also the amount of reduction in prestress.

Therefore, the design values of creep coefficients were calculated by (4) based on (1) to (3) and the commonly used Whitney rule, referring to the study [12] in the JSCE Standards enacted in 2017. This is calculated as the residual creep from the time of each loading to the design service life in relation to the creep at the time of prestressing as the design creep value for the age of the material at the time of each loading.

$$\varphi(t,t'_i)=\varphi(t,t'_1)-\varphi(t'_i,t'_1) \tag{4}$$

where, $\varphi(t,t'_i)$: creep coefficient at age t (days) of concrete first loaded at age t'_i (day), where t'_1 is 7 days (N, BB, FB) or 4 days (H). The value of t was set to t = 38,000 (days) to ensure a service life of 100 years, which is a rather large value considering the time until the start of in-service.

As shown in Table 2, the creep coefficient of early-strength cement is slightly smaller than that of ordinary cement when loaded at relatively early ages (Fig. 4). On the other hand, the creep coefficients of blast-furnace cement Class B and fly ash cement Class B were almost the same as those of ordinary cement (Fig. 4), suggest-

Table 2 Design values of creep coefficient of concrete for effective prestressing calculation

Source/method of study	Type of cement	Age of concrete at introduction of prestress, age of concrete at loading (day)						
		4	7	4-7	14	28	90	365
The 2004 Railway Standard	-	-	-	2.7	1.7	1.5	1.3	1.1
Equations (1) to (4)*	N	-	3.1	-	2.5	2.2	1.8	1.4
	H	2.9	2.5	-	2.3	2.0	1.7	1.3

*N: Ordinary Portland cement (blast-furnace cement Class B and fly ash cement Class B are also applicable), H: High strength Portland cement

Table 3 Trial design conditions

Design conditions	PC			PRC	
	T-shaped girder	Box girder	Through girder	T-shaped girder	Box girder
Number of lines	1	2	1	2	2
Bridge length	24 m	31.3 m	31 m	38 m	34 m
Type	Shinkansen	Conventional line	Conventional line	Conventional line	Shinkansen
Design speed	260 km/h	90 km/h	110 km/h	160 km/h	260 km/h

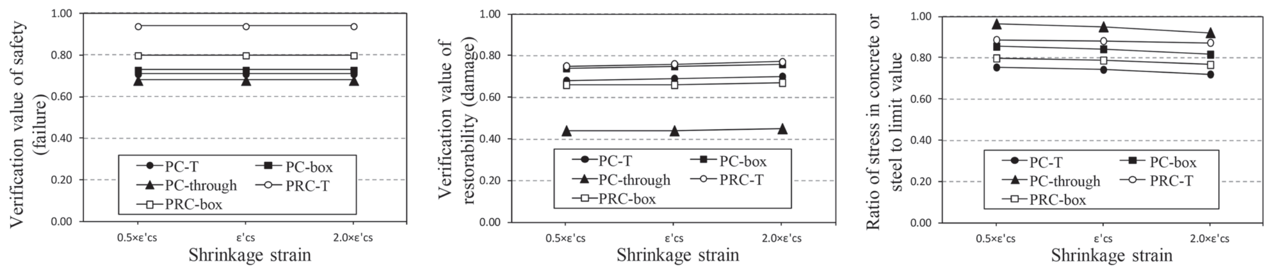

(a) Verification value of safety (failure) (b) Verification value of restorability (damage) (c) Examination of "Requirements for application"

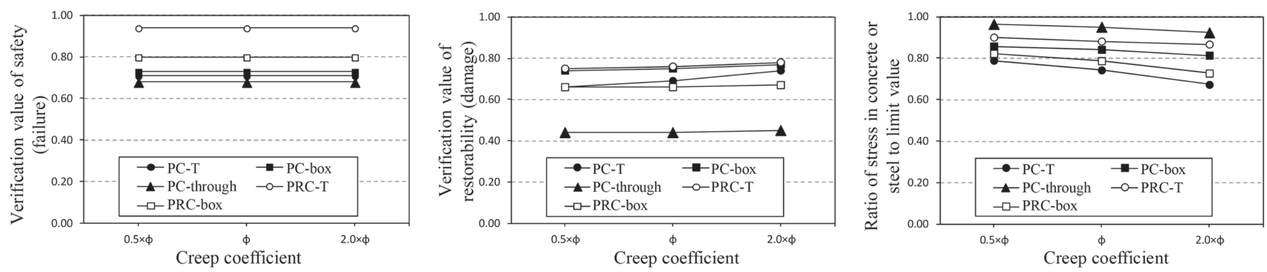

(d) Verification value of safety (failure) (e) Verification value of restorability (damage) (f) Examination of "Requirements for application"

Fig. 6 Results of trial design of various PC and PRC girders (Upper: with different amount of shrinkage strain, lower: with different creep coefficient)

ing that the values of ordinary cement should be applied as design values. As a result, the creep coefficient increases in the range of 0.3 to 0.8, but the creep curve does not differ significantly from the 2004 Railway Standard.

3.2 Influence of design values on verification of simple PC and PRC girders

The effects of shrinkage strain ε'_{cs} and creep factor φ on the verification results of each performance item for PC and PRC girders were investigated. Table 3 shows the main test design conditions of the girders for which trial designs were conducted. One example, each of PC-T girders, PRC-T girders, PC-box girders, PRC-box girders, and PC-through girders were selected. $\varepsilon'_{cs} = 200 \times 10^{-6}$ and $\varphi = 2.7$ [1] were used as the base values. The verification results were checked when the values of ε'_{cs} and φ were increased or decreased by a factor of 0.5 and 2.0, respectively. The design standard strength of the concrete is 40 N/mm^2 (34 N/mm^2 when introduced) with a maximum water cement ratio of 50%.

Figure 6 shows the calculation results. Here, safety (failure), recoverability (damage), and "Assumptions for verification," which are the determining factors in the design, are presented. In "Assumptions for verification," the stress levels of concrete and steel were examined, and it was confirmed that the compressive stress σ'_c at the edge of concrete due to permanent action is less than 40% of the design compressive strength f'_{cd} of concrete, and the tensile stress σ_p of PC steel due to variable action is less than 70% of the design tensile strength f_{pud}. The tensile stress σ_p of the PC steel due to the variation is less than 70% of the design tensile strength f_{pud}.

Regardless of the girder type, the shrinkage strain ε'_{cs} and creep factor φ have a small influence on the verification results. In particular, for girders, the sensitivity of ε'_{cs} and φ is not found in safety (failure), which is the determining factor in design. In addition, in the case of the "verification assumption," which is verified using the steel stresses, the verification results varied slightly, but there was no increase in the verification values to the extent that it became a determining factor. Thus, in the design of simple PC girders, the increase or decrease of shrinkage strain ε'_{cs} and creep factor φ has a small effect on the verification results. In other words, as shown in Table 2, although the design values of the creep coefficients increased from the 2004 Railway Standard, the effect on the verification values for the different girders is considered to be small.

4. Conclusions

(1) Based on the previous experimental results showing that the effect of cement type on unit creep strain was relatively small, it is considered that creep of mixed cement concrete can be generally expressed by considering the difference in compressive strength development of concrete in the creep strain calculation equation of the 2004 Railway Standard.
(2) Based on the existing compressive strength estimation equation, the compressive strength estimation equation under loading was formulated for the calculation of creep strain. Creep coefficients for effective prestress calculations considering cement types are presented.
(3) In the trial design of simple PC girders and PRC girders, the effects of the shrinkage strain ε'_{cs} and the creep coefficient φ on the verification results were confirmed. Although the design values of creep coefficients were increased in this report, the effects on the verification results of these girders were confirmed to be small.

References

[1] Ministry of Land, Infrastructure, Transport and Tourism, and Railway Technical Research Institute, *Design Standard for Railway Structures and its Commentary (Concrete Structures)*, Maruzen, 2004 (in Japanese).
[2] Japan Society of Civil Engineers, *Standard Specifications for Concrete, 2017 [Design Edition]*, Maruzen, 2018 (in Japanese).
[3] Otani, T., Hamanaga, Y., Ueda, K., and Sato, Y., "Evaluation of shrinkage cracking resistance of concrete admixture by buried reinforcement test," *Proc. of Japan Concrete Institute*, Vol. 33, No. 1, pp. 221-226, 2011 (in Japanese).
[4] Otani, T., Yan, S., Ito, N. and Sato, Y., "Study on shrinkage and cracking characteristics of fly ash concrete by boundary test with buried steel bars," *Proc. of Japan Concrete Institute*, Vol. 34, No. 1, pp. 136-141, 2012 (in Japanese).
[5] Nakamura, M., Watanabe, K., "Study on design value of creep factor of concrete considering cement type," *Proc. of symposium on development of prestressed concrete*, Vol. 30, pp. 515-518, 2021 (in Japanese).
[6] Japan Society of Civil Engineers, *2007 Standard Specification for Concrete [Design Edition]*, Maruzen, 2008 (in Japanese).
[7] Japan Concrete Institute, *Crack Control Guidelines for Mass Concrete 2008*, Japan Concrete Institute, 2008 (in Japanese).
[8] Oi, T., Morino, K. and Naito, Y., "Curing temperature conditions and strength development of concrete," *Proc. of Japan Concrete Institute*, Vol. 1, No. 1, pp. 5-8, 1979 (in Japanese).
[9] Kokuhu, K., Ueno, A. and Hirano, S., "Quantitative evaluation of curing temperature and age effect on strength development of fly ash," *Proc. of Japan Concrete Institute*, Vol. 22, No. 2, pp. 79-84, 2000 (in Japanese).
[10] Wu, F., Masuda, Y., Nakamura, N. and Niinuma, D., "Effect of curing change on strength development of concrete using fly ash," *Proc. of Japan Concrete Institute*, Vol. 25, No. 1, pp. 569-574, 2003 (in Japanese).
[11] Fukagawa, M., Nakamura, N., Masuda, Y. and Abe, M., "Mechanical properties and durability of high-strength concrete using classified fly ash," *Proc. of Japan Concrete Institute*, Vol. 19, No. 1, pp. 205-210, 1997 (in Japanese).
[12] JSCE, *Concrete Library 138, Revision of the 2012 standard specification for concrete - basic principles, design and construction* -, Maruzen, 2013 (in Japanese).

Authors

Ken WATANABE, Ph.D.
Senior Chief Researcher, Head of Concrete Structures Laboratory, Structures Technology Division
Research Areas: Design and Maintenance of Concrete Structures

Mami NAKAMURA, M.E.
Assistant Senior Researcher, Concrete Structures Laboratory, Structures Technology Division
Research Areas: Design and Maintenance of Concrete Structures

Summaries of Papers in RTRI REPORT (in Japanese)

Verification of Finite Element Analysis Accuracy through Collision Test Using an Actual Railway Carbody Structure and a Dump Truck

Tomohiro OKINO, Keisuke NAGATA, Jun-ichi TAKANO

(Vol.38, No.11, 1-9, 2024.11)

It is impractical to conduct collision tests with the actual train unit to design the crash safety structure. Consequently, numerical simulation is effective and it is important to validate the analytical accuracy. Therefore, the authors conducted the collision test of a full size partial stainless-steel carbody structure of a railway leading vehicle and a typical large dump truck. In addition to the test, FE analysis was conducted under the same conditions as the experimental test in order to compare the numerical result with the experimental one. As a result, the numerical result was in agreement with the experimental result. Finally, using the FE analysis, the authors estimated the impact deformation and fracture behavior of the railway carbody under the actual level-crossing accident.

Development of Driver Advisory System Using Speed Estimation for Freight Train

Tomoyuki OGAWA, Toshihide YOKOUCHI, Yoko TAKEUCHI

(Vol.38, No.11, 11-17, 2024.11)

In this study, we have developed a driver advisory system for freight trains using a speed estimation technique aiming to improve energy-saving and punctuality. The driver advisory system focuses on the maneuvering of freight trains in cruising mode, with the aim of passing through stations on time. The driver advisory system proposes a recommended driving operation for each passing station. We have developed a method for assigning driving operations using the speed estimation, which switches between constant-speed and saw-toothed driving operations depending on speed and load characteristics. Then, we present a trial result with regard to energy consumption. We confirm the energy-saving effect by comparing the energy consumption with and without the developed driver advisory system.

Evaluation of Shear Capacity of RC Pile Head Based on Equivalent Shear Span Method

Yuki NAKATA, Haruyuki KITAGAWA, Ken WATANABE, Toshiya TADOKORO

(Vol.38, No.11, 19-26, 2024.11)

In the verification of reinforced concrete (RC) piles, the design shear capacity V_{yd} of bar members is used based on the experimental results of simply supported RC beams. On the other hand, since RC piles are subjected to ground reaction forces, unlike simply supported conditions, the shear capacity may be greater than V_{yd}. In this paper, we used nonlinear finite element analysis to evaluate the shear capacity of RC pile heads taking into account ground reaction forces. We have shown that the equivalent shear span method, which is applied to the analysis of slabs of underground box structures, can also be applied to the analysis of RC pile heads.

Method for Calculating of the Design Shear Capacity of Reinforced Concrete Members with Continuity of Ratio of Shear-span to Effective Depth

Yuki NAKATA, Ken WATANABE, Yukihiro TANIMURA

(Vol.38, No.11, 27-35, 2024.11)

The safety of RC structures for shear force is verified by confirming that the shear force does not reach the design shear capacities (V_{yd}, V_{dd}). V_{yd} and V_{dd} are determined on the basis of experimental results and are expressed as a function of the ratio of shear span to effective depth (a/d). Therefore, there may be a significant difference between V_{yd} and V_{dd} at $a/d = 2.0$ in the case of RC beams with larger shear reinforcement ratios. This is due to the fact that the contribution of large amounts of stirrups to the shear capacity of RC beams has not been clarified. Based on experimental results, this research has investigated the contribution of stirrups and load plates to the shear capacity of rectangular cross section RC beams. Finally, a method for calculating the design shear capacity of RC beams with continuity of a/d has been proposed.

Method for Determining Resumption of Train Service on Railway Embankment Damaged by Rainfall

Taketo SATO, Takaki MATSUMARU, Kazuki ITO, Takumi OZAKI

(Vol.38, No.11, 37-43, 2024.11)

Since the stability of railway embankments damaged by rainfall is not easily assessed, the need for temporary restoration is often determined by the inspector's experience, or the damaged embankment is simply restored to its original shape. As a result, there are cases where temporary restoration is carried out with excessive specifications for embankments that meet the performance requirements for train operation. This study proposes a method to evaluate the performance of damaged embankments or temporary restoration embankments in terms of stability and settlement during train operation, and to quickly determine the resumption of train operation on the damaged embankment.

Effect of Snow Cover on Embankment Stability during Rainfall and Snowmelt

Tsuyoshi TAKAYANAGI, Shoma FUJIWARA, Ryota SATO

(Vol.38, No.11, 45-53, 2024.11)

In this study, the effect of snow cover on slope stability was examined to evaluate the risk of snowmelt disasters more accurately. At first, strength characteristics of snow were obtained through laboratory tests. In addition to the laboratory tests, precipitation experiments were conducted on a snow-covered embankment model to observe the moisture response and deformation of the embankment. Furthermore, slope stability analysis using finite element method were conducted on the snow-covered embankment model. As a result, it was confirmed that restriction of the surface layer of embankment could slightly improve the effect of snow cover on the slope stability.

Image Measurement of Bridge Girder Deflections on Conventional Line at Night with Reflective Stickers

Seiya HOKIMOTO, Kodai MATSUOKA

(Vol.38, No.11, 55-61, 2024.11)

Image measurement of bridge girder deflection using a video camera has been used on actual railway. However, its applications are limited to daytime when illumination can be secured sufficiently. In this study, the authors investigated an image measurement method for bridge deflection at night using light, small, and simple reflective stickers in addition to a minimal amount of lighting equipment. As a result of the investigation, it was decided to make appropriate use of the contrast between the reflective sticker and the surroundings, and the effectiveness of the proposed method was confirmed by measuring the girder deflection of actual bridges on a conventional line. The result of the actual bridge measurement showed that the girder deflection of the bridge at a distance about 20 meters could be measured with the same accuracy as during the daytime.

Vibration Test Method for Connectors of Overhead Contact Line Based on OCL Vibration Analysis

Takuya OHARA, Chikara YAMASHITA

(Vol.38, No.11, 63-69, 2024.11)

Electrical connectors connecting contact wires and messenger wires are sometimes subject to fatigue-failure due to vibration caused by train passage. It is therefore desirable to establish a method for evaluating the fatigue resistance of the connectors. Therefore, the authors proposed a test method consisting of two types of vibration tests that take into account the two fatigue factors of the connectors: the relative displacement of the contact wire and their resonance. The test conditions were determined by analyzing overhead contact line vibration using an OCL-pantograph simulation. Furthermore, the authors carried out vibration tests on real connectors and confirmed that the test results were consistent with the actual failure status of the connectors.

Development of a Gaze Distribution Data Feedback System for Train Drivers

Daisuke SUZUKI, Fumitoshi KIKUCHI, Takaharu KOIKE

(Vol.38, No.11, 71-77, 2024.11)

This study aimed at developing gaze data feedback system for conducting a driving simulator training using quantitative gaze data of train drivers. The system can preset driving scenes to efficiently instruct trainees within a limited training time. The system can also to compare trainees with experts on face direction and gaze data graphs to clarify the characteristics of trainees' visual search. In addition, the system can visualize the gaze data and clearly show the objects that trainees were looking at while driving. An instructor from a railway company tried the system and gave it a positive evaluation as a training tool for trainees' visual search.

Development of Unloosening Rail Fastening System with Leaf Spring Clip and Existing Concrete Sleeper

Daiki YAMAOKA, Tadashi DESHIMARU, Shingo TAMAGAWA

(Vol.38, No.12, 1-6, 2024.12)

Rail fastening systems using leaf spring clips and bolts are widely used in Japan. This rail fastening system requires regular maintenance to prevent the bolts from loosening. Some railway companies are replacing rail fastening systems using leaf spring clips with boltless rail fastening system using round bar clips in order to eliminate the need for re-tightening of bolts. This replacement involves replacing existing concrete sleepers with dedicated sleepers for round bar clips. Therefore, some railway companies find it difficult to introduce boltless rail fastening systems using round bar spring clips due to construction costs and labor. In response to this problem, we have developed unloosening rail fastening systems using leaf spring clips and existing concrete sleepers.

Method for Repairing Track Slabs with Frost Damage

Takatada TAKAHASHI, Masaru HOJO, Narita TAKAHASHI

(Vol.38, No.12, 7-13, 2024.12)

We have clarified the deterioration mechanism of cross-sectional repair sections in track slabs laid in open sections in cold regions. We also evaluated the residual strength of rail fastening systems on track slabs simulating frost damage. Furthermore, we confirmed the effectiveness of silane/siloxane type surface penetrants in suppressing the progression of frost damage by freezing and thawing tests. Based on these results, we proposed a method for repairing track slabs laid in open sections in cold regions.

Rail Gas Pressure Welding of Low Upset Length Using Variable Pressure Method

Hajime ITOH, Yuki KONAYA

(Vol.38, No.12, 15-20, 2024.12)

In order to reduce the bulge of gas pressure weld and finish by grinding only, the authors carried out rail gas pressure welding tests and numerical analysis for reduction of the upset length. In the tests, a new rail gas pressure welding method using the variable pressure method was achieved with a compression of the upset length of about 6 mm, which is 1/4 of the conventional method, with sufficient strength for practical use. As the trimming process is not necessary, the trimming device is not required. This also reduces the weight of the gas pressure rail welding machine.

Practical Method for Setting Nonlinear Response Spectrum for Seismic Design of Railway Bridges and Viaducts

Kimitoshi SAKAI

(Vol.38, No.12, 21-27, 2024.12)

A Non-linear Response Spectrum Method is one of the methods used to calculate the seismic response values of railway bridges and viaducts. In this study, a method for expressing the non-linear response spectrum was proposed using a relatively simple mathematical equation. In addition, a procedure for estimating the parameters to be input into this equation was proposed. The proposed method was applied to seismic records. The result confirmed that the proposed method can automatically represent the overall trend of the spectra of seismic records while significantly reducing the number of parameters used compared to conventional methods.

Method for Evaluating Crashworthiness of Railway Vehicles Based on Correlation with Injury Severity of Passengers Occupying Longitudinal Seats

Kazuma NAKAI, Tomohiro OKINO, Shota ENAMI, Keisuke NAGATA

(Vol.39, No.1, 1-9, 2025.1)

It is important to enhance the safety of passengers on board railway vehicles in the event of a collision. The railway vehicle standard in European countries and the U.S. provides a framework for structural crashworthiness design. On the other hand, there is still no established method for evaluating the crashworthiness design of railway vehicles in Japan. The aim of this study is to propose a safety index for railway vehicles with longitudinal seats. The severity of passenger's head injury in a level crossing accident was estimated using numerical simulation. The correlation between the injury severity of an Anthropomorphic Test Device (ATD) model and the safety indices of vehicles, that is, the integral of the deceleration waveforms, the mean deceleration waveforms and the maximum waveforms, was compared. It was found that the integral of the deceleration values had the highest correlation with the injury values of ATD. We proposed the integral of the deceleration as a method for evaluating the crashworthiness design of railway vehicles with longitudinal seats.

Method for Measuring the Pantograph Contact Force in Overhead Contact Line System Using Sparse Modelling

Takayuki USUDA, Yoshitaka YAMASHITA, Masaki TAKAHASHI

(Vol.39, No.1, 11-19, 2025.1)

In order to understand the wear mechanism of contact wire and to efficiently prevent OCS failure, the authors have so far developed a method for measuring contact forces of all pantographs during trains passing on sections with sensors installed on the overhead contact line. However, some difficult issues remain in the method for computing the inertial force from contact wire acceleration measured at some measurement points. This paper proposes a method for selecting effective measurement points for contact wire acceleration. LASSO regression, known as one of the sparse modelling techniques, is applied to the proposed method so that suitable points for measuring acceleration are selected for computing inertia force. The results obtained by the proposed method are shown using dynamic simulation data.

Development of Low-cost Train Patrol Support Method Using Smartphone

Hirofumi TANAKA, Boyu ZHAO, Di SU, Tomonori NAGAYAMA

(Vol.39, No.1, 21-27, 2025.1)

Although regional railway companies are facing a difficult business environment, they need to properly inspect and maintain railway facilities and rolling stock to ensure safe and stable train operations. In this study, we developed a smartphone-based train patrol support application as a low-cost track condition management method that can be introduced even by regional railway companies. We then carried out test measurements using the developed application on a commercial line and investigated the use of the measurement data. The results show that the acceleration data are effective for train vibration management, and that the forward view video data are effective for understanding track conditions during desk review.

A Method for Proposing Countermeasures against Ground Vibrations along Railway Lines based on Numerical Simulation

Masanori NOYORI, Hidefumi YOKOYAMA

(Vol.39, No.1, 29-37, 2025.1)

There have been many studies on countermeasures against train-induced ground vibration. However, in many of the countermeasures, the mechanisms and reduction values have not been clarified. Therefore, countermeasures are generally selected on the basis of previous cases or empirical judgments. Using a numerical simulation consisting of a running train, tracks, supporting structures and the ground, we investigated a method for extracting primary factors of the vibration. Then, a method for proposing countermeasures considering the primary factors was investigated. In addition, this report presents a flow chart which shows the relationship between the primary factors and the proposed countermeasures.

QUARTERLY REPORT of RTRI

第 66 巻　第 1 号	Vol. 66, No. 1
2025 年 2 月 1 日　発行	Published date: 1 February 2025
監修・発行所：公益財団法人鉄道総合技術研究所	Supervision/Publisher: Railway Technical Research Institute
〒 185-8540　東京都国分寺市光町 2-8-38	Address: 2-8-38 Hikari-cho, Kokubunji-shi, Tokyo 185-8540, Japan
発行人：芦谷公稔	Issuer: Dr. Kimitoshi ASHIYA
問い合わせ：鉄道総研広報	Contact us: Public Relations, Railway Technical Research Institute Mail Address: rtripr@rtri.or.jp

QUARTERLY REPORT of RTRI

RAILWAY TECHNICAL RESEARCH INSTITUTE

Printed in Japan